INFORMATION TO USERS

This manuscript has been reproduced from the microfilm master. UMI films the text directly from the original or copy submitted. Thus, some thesis and dissertation copies are in typewriter face, while others may be from any type of computer printer.

The quality of this reproduction is dependent upon the quality of the copy submitted. Broken or indistinct print, colored or poor quality illustrations and photographs, print bleedthrough, substandard margins, and improper alignment can adversely affect reproduction.

In the unlikely event that the author did not send UMI a complete manuscript and there are missing pages, these will be noted. Also, if unauthorized copyright material had to be removed, a note will indicate the deletion.

Oversize materials (e.g., maps, drawings, charts) are reproduced by sectioning the original, beginning at the upper left-hand corner and continuing from left to right in equal sections with small overlaps. Each original is also photographed in one exposure and is included in reduced form at the back of the book.

Photographs included in the original manuscript have been reproduced xerographically in this copy. Higher quality 6" x 9" black and white photographic prints are available for any photographs or illustrations appearing in this copy for an additional charge. Contact UMI directly to order.

UMI

A Bell & Howell Information Company
300 North Zeeb Road, Ann Arbor MI 48106-1346 USA
313/761-4700 800/521-0600

The Dynamics of Benzylic Radical Pairs in Organized Media:
Binding and Mobility

by

Mark Howard Kleinman
B.Sc., Concordia University, 1993

A Dissertation Submitted in Partial Fulfillment of the
Requirements for the Degree of

DOCTOR OF PHILOSOPHY

in the Department of Chemistry

We accept this dissertation as conforming
to the required standard

Dr. Cornelia Bohne, Supervisor (Department of Chemistry)

Dr. Peter Wan, Department Member (Department of Chemistry)

Dr. Charles Qian, Department Member (Department of Chemistry)

Dr. Dorothy Paul, Outside Member (Department of Biology)

Dr. Miguel García-Garibay, External Examiner (Department of Chemistry and Biochemistry, University of California, Los Angeles)

Supervisor: Dr. C. Bohne

Abstract

Through the use of laser flash photolysis and product studies, the photochemistry of dibenzyl ketone and its derivatives in SDS micelles shows that these aggregates impart some constraint on the dynamics of benzylic radical pairs. The enhancement of the geminate/cross-termination product occurring within the micellar interior is termed the geminate cage effect. Under conditions where all radicals exit from the supramolecular system, a substantial amount of the cross-termination product is observed in the product studies. This experimental evidence cannot be explained with conventional models, and a new proposal is put forth which suggests that some of the cross-termination product arises from radicals that exit the micelle and then recombine upon re-entry. This new approach is based on the binding of solutes to the micelle and is called the partition effect.

Two sizes of DODAC vesicles were investigated. In small unilamellar vesicles with a diameter of 30 nm, the cage effect derived from product studies showed a significant enhancement of the cross-termination product. Time-resolved experiments showed that all radicals separate, which implies that all of the enhanced cross-termination reactions from the product studies are derived from random radical encounters.

Product studies in large vesicles (~150 nm diameter) demonstrated that the cross-termination product is enhanced, but not to the same extent as for SDS micelles or small vesicles. Calculations reveal that a significant proportion of the random encounters occur in the bulk aqueous phase.

The proposed model suggests that it is not necessary to generate a triplet radical pair in order to observe a magnetic field effect on product distribution.

In summary, this new proposal predicts that magnetic field effects in biological systems can be observed as long as mobility between different solubilization sites occurs.

Examiners:

Dr. Cornelia Bohne, Supervisor (Department of Chemistry)

Dr. Peter Wan, Department Member (Department of Chemistry)

Dr. Charles Qian, Department Member (Department of Chemistry)

Dr. Dorothy Paul, Outside Member (Department of Biology)

Dr. Miguel García-Garibay, External Examiner (Department of Chemistry and Biochemistry, University of California, Los Angeles)

Table of Contents

List of Tables

List of Figures

List of Schemes

Acknowledgements

I wish to express my sincere appreciation to my supervisor Dr. Cornelia Bohne for her guidance and assistance throughout this research project. She is my mentor and an inspiration.

Special mention must be given to Tatiana Shevchenko who completed some of the product studies described within and Dr. Luis Netter who helped in too many way to count.

I would also like to thank Laurel Clouston, Scott Murphy, Brian Eastman and Dr. Dave Budac for their professional assistance and their friendship.

I appreciate the support received from Olga Rinco, Cynthia Ju and Sarah Monahan.

I would like to thank Dr. Dave McGillivray for providing the mass spectra and Chris Greenwood for help with NMR spectrometers. I would like to credit the cooperation and support from the technical staff in the instrument, mechanical and glass shops, and I would also like to thank my fellow graduate students for creating an enjoyable working environment.

This dissertation is dedicated to

My Family and Friends

List of Abbreviations

$\Sigma\alpha_2$	hydrogen bond acidity of the solute
Abs	absorbance
ΔA	change in absorbance (absorbance measured using LFP)
ΔA_{fast}	sum of all transient absorbances for the fast process in a LFP kinetic trace
ΔA_{max}	maximum transient absorbance in a LFP kinetic trace
ΔA_{∞}	residual absorbance remaining after decay on the LFP experimental time scale
$\Sigma\beta_2$	hydrogen bond basicity of the solute
BB	bibenzyl
4-*t*-bBB	4-*t*-butylbibenzyl
4-*t*-butylDBK	4-*t*-butyldibenzyl ketone
c	velocity of light (3×10^8 m/s)
cmc	critical micelle concentration
cmt	critical micelle temperature
CTAC	cetyl (C_{16}) trimethylammonium chloride
CTP	cross termination product (asymmetric product)
$[D_{total}]$	total concentration of detergent
DBK	dibenzyl ketone
4,4'-dmBB	4,4'-dimethylbibenzyl
DODAC	dioctadecyldimethylammonium chloride
DPA	1,1-diphenyl acetone

DPM	diphenylmethane
ε	molar absorptivity ($M^{-1}cm^{-1}$)
E	energy
E_{TS}	triplet-singlet energy gap
exp	number of experiments
4,4'-dtBB	4,4'-di-*t*-butylbibenzyl
F	fluorescence
FID	flame ionization detector
f_s	singlet probability
GC	gas chromatography (gas chromatogram)
h	hours
h	Planck's constant (6.63×10^{-34} J·s)
hfc	hyperfine coupling
HOMO	highest occupied molecular orbital
I	intensity
I_o	initial intensity
IC	internal conversion
ISC	intersystem crossing
K	partition coefficient (equilibrium constant)
$2k/\varepsilon l$	rate constant product for the random recombination process
k_+	entry rate constant
k_-	exit rate constant
k_B	Boltzmann constant (1.38×10^{-23} J·K^{-1})
k_{-CO}	decarbonylation rate constant
k_e	rate constant for the frequency of encounters

k_f	rate constant for fluorescence
k_{fast}	rate constant for the fast decay that corresponds primarily to recombination of the primary radical pair
k_{IC}	rate constant for internal conversion
k_{ISC}	rate constant for intersystem crossing
k_{nr}	rate constant for sum of all non-radiative decay pathways
k_o	intrinsic decay rate constant
k_{obs}	observed rate constant
k_q	quenching rate constant
k_r	radiative rate constant
k_{vr}	rate constant for vibrational relaxation
λ	wavelength (usually in nm)
l	pathlength (cm)
LFP	laser flash photolysis
LUMO	lowest unoccupied molecular orbital
4-MBB	4-methylbibenzyl
4-MeDBK	4-methyldibenzyl ketone
min	minutes
MF	magnetic field
MFE	magnetic field effect
MS	mass spectroscopy (mass spectrum)
ν	frequency (s^{-1})
$\bar{\nu}$	wavenumber (cm^{-1})
$\bar{n}$	average number of solutes per micelle
N_{ag}	aggregation number (number of monomers per assembly)

NMR	nuclear magnetic resonance (spectroscopy/spectrum)
π_2	solute dipolarity
P	phosphorescence
PMAP	1-phenyl-*p*-methylacetophenone
PMT	photomultiplier tube
PRP	primary radical pair
Q	quencher
R_2	solute excess molar refraction
S	solute
$[S]_{aqueous}$	concentration of solute in the bulk aqueous water
$[S]_{micelle}$	concentration of solute within the micelle
SDS	sodium dodecyl sulfate
SOC	spin-orbit coupling
SRP	secondary radical pair
τ_o	intrinsic lifetime (also equal to $1/k_o$)
τ_{obs}	observed lifetime (also equal to $1/k_{obs}$)
TPA	1,1,3,3-tetraphenylacetone
$T\text{-}T_{abs}$	triplet-triplet absorption
VR	vibrational relaxation
V_X	solute molar volume

CHAPTER 1: INTRODUCTION

1.1 Photophysics

1.1.1 Electromagnetic Spectrum

Electromagnetic radiation is energy that is propagated as a wave, but exhibits point charge characteristics as well. Light is delivered in discrete, quantized packets of energy called photons. Monochromatic light consists of photons with energy of a single frequency, where the energy of the photon can be calculated as:

$$E=h\nu \qquad (1.1)$$

where E is energy (J);
h is Planck's constant (6.63×10^{-34} J·s);
ν is the frequency of light (s^{-1})

As the frequency of light increases, so does the energy of the photon. In organic photochemistry, it is common to report the energy of light as the wavelength (λ) measured in nanometers (nm). Equation 1.1 can then be transformed into Equation 1.2, where the wavelength of light is inversely proportional to the energy.

$$E = hc/\lambda \qquad (1.2)$$

Figure 1.1 shows that there is a wide range of available electromagnetic radiation.

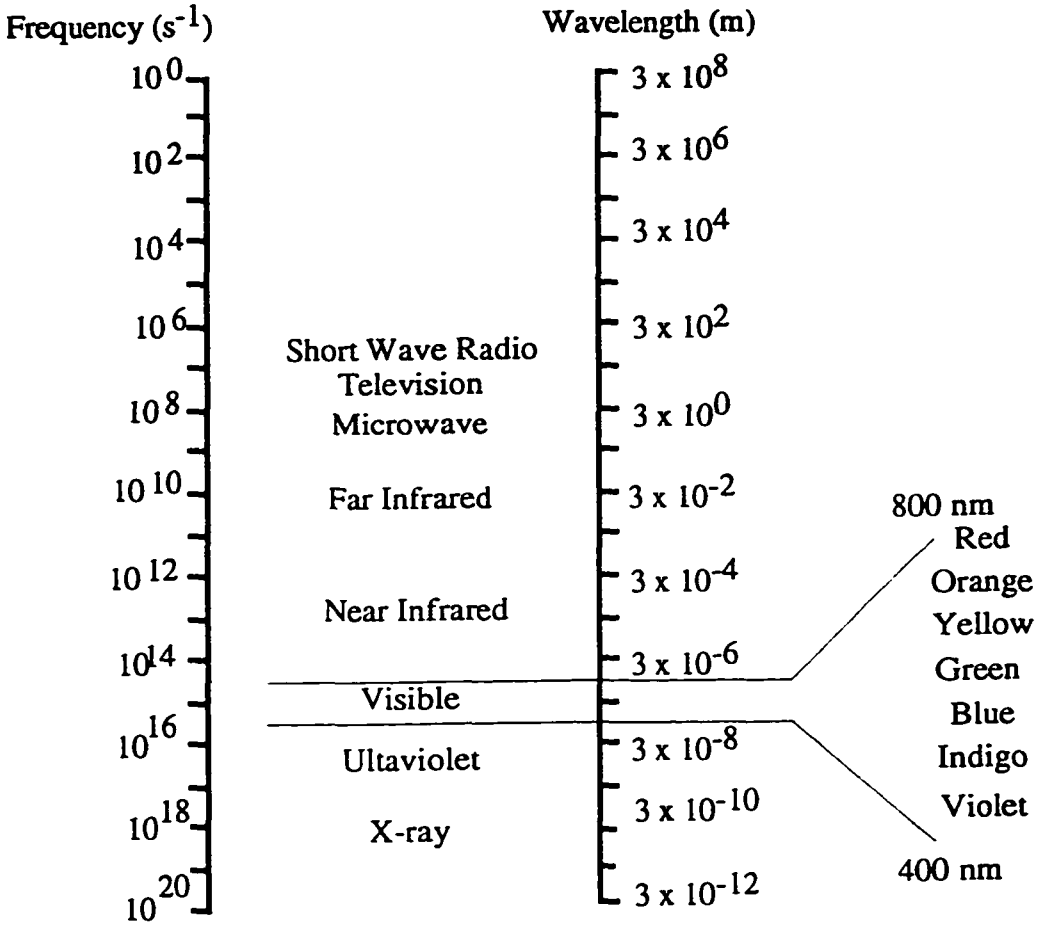

Figure 1.1: Electromagnetic spectrum. Typical excitation of organic molecules is in the UV-Vis region.

After a photon interacts with a molecule, the molecule may become excited and electronic, vibrational or rotational transitions can occur. Microwave excitation can lead to nuclear spin inversion (*i.e.* nuclear magnetic resonance spectroscopy, NMR). Infrared (IR) based transitions include changes in the vibrational and rotational states of molecules. X-rays and γ-rays may excite innershell electrons and may lead to radioactive emissions. In this study, ultraviolet light is used to provide enough energy for an outer, valence shell transition.

1.1.2 Electronic Excitation

1.1.2.1 Ground State Multiplicity

Closed-shell organic molecules usually exist in singlet ground states where all electrons are paired. The multiplicity of the molecule can be calculated by multiplying the total electron spin (S) by 2 and then adding 1. Thus, a singlet multiplicity arises from two paired electrons (S=0). Oxygen is one of the rare molecules which in the ground state has two unpaired electrons leading to a triplet ground state. If a molecule has only one unpaired electron, it is a doublet and these molecules are called free radicals. This latter type of molecule is usually quite reactive and prone to dimerization.

Upon excitation an electron is transferred from the highest occupied molecular orbital (HOMO) to the lowest (previously) unoccupied molecular orbital (LUMO). For aromatic molecules, this will involve an electronic transition from a π bonding orbital to a π^* antibonding orbital (π,π^* state). If the molecule being excited contains a nonbonded electron pair such as those on an oxygen atom in a carbonyl moiety, one of the nonbonded electrons can be excited into an antibonding

orbital leading to an excited state with a n,π^* configuration. This latter transition is symmetry forbidden because the orbitals are orthogonal to each other and thus the transition has a low probability of occurring.

1.1.2.2 Electronic Excitation and Deactivation

Radiant energy is quantized, so if there is more energy than needed for an electronic transition, the excess energy will be put to use in other transitions (*e.g.* rotational or vibrational). This electronically excited molecule may undergo a number of different physical deactivation pathways that return the molecule to its ground state. Deactivation pathways that preclude emission of radiation are classified as non-radiative processes, whereas those that involve emission are termed radiative processes. Both processes take the molecule from the excited state to another state with lower energy. An energy level diagram detailing the possible excitation and subsequent deactivation pathways is called a Jablonski diagram[1] (Figure 1.2).

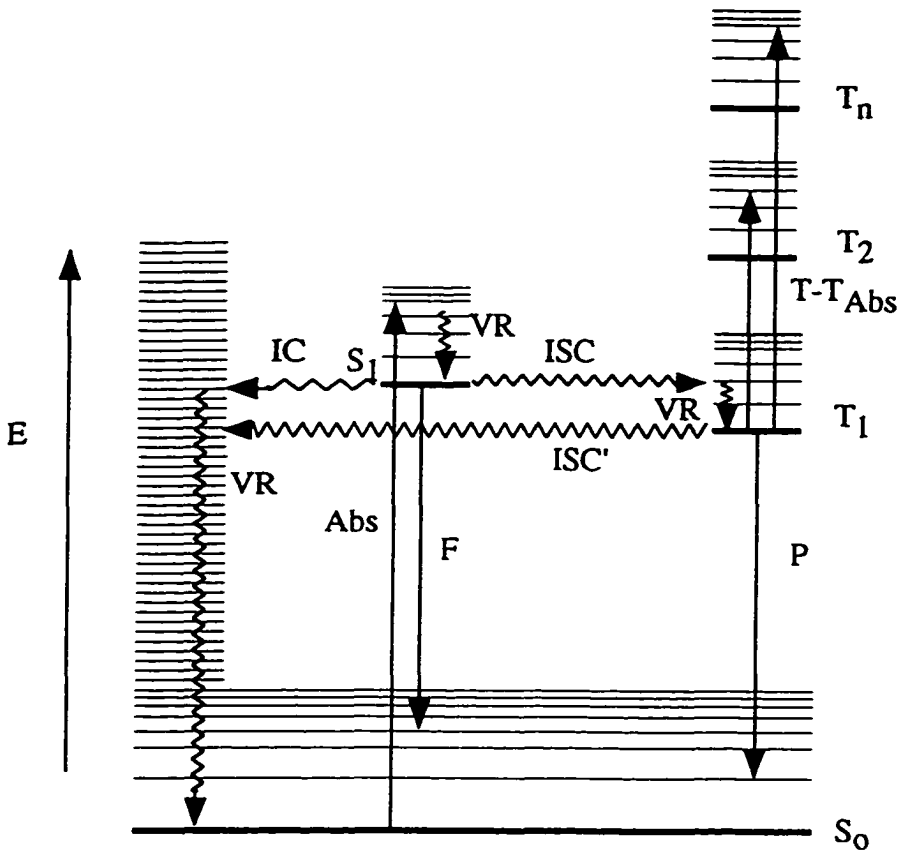

Figure 1.2: Modified Jablonski energy level diagram. IC, ISC, VR represent internal conversion, intersystem crossing and vibrational relaxation, respectively; Abs, F, P and $T\text{-}T_{abs}$ represent absorption, fluorescence, phosphorescence and triplet-triplet absorption, respectively.

1.1.2.2.1 Nonradiative Processes

Nonradiative processes found in Figure 1.2 include internal conversion (IC), intersystem crossing (ISC, ISC') and vibrational relaxation (VR). Nonradiative transitions between electronic states of the same spin multiplicity (*e.g.* $S_1 \rightarrow S_0$ and $S_2 \rightarrow S_1$) are called internal conversion. ISC involves a transition between electronic states with different multiplicities (*e.g.* $S_1 \rightarrow T_1$ and $T_1 \rightarrow S_0$). Any process that involves a spin flip is a forbidden process. The term "forbidden" typically means not probable, but these processes may still be possible. Vibrational relaxation is a transition between vibrational levels of the same electronic state (*e.g.* two vibrational levels within S_0). In solution phase, excess vibrational energy can be rapidly (10^{-13} s) removed by collisions with solvent molecules.

1.1.2.2.2 Radiative Processes

Radiative deactivation processes involve the emission of light. Emission with concomitant energetic deactivation and retention of spin multiplicity is called fluorescence. The most probable fluorescence emission involves a transition from S_1 to S_0. Although only one arrow is shown for fluorescence in Figure 1.2, it can occur between any two vibrational levels in different singlet electronic states providing that the end electronic state is lower in energy.

Phosphorescence involves a transition between two states of different multiplicity with emission of light. The most common form of phosphorescence involves a $T_1 \rightarrow S_0$ transition. Few organic molecules are capable of high yields of phosphorescence as this process is in competition with intersystem crossing. Benzophenone is probably the most notable organic molecule that is capable of phosphorescing, and at room temperature 10% of the absorbed light is emitted as phosphorescence.[2] The energetic difference between the two states (shown by the

F and P arrows) shows that fluorescence will normally have some overlap in the excitation spectrum and emission spectrum (0-0 band), but the remaining portions of the emission spectrum will be red-shifted to lower energies. Since the triplet state is lower in energy than the singlet state, the phosphorescence will be even further red-shifted to lower energies (longer wavelength) in comparison to the ground state absorption spectrum.

1.1.3 Quantum Yields and Lifetimes

Upon excitation, molecule M, can undergo a radiative process as shown in Equation 1.3 where ν must be of equal or lower frequency (lower energy) than the excitation energy.

$$M^* \rightarrow M + h\nu \qquad (1.3)$$

If the emission occurs (*i.e.* fluorescence from S_1 to S_o), the rate of depopulation of the excited state can be written as shown below, with k_r being the rate constant for the first order radiative process.

$$-\frac{d}{dt}[M^*] = k_r[M^*] \qquad (1.4)$$

This is true for any radiative process such as fluorescence or phosphorescence in the absence of nonradiative pathways. Integration of Equation 1.4 yields Equation 1.5; where M^*_o corresponds to the concentration of excited M at time equal to 0 (t=0).

$$[M^*]=[M^*]_o e^{-k_r t} \qquad (1.5)$$

For the first order radiative process, a single exponential decay is expected. The lifetime of the process (τ_o) is the reciprocal of the sum of the rate constants for all unimolecular deactivation pathways (Equation 1.6); where k_r corresponds to the radiative rate constant and k_{nr} refers to the sum of all of the nonradiative paths for M^* (*e.g.* k_{IC} and k_{ISC}).

$$\tau_o = \frac{1}{k_r + k_{nr}} = \frac{1}{k_o} \qquad (1.6)$$

Furthermore, a general definition of a quantum yield is the ratio of molecules undergoing a process relative to the total deactivation/reaction pathways. It can be written in terms of rate constants. For example, the fluorescence quantum yield (Φ_f) can be calculated as shown below:

$$\Phi_f = \frac{k_f}{k_f + k_{nr}} = k_f \tau_o \qquad (1.7)$$

1.2 Overview of Laser Flash Photolysis

Much of the information regarding the nature of transients in this study is obtained with laser flash photolysis (LFP). This technique is based on conventional flash photolysis for which Porter and Norrish[3,4] shared a Nobel prize in 1967. The ease of use of conventional flash photolysis[5] inspired further technical development and so LFP was pioneered in the late 1960's.[6,7] Subsequent modernization occurred with the use of gated photomultipliers,[8] optical multi-channel analyzers,[9] digitization and computers.[10,11] The description of the LFP

system used in this study has been published[12] and the details of the apparatus are also presented in Chapter 2. This method provides a mean to directly monitor the absorption and kinetics of an excited state and subsequent intermediates. In short, these molecular excited states are generated by a short laser pulse (5-10 ns full width at half height for the excimer laser used). An analyzing beam is passed through the sample and the change in absorbance is monitored. The absorbance change can be inspected on a timescale of tens of nanoseconds to hundreds of microseconds. As absorbance is proportional to concentration, the reactive intermediate can be followed in time using kinetic treatments. So, lifetimes and rate constants can be determined for processes occurring in these fast time regimes. It is important to note that absorbances in LFP are measured as ΔA (change in absorbance) because the absorbance of the transient is measured relative to the absorbance of the chromophore before the laser flash.

The spectral characteristics (the dependence of molar absorptivities or absorbances on wavelength) can be measured by using diode array detection or by observing kinetic traces in different experiments at various wavelengths. A transient spectrum can be obtained by plotting the ΔA obtained at the same time in each kinetic trace and at each of the wavelengths monitored.

1.3 Excited State Quenching

Quenching is a process through which an excited state is deactivated by external means.[13] The deactivation is commonly brought about by another molecule, known as the quencher (Q). Quenching experiments are useful as they can be applied to almost any system as long as a property (lifetime, absorbance or fluorescence intensity) is altered by the addition of the quencher. Quenching studies

can be used to investigate the primary photochemistry or photophysics as well to probe the topological features of supramolecules. This extra mode of deactivation speeds up the decay of the transient (Equation 1.8) where k_{obs} ($1/\tau_{obs}$) and k_o ($1/\tau_o$) are the observed and intrinsic decay rate constants.

$$k_{obs} = k_o + k_q[Q] \qquad \text{or} \qquad 1/\tau_{obs} = 1/\tau_o + k_q[Q] \tag{1.8}$$

These equations represent the common case of bimolecular quenching so k_q has a value in units of $M^{-1}s^{-1}$. These quenching processes can occur by different mechanisms such as energy transfer, charge transfer and electron transfer. Due to the large number of possible mechanisms, quenching can occur via collision, and at short or long separation distances.

1.4 Self-Assembled Supramolecular Systems

Supramolecular systems can be defined as a collection of molecular units which are held together by non–covalent interactions. Chemical and physical properties of supramolecular systems are different from the sum of the individual properties of each respective unit. These systems involve equilibria and are held together by non-covalent interactions such as any combination of charge and dipole interactions (*e.g.* charge-charge and charge-dipole), hydrogen bond formation, Lewis acid/base interplay, van der Waals forces and the hydrophobic effect. The charge-charge interaction is the strongest, while the van der Waals forces provides the weakest induction. Changes in the partitioning of solutes, the association/dissociation rate constants of solutes or monomers as well as other equilibria have significant implications on the function of the supramolecular systems.[14]

The term self-assembly implies that non-covalent interactions induce formation of an aggregate under specific environmental conditions. The structural characterization of each individual unit in a self–assembled aggregate involves the determination of parameters such as size, number of monomers in the aggregate (aggregation number), and polydispersity. The next level of characterization is related to the physical properties of regions or complexation sites involved in supramolecular function. This includes the resolution of the size and shape of complexation sites, the characterization or identification of specific interactions, and the determination of local polarity and viscosity. In the following sections, two types of self-assembled systems are discussed.

1.4.1 Micelles

Micelles are self-assemblies (Fig. 1.3) formed from surfactants that have an alkyl chain (usually 8-18 carbon atoms long) and a hydrophilic headgroup that may be charged. When solubilized in aqueous solution, the hydrophobic portions tend to group together as a consequence of the hydrophobic effect.[15] The region of a few angstroms where the charge and counterions exist is called the Stern Layer. Even further from the hydrophobic core, the Gouy-Chapman layer takes up to several hundred angstroms.[16] Systems such as micelles can be viewed as forming separate pseudo–phases from the bulk solvent.

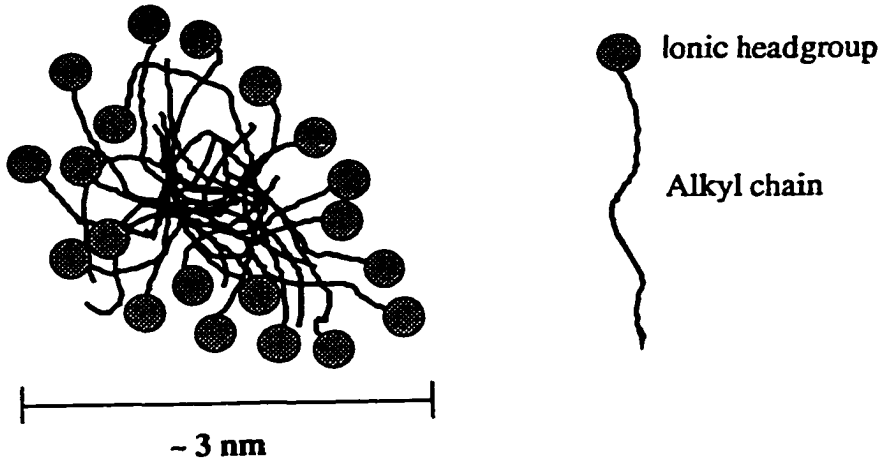

Figure 1.3: Structure of a micelle. The interior of the micelle with the long alkyl chains (—) is hydrophobic, while the charged headgroup (•) normally interacts with the bulk water.

The headgroups repel others with the same charge so both the hydrophobic effect and charge-charge interactions play a role in the determination of the structure of the aggregate. The headgroups are as far away from each other as possible and the chains have a large degree of surface area overlap. In fact, for many years micelles have been modeled as spheres with the monomers resembling the "spokes on a wheel". Current thought is that the hydrocarbon chains are quite flexible,[17] undulate chaotically and are quite dynamic. Due to the dynamics of the structure, there is substantial water penetration into the more hydrophobic regions.[18]

These self-assemblies are cheap, easy to produce and are fairly well understood,[19] so they have often been used to improve understanding of the mobility of small solutes situated within biological membranes.[20] The key

similarities between micelles and biological membranes are that they are both self-assembled, consist of amphiphilic molecules, and are capable of partitioning molecules between a hydrophobic region and the bulk water.[21]

1.4.1.1 Properties of Micelles

These self-assemblies are very dynamic, with monomer exchange occurring in microseconds and with a lifetime of the self-assembly of milliseconds.[22] The critical micelle concentration (cmc) represents the concentration of monomer above which micelles can form. The cmc ranges widely for different surfactants and usually decreases with an increase in the hydrophobic chain length.[23,24] Below the cmc, the surfactant molecules exist as monomers or small oligomers and above the cmc additional monomers are incorporated into micelles, so that the free monomer concentration is constant. The number of monomers in a micelle is given by the aggregation number (N_{ag}). Properties such as electrical conductivity,[25] light scattering,[26] surface tension[27] or the UV-Vis or fluorescence spectrum of a bound reporter molecule[25] can change upon micelle formation and can be employed to determine the cmc of a surfactant. Knowing the cmc and the concentration of monomer in solution, the concentration of micelles can be calculated (Equation 1.9).

$$[\text{micelle}] = \frac{[\text{total monomer}] - [\text{cmc}]}{N_{ag}} \qquad (1.9)$$

1.4.1.2 Properties of Sodium Dodecyl Sulfate Micelles

One of the most commonly used micelles is made with sodium dodecyl sulfate (SDS), a molecule that contains a 12 member carbon chain attached to a SO_4^-

headgroup. The cmc for SDS micelles has been reported to be 8.2 mM.[27] A 25 mM solution of SDS monomer consists of about 60 monomers per micelle at room temperature[24] and each micelle has a diameter of about 2-3 nm.[26,28] However, as the concentration of monomer increases, the aggregation number can increase up to 89 monomers (for [SDS]=200 mM).[27,29]

Many alkali salts increase N_{ag}[30] and for example, Table 1.1 demonstrates that the size of SDS micelles increases with NaCl addition.

Table 1.1 Aggregation number of SDS micelles in the presence of NaCl. Fluorescence spectroscopy and light scattering are designated as flu and LS, respectively.

[NaCl] (M)	Aggregation Number	Technique	Reference
0	60	1-Methylpyrene (flu)	24
0.1	89,97	LS	31,32
0.45	130	1-Methylpyrene (flu)	24
0.5	148	LS	32
0.8	~1000	LS	31,32

This growth in micellar size leads to rod-shaped micelles and these elongated shapes have been observed by light scattering.[26,28,31-35] Under these conditions, the micelles are exceptionally elongated and have a long diameter greater than 20 nm.[26]

In addition to the cmc, micelles also possess a critical micelle temperature (cmt). Micelles are only formed above the cmt, and usually form cloudy solutions below the cmt. The cmt for SDS micelles has been determined to be 15.5°C and 25°C at 0 M and 0.6 M NaCl.[33] As the temperature of the solution is increased, the

micelles shrink in size. For example, N_{ag} for a 0.1 M solution of SDS decreases from 67 to 34 when the temperature is raised from 20°C to 80°C.[36] Most of the decrease takes place from 20-60°C, above which N_{ag} remains fairly constant as measured by pyrene excimer fluorescence.[36] The addition of salt promotes a more rapid decline in size as the temperature is raised.[26,28,34,36] Extrapolation from the plots of the temperature dependence of the aggregation number[36] shows that a minimum of approximately 30-40 monomers is required to form a stable micelle regardless of salt concentration or temperature.

1.4.1.3 Addition of Probe Molecules into Micelles

There are five general types of effects that micelles can provide to alter a given reaction: (*i*) cage effects; (*ii*) local concentration effects; (*iii*) microviscosity effects; (*iv*) polarity effects; and (*v*) electrostatic effects.[16] Micelles are able to sequester hydrophobic molecules in their core and can hold two or more of these molecules within their confines long enough to enhance the rate of a reaction. Solubilization of molecules inside the micelle also increases the local concentration of reactants and can therefore increase the rate of reaction. Due to the nature of the interior of the micelle, there is also an increase in the local microviscosity. Microviscosities are typically higher than in homogeneous, organic solvents and range from 15 cP-100 cP for ionic micelles.[16] In the case of non-polar solutes, the solute interacts with the polar head group and penetrates somewhat into the core, so that it is bound at the micelle-water interface. If a charge is present on the solute and it is complementary to that of the micelle, it may bind as a counterion.[18] Reactions that are affected by polarity can have their rates altered depending on the binding locus. Lastly, the electrostatic interactions of a micelle can play a role in determining the outcome of a reaction because charged species can bind to the Stern

layer. This may bring a charged reactant close to a hydrophobic molecule so that a reaction can occur, or can help separate a reactant from a product if one is neutral and the other charged. Overall, partitioning of solutes between the micellar pseudophase and the bulk water is key in many of the micellar effects listed above.

The number of probe molecules per micelle can be established by using statistical distributions (typically a Poisson distribution).[18] In a similar manner to balls (probes) in a box (micelle) where the box can hold an infinite number of balls, the number of micelles containing *i* number of solutes can be calculated as shown below.[18] This analysis assumes that there is an equal chance of binding a probe regardless of whether a micelle already has one or more probes bound to it.

$$\frac{[M]_i}{[M]} = \left(n^i e^{-n} \right) \qquad (1.10)$$

where [M] is the concentration of micelles

$\bar{n}$ is the average number of solutes per micelle; $n = [S]/[M]$;
S is the total number of solutes introduced
$[M]_i$ is the concentration of micelles with *i* number of solutes

When [S] << [M] (*i.e.* $\bar{n}$=0.1), most of the micelles are empty. If $\bar{n}$=1.0, 37% of the micelles are empty, but 26% of the micelles contain two or more probes. The main consequence of having too many solutes in a micelle is that solute-solute interactions come into play and the experiment may monitor the conduct of the solutes as well as the structure and behaviour of the macromolecular aggregate.

1.4.2 Vesicles and Membranes

Biological membranes are an integral part of all cells. They allow a cell to separate individual components from a bulk solution. The plasma membrane

separates the interior of the cell from its outside environment, while the mitochondrion (energy producer of the cell) possesses a double membrane in order to help separate charges in oxidative phosphorylation and to separate itself from the rest of the cell. Other areas inside the cell use membranes to ensure that degradative enzymes work in a highly controlled environment. Cell membranes are made up mostly of phospholipids (two fatty acid groups covalently connected to a phosphate group via glycerol). Cholesterol and membrane proteins are also found in biological membranes. Cholesterol controls membrane fluidity by interacting with the fatty acid chains. As the strength of the interaction increases, the transition temperature decreases, thus, as the concentration of cholesterol in the membrane increases, the fluidity of the membrane is elevated.[37] Proteins are vital for proper cell function and in many cases, they are embedded either wholly or partially in the membrane. As membranes are very complex, simpler systems are required in order to understand their structure-function relationship. Vesicles have been used as models because they consists of lipid bilayers and proteins may be reconstituted in them so that the protein-bilayer interaction may be studied. Liposomes have been tested as drug delivery agents due to their potential for encapsulating solutes.[20]

Vesicles (liposomes) are self–assemblies formed by phospholipids or synthetic surfactants containing two hydrophobic chains that form bilayers (Fig. 1.4). Vesicle systems are defined by three different regions, the internal water pool, the hydrophobic bilayer and the homogeneous water phase. In a similar manner as in micelles, the headgroups are exposed to the water regions and the hydrocarbon chains align themselves in the inner core of the bilayer. Vesicles are more ordered than micelles because of their higher level of organization (bilayer vs. oil drop) and contain an internal, trapped pocket of water.

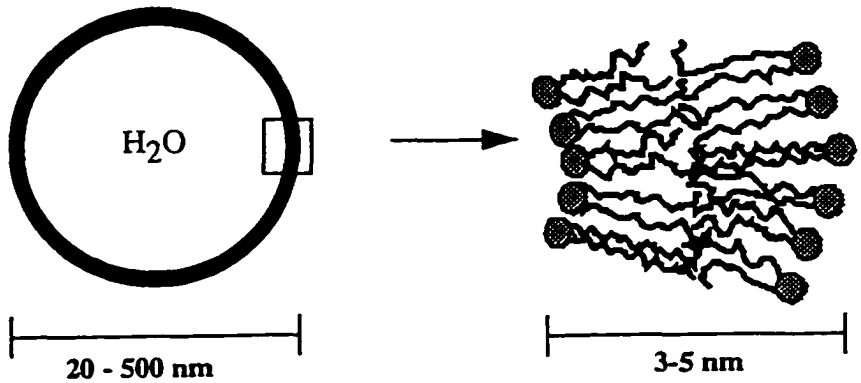

Figure 1.4: Structure of vesicles.

The size of vesicles depends on the method of preparation. Small unilamellar (single bilayer) vesicles (SUV) have diameters ranging from 20 nm to 50 nm, whereas large unilamellar vesicles (LUV) have diameters from 50 nm to 500 nm.[20] There is also the possibility of multilamellar vesicles where many bilayers exist in a single aggregate.[18]

1.4.2.1 Geometric Considerations

Surfactants/phospholipids form either micelles, vesicles or bilayers depending on their overall shape. These amphiphilic molecules can be classed as cones, cylinders or inverted cones.[20] If the headgroup encompasses a larger or much larger volume than the acyl chains (inverted cone shape), the lipid will form spherical or rodlike micelles, respectively. Cylindrical-shaped molecules can form bilayers and vesicles, whereas cone shaped molecules (acyl chains in the lipid take up more volume than the headgroup) form reverse micelles in which the hydrophobic tails are extended outward and the charged headgroups are solubilized in the center by a small pool of water.

Smaller vesicles have more curvature in the bilayer. For this reason larger vesicles are more representative of cell membranes. The small radius presents difficulties in lipid packing because the surface area of the outer monolayer (leaflet) is almost twice that of the inner lipids and as much as 70% of all lipids pack in the outer monolayer.[20] The packing problem is diminished in LUV's. In a similar manner to cell membranes, this asymmetry leads to different lipid preferences regarding their location.[20] Lipids with inverted cone shapes (*e.g.* phosphatidylcholine) will preferably partition into the outer monolayer.

1.4.2.2 Transition Temperatures

In contrast to micelles, which are quite dynamic aggregates, the bilayer in vesicles is more structured and undergoes a phase transition at a defined temperature. At the phase transition, the bilayers go from an ordered, fairly rigid structure to one where the alkyl chains are quite flexible. Transition temperatures range from -22°C for dioleoylphosphatidylcholine (C_{18}-1,9-*cis*) to 82°C for disteroylphosphatidylethanolamine, but most are in the range of 40°C-60°C. Synthetic cationic vesicles made up of dioctadecyldimethylammonium chloride ($[(C_{18}H_{37})_2N(CH_3)_2]^+ Cl^-$, DODAC) have melting temperatures around 35°C.[38,39] The benefit of using synthetic amphiphiles is the lower cost, the lack of degradation of monomer and the fact that they have been well characterized.[39,40] In addition, DODAC vesicles can exist as either SUV's with a 30 nm diameter,[39,40] or LUV's of ~300 nm diameter.[39] Small sizes of many types of vesicles are usually formed by sonication,[41] whereas larger sized liposomes can be produced by slowly injecting the surfactant in low boiling organic solvents into very hot water.[42]

1.4.2.3 Dynamics of Monomers Within the Bilayer

Monomers in vesicles have defined motions each with its respective rate constant, while micelles have monomer exchange that occurs on the order of microseconds.[43] In the plane of the bilayer, there is fast lateral diffusion. Diffusion coefficients of approximately 10^{-8} cm^2s^{-1} have been measured by NMR, ESR and fluorescence techniques.[18] This lateral diffusion process occurs with a frequency of about 10^7s^{-1}.[18]

Flip-flop of a phospholipid monomer from either the inner leaflet to the outer monolayer or vice-versa is a fairly rare event. The transversal movements have rate constants in the regime of one per several days in model and biological membranes.[18] The process is hampered because the charged headgroup must cross the hydrophobic region of the bilayer.

1.5 Common Probes

Probe molecules report on the properties of their surroundings. Those molecules with finite lifetimes, such as excited states, will only report information regarding the volume that is explored before decaying back to their ground states. In order to get information on different time scales, probes with different lifetimes can be used. If the probe has a much shorter lifetime than the dynamic process of interest, it reports on a static environment, since changes do not occur during the lifetime of the probe molecule. For dynamic information to be recovered, the lifetime of the probe should be of the same order of magnitude as the rates of the processes being investigated. Reporter molecules may be either unreactive or reactive and they may possess different multiplicities. Scheme 1.1 displays some of the many types of reporter molecules used in organic photochemistry.

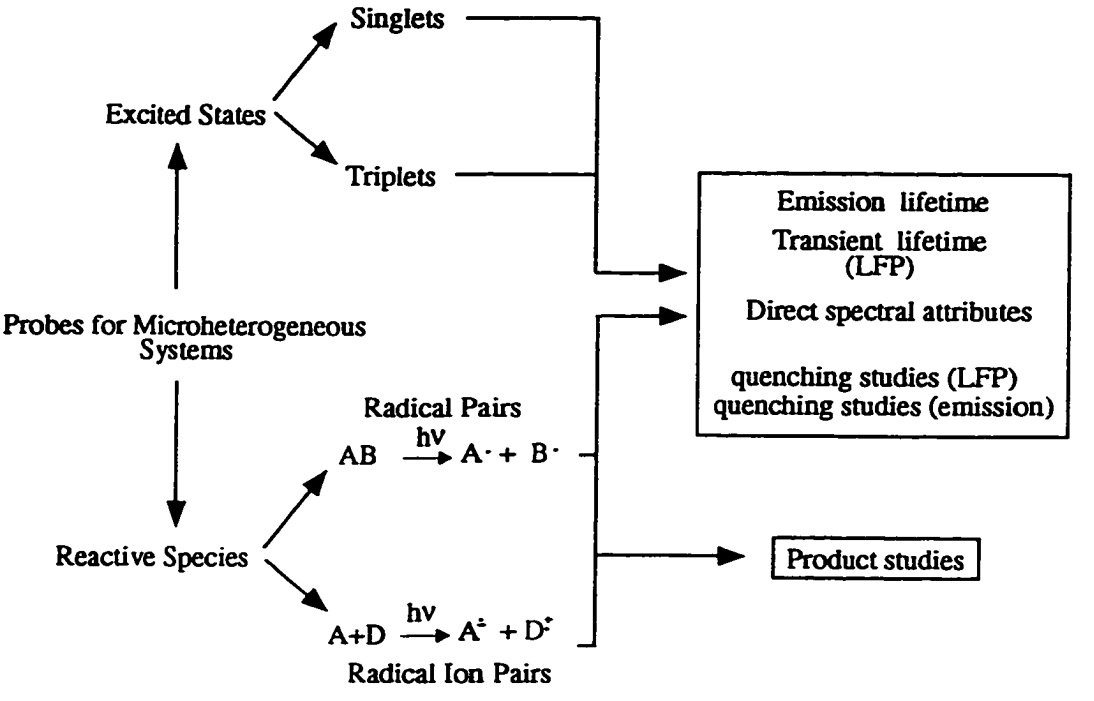

Scheme 1.1: Types of probe molecules used in organic photochemistry

1.5.1 Unreactive Excited State Probes

In some cases, excited singlet and triplet states are not reactive under experimental conditions and consequently these molecules may be used as probes. Excited singlet states of organic molecules normally live less than 10 ns. Due to their short lifetimes, fluorescent probes can only explore a small volume and therefore report on their local environment and the static nature of the macroassembly. Although the short lifetimes of fluorescent probes bar their use for direct relocation studies, the excited state can be employed as a marker for the access of quenchers to the site where the probe resides. This is an indirect method

since the excited probe is employed to report on the mobility of an "invisible" molecule, *i.e.* the quencher.

Organic molecules in their excited triplet state have long lifetimes, since the decay to the singlet ground state is a spin forbidden transition. Relative to singlet species, the longer lifetime of triplet states meets the requirement for organized systems that the lifetime be comparable to the rate of the dynamic processes being studied.

Triplet excited state probes can be monitored by phosphorescence emission, absorption characteristics, emissive or absorptive lifetimes or by quenching studies (Scheme 1.1). Direct spectroscopic characterization is the best method for monitoring dynamics. This method can be applied when the triplet excited state has spectral characteristics that depend on its environment, however, only xanthone is known to possess this useful property.[11] Quenching studies can be employed under conditions where the probe is less accessible inside the organized system than in the bulk aqueous solution.[44]

1.5.2 Reactive Probes: Radical (Ion) Pairs

Biradicals, (neutral) radical pairs and radical ion pairs are good probes for microheterogeneous system as they can be investigated by product studies and by the application of time-resolved techniques (Scheme 1.1). Radical pairs are excellent probes for diffusional activities because the radicals must encounter another reactive species to form products. In this manner, the application of these probes provides beneficial information regarding dynamic behaviour.

Radical ion pairs are formed when upon excitation, the donor molecule transfers an electron to an acceptor molecule producing a positively charged and a negatively charged radical (radical cation and radical anion). Before separation, the contact radical ion pair may be either in a triplet or singlet multiplicity. For

example, species residing inside the micellar or vesicular pseudophases such as pyrene can act as electron acceptors after photoionization of dimethylaniline which is bound in the Stern layer.[45] Since charged molecules are formed, one species becomes attracted to the micelle, while the other is repelled.

A molecule that contains a single unpaired electron has a doublet multiplicity and is called a radical. When two radicals are tethered together by a covalent chain (usually a methylene chain), the molecule is called a biradical. A radical pair consists of two radicals that can interact for a period of time longer than the lifetime of a typical solvent cage (10^{-13} s), but that are not covalently linked. One of the many key aspects of this type of probe the spin multiplicity because biradicals and radical pairs may exist in either singlet or triplet multiplicities. This is crucial as only singlet radical (ion) pairs can react, so a triplet intermediate must undergo intersystem crossing before reacting. Scheme 1.1 shows that radical (ion) pairs may be useful as probes for microheterogeneous systems as the species may be observed by emission spectroscopy, quenching studies or through direct observation of their transient absorbances by LFP. Most importantly, investigations using reactive probes offer the opportunity to study the products derived from the photochemical reaction.

Biradicals and radical pairs can be formed from ketone precursors. Ketones that undergo Norrish Type I reactions (Scheme 1.2) are good starting points to create radical pairs as they undergo photoinduced homolytic α-cleavage to yield an acyl radical and an alkyl radical. Note that if a cyclic ketone is used, a biradical is generated.

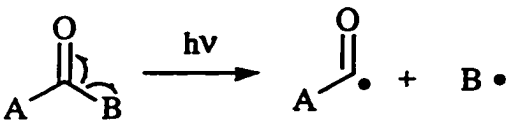

Scheme 1.2: Norrish Type I reaction of ketones.

It is also worth noting that the reactivity of n,π* triplet states is usually about 100 times greater relative to singlet states with n,π* configuration because there is no electronic correlation between the singlet excited state and the ground state radical products.[46]

Another reaction of n,π* ketones is hydrogen abstraction. In the presence of a hydrogen donor, the n,π* ketone can abstract a hydrogen atom to yield a ketyl radical and a radical on the hydrogen donor (Scheme 1.3).

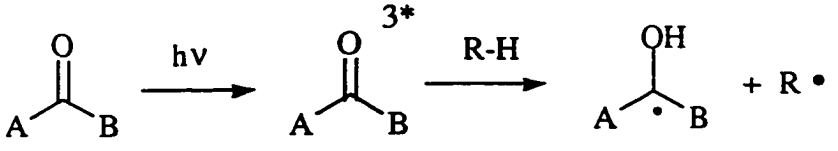

Scheme 1.3: Photoinduced hydrogen abstraction reaction of n,π* ketones

The case of intramolecular γ-hydrogen abstraction .to form products is called a Norrish Type II mechanism. Competition between Type I and Type II processes have been used to investigate the behaviour of micelles.[47] The micellar

environment favours certain conformations of the ketone probe which then leads to the preference of one of the reactions.[48]

Both of these photoreactions provide excellent means to generate radical pairs. Norrish Type I radical pairs are preferred as they are generated by a single molecule and so diffusion is not involved in the formation of the radical pair. In the case of some intermolecular hydrogen reactions, an external hydrogen donor has to be added in order to eliminate the slow diffusional process needed to create the radical pair. If a micelle is being probed, then this hydrogen donor is situated close to the ketone (*e.g.* benzophenone/1,4-cyclohexadiene).[49,50]

1.6 Dibenzyl Ketone

1.6.1 Dibenzyl Ketone in Homogeneous Solution

Radicals with chromophores can be investigated using LFP. A radical that can be conjugated to an aromatic ring system will have an increased lifetime due to the additional conjugative stability.[51] One of the most common probes is dibenzyl ketone (DBK). Upon excitation, it undergoes Norrish Type I cleavage to form two benzyl radicals (after decarbonylation of the phenylacetyl radical) which ultimately recombine to form bibenzyl (Scheme 1.4).

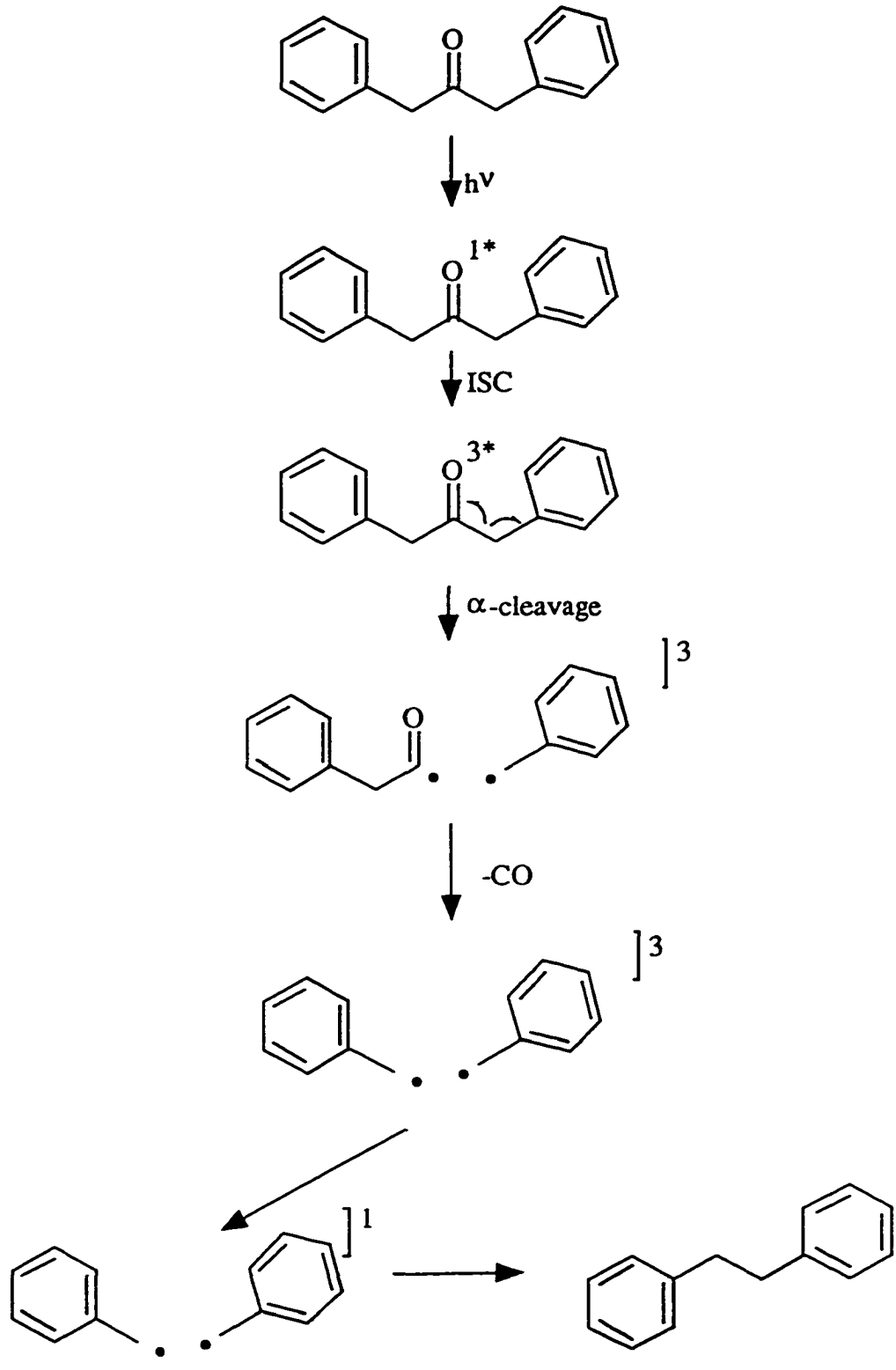

Scheme 1.4: Mechanism for product formation for photolysis of DBK.

The ground state of DBK is a singlet. Excitation leads to a singlet excited state in an n,π^* configuration with a lifetime of ~2-3 ns.[52,53] Intersystem crossing leads to an n,π^* triplet excited state.[54,55] The α-cleavage occurs to yield a phenylacetyl radical and a benzyl radical. The phenylacetyl radical was once believed to decarbonylate exceptionally fast (<3.6 ns),[56,57] but it has now been determined that decarbonylation occurs within a few hundred nanoseconds.[58,59] In addition, it has been reported that the decarbonylation reaction is solvent dependent.[58-60] As the solvent gets increasingly polar, the phenylacetyl radical is stabilized relative to the benzyl radical, so that the reaction progresses at a slower rate.[58-60] After decarbonylation, two benzyl radicals can recombine to form the diarylethane in almost quantitative yield.[56,57,61] The fact that all of the radicals generated by photolysis lead to a single product (>90%) make DBK an ideal probe for microheterogeneous systems.

1.6.2 Dibenzyl Ketone in Micelles - Mechanism

The photolysis of DBK in micelles can give crucial information regarding the dynamics and general behaviour of radical pairs in these supramolecular assemblies. Scheme 1.5 demonstrates the more complex mechanism in micelles relative that in homogeneous solution shown in Scheme 1.4.

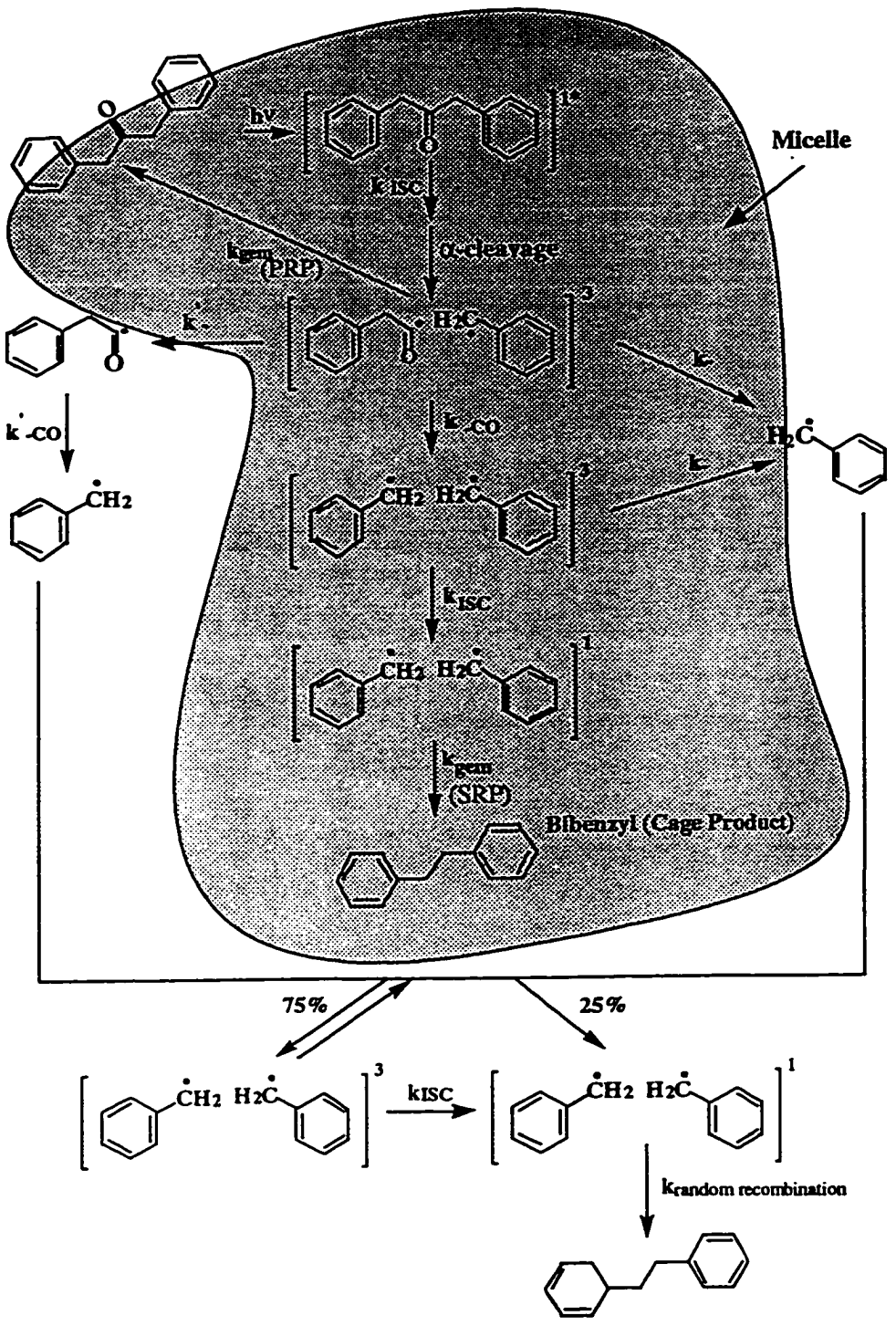

Scheme 1.5: Mechanism for photolysis of DBK in micelles The brackets represent a contact radical pair.

The ketone is solubilized within the micelle. Scheme 1.5 reveals two very important features. First, there is the existence of a primary radical pair (k_{gem}, PRP) recombination process. The first radical pair is formed immediately following α-cleavage. The micelle can act as a "supercage"[16,62-64] and enhance radical recombination within its confines. The radical pairs will then be able to increase the number of encounters between each partner instead of rapidly escaping as in homogeneous solution. This is an example of a geminate ("twin") process in which the two radicals derived from the same precursor molecule recombine before reacting with other extraneous radicals (derived from other ketone precursors). The quantum yield for the disappearance of DBK in cetyltrimethylammonium chloride (CTAC) micelles is 0.3, whereas the same quantum yield is 0.84 in benzene.[65] Thus, the micelle is enhancing the recombination of the primary radical pair (phenylacetyl-benzyl) so there is more reformed starting precursor. If the primary radical pair does not react immediately, either partner can escape into the aqueous phase. The paradigm of radical pair dynamics[16,62] states that decarbonylation occurs in the micelle and the secondary radical pair (SRP) can undergo a second geminate reaction to yield bibenzyl whose yield is increased in micelles. However, there is also a possibility that the radicals can escape into the aqueous phase, react there or enter a secondary micelle. According to the paradigm, after escape, scrambling of the radicals occurs, and the obtained products are termed random recombination products. In the case of DBK, the geminate and random product is the same. However in the case of 4-methyldibenzyl ketone (4-MeDBK) or other asymmetric ketones, photolysis does not lead to the same products for both geminate and non-geminate reactions. One expects only 4-methylbibenzyl as the lone geminate product plus two other products from the scrambled, random

recombination products (Scheme 1.6). These products include bibenzyl (AA), 4-methylbibenzyl (AB) and 4,4'-dimethylbibenzyl (BB).

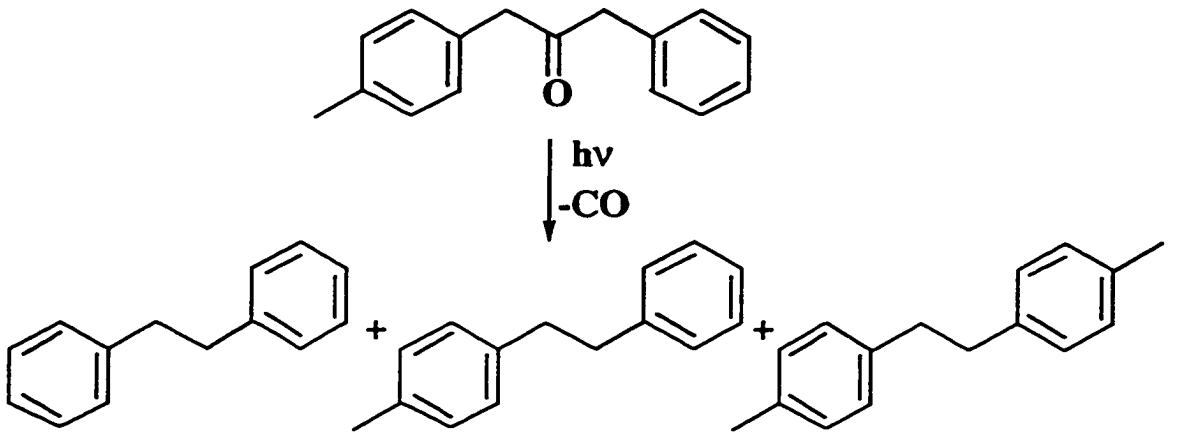

Scheme 1.6: Products derived from the photolysis of 4-MeDBK.

In homogeneous solution, complete randomization of the radicals leads to a statistical ratio of 1:2:1 for AA:AB:BB. The enhancement of the asymmetric product relative to the total amount of product represents the relative amount of product derived from the photolysis of 4-MeDBK formed by geminate reactions. This enhancement of the geminate reaction is called the cage effect.[66] This idea was first tested with 4-MeDBK in micelles in 1978 and the net enhancement of the asymmetric product relative to the total amount of symmetric product (cage effect = AB/(AA+BB), *N.B.*: this is not the current definition of the cage effect) increased from ~0% at concentrations below the CTAC cmc to ~50% (>98% of all products were 4-methylbibenzyl) above the cmc.[67] Current determination of the cage effect value uses Equation 1.11.[68]

$$\text{Cage Effect (\%)} = \frac{AB - (AA + BB)}{AA + AB + BB} \times 100\% \qquad (1.11)$$

In essence, the cage effect reflects the amount of asymmetric product compared to the total products formed and depicts the overall set of dynamic processes that occur under steady-state conditions.

In addition to the use of an asymmetric ketone, there is yet another way in which the cage effect can be measured for this system.[68] Using DBK, one can scavenge all of the escaped radicals by adding a cationic quencher (Q) that cannot enter into the micelle. This can be done using CuCl for benzyl radical pairs in CTAC. So, the final products would be AA from a geminate process and AQ from escape processes. The cage effect can then be measured by:

$$\text{cage effect } \% = \frac{AA}{[DBK]_{rxn}} \times 100\% \qquad (1.12)$$

where $[DBK]_{rxn}$ corresponds to the amount of reacted ketone. This method can be used separately to yield the same cage effect,[68] but even more importantly, furnishes a value for the cage effect for symmetric ketones.

Using these methods to determine the cage effect, many correlations were developed.[68] An increase in the hydrophobicity of the ketone (DBK to 4,4'-dimethylDBK to 4,4'-di-*t*-butylDBK) leads to an increase in the cage effect (31% to 59% to 95%) in CTAC micelles. Moreover, as the chain length of the alkyl sulfate surfactant increases to generate larger micelles (SC_8S to $SC_{16}S$), the cage effect increased from 8% to 55%.[68] It was also found that an increase in temperature up to 69°C and of the pressure (up to 2000 bar) had little effect (<10%) on the value of

the cage effect.[68] Also, the addition of salts (0.5 M NaCl) increased the cage effect in the larger micelles by ~25%.[68]

1.6.3 DBK - A Historical Perspective

In order to fully comprehend the steady-state product studies, a historical overview of kinetic studies involving dibenzyl ketones is necessary as this technique can further explain the details of radical dynamics. From LFP measurements, no evidence of a decarbonylation process was initially found, and the information mirrored the 1970's model that proposed that decarbonylation was fast ($\sim 10^8$ s^{-1}). This would imply that all processes measured by LFP were occurring with the secondary radical pair (benzyl-benzyl). LFP showed the existence of both a fast (τ=400 ns) and a slow (~50 μs) exponential decay.[69] The fast decay was ascribed to spin correlated geminate radical pair recombination which would occur before exit from the micelle. It was hypothesized that the slow decay could not be arising from random recombination because (*i*) the amplitude of the decay was the same for 4,4'-di-*t*-butyldibenzyl ketone and for DBK and according to the cage effect values (from product studies), almost no escape occurred for the di-*t*-butyl derivative; (ii) 2nd order kinetics would be observed for random encounters; and (*iii*) quenching experiments with 4 mM Cu(II) did not affect either decay. So, the slow decay was attributed to recombination of a relaxed geminate radical pair,[10,69] which would be generated after some diffusion within the initial micelle. Note that the final two reasons were later revised by others (see below). Sakaguchi *et al.* proposed that the slow decay corresponded to the recombination of benzyl radicals following escape from the micelle[70] and showed it to follow second order kinetics.[71] Thus, the fast reaction was ascribed to

recombination of a secondary geminate radical pair, while the slow kinetics were found to be characteristic of random encounters.

The decarbonylation of DBK was investigated in 1983. The rate constant for decarbonylation was found to be solvent dependent and in the range 5×10^6 s^{-1} to 1×10^7 s^{-1}.[58,59] It follows that the interpretation of early LFP results is tainted because it was assumed that the decarbonylation was fast. This led to false conclusions regarding the nature of the fast decay which was attributed to a benzyl-benzyl secondary radical pair in the case of DBK.

In 1993, kinetics with a fast decay (τ=50 ns in SDS micelles), a growth (τ=285 ns) and a slow decay were observed for the DBK/SDS system.[72] The fast kinetics were attributed to the recombination of both the primary radical pair as well as the secondary radical pair. The growth was credited to the decarbonylation process which forms benzyl radical. The slow decay was fitted well to second order kinetics and was ascribed to the recombination of radical pairs after exit from a micelle. It was also proposed that much of this slow decay kinetics may be occurring after re-entry of the radical into a micelle.[72]

1.6.4 DBK - Dynamics of Radicals in Micelles

From the studies discussed above and similar investigations, the exit rate constant for the phenylacetyl radical was reported to be ~6.6×10^6 s^{-1} [72] compared to 1.4×10^6 s^{-1} for benzyl.[30,73,74] The values of the entry rate constants are generally diffusion controlled[75] and are bimolecular because the process involves a radical and a micelle. Typical diffusion rate constants for arenes in micelles are on the order of 10^9 - 10^{10} $M^{-1}s^{-1}$.[75] The partition coefficient is the ratio of the entry, k_+

and exit, k_{-}, rate constants, so, it is the exit rate constant that usually determines the partition coefficient.

1.7 Electronic and Magnetic Field Effects on Radical Pairs

As shown explicitly in Scheme 1.5, recombination within micelles requires intersystem crossing of a triplet radical pair to a radical pair with singlet multiplicity. If ISC does not happen, exit from the micelle to yield random radical encounters occurs. The application of magnetic fields can slow down ISC and therefore provides a means to alter the dynamic behaviour of the system.

1.7.1 Electron Spin Vector Model

The following mechanistic discussions will center around the electron spin vector model. A simplified picture of precessing electronic magnetic moment vectors is shown below (Figure 1.5). In essence, the magnitude of each electron spin is the same. The differences lie in the direction of the vector (*i.e.* the projection of the spin angular momentum). In the singlet state, the two electrons precess exactly out of phase, and in the opposite direction, so that the forces of the spins cancel out. In the case of the triplet species, there are two possibilities where the electrons are in phase and have the same spin vector direction (T_{-} and T_{+}). On the other hand, T_0 has electrons that are in phase, but the directions are opposite. It can be said that T_{+} and T_{-} are spin correlated and spin polarized as their spins are in the same direction, and that of T_0 and S are spin correlated but *not* spin polarized.[76] Spin correlation can be defined an electron "knowing" where the spin of the other electron is.

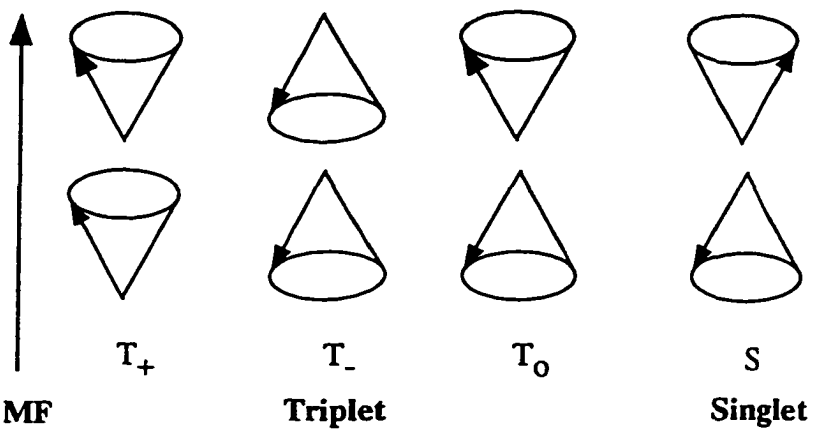

Figure 1.5: Simplified schematic of the electron spin vector model.

1.7.2 Magnetic Field Effects on Intersystem Crossing

In order for an applied magnetic field to alter the kinetics or fate of a chemical reaction, there must be a paramagnetic reaction intermediate (usually with unpaired electron spins).[77] An electron has a small mass, is charged and spins. These characteristics generate a magnetic field which can interact with other magnetic fields. The magnitude of the energy generated by a magnetic field interacting with an electron can be written as:

$$\Delta E_{spin} = N_A \times g \times \mu_\beta \times B \qquad (1.13)$$

where N_A is Avogadro's number (6.02×10^{23} mol^{-1});
g is the electronic g-factor (very close to 2.00 for organic molecules and represents the interaction between spin and orbital angular momentum)
μ_β is Bohr's magneton (9.27×10^{-24} $J \cdot T^{-1}$)
B is the magnetic field (T)

An interaction with 1 mol of unpaired electrons (g = 2.000) with a strong magnetic field of 1 T (10^4 G) yields an energy difference of 11 J/mol or (4.4×10^{-3}) $\times$ RT (R is the gas constant and T is the temperature) at 300 K. A significant change in the activation energy of a reaction is unlikely because of the small magnitude of the energy difference relative to the thermal energy supplied at room temperature. However, if activation energies of two competitive pathways that differ in spin (two different multiplicities) are close in energy and the magnetic field can induce a small change in the rate of interconversion then alterations are possible.[77] In other words, when there is competition between two mechanistic steps, an increase in the rate constant of one can alter the course of the reaction.

1.7.3 Zeeman Splitting

It has been shown for biradicals and caged radical pairs that the triplet state T_o lies above the singlet state.[78,79] As one applies a magnetic field, the normally degenerate triplet sublevels (T_+, T_-) are split from T_o. Figure 1.6 illustrates the effect of a magnetic field on the electronic energies (Zeeman splitting) in a biradical or radical. It is important to note that the T_+ and T_- split in opposite direction, but with the same magnitude with respect to the energy for T_o. There is also a certain magnitude of the magnetic field where $E_S = E_{T-}$.

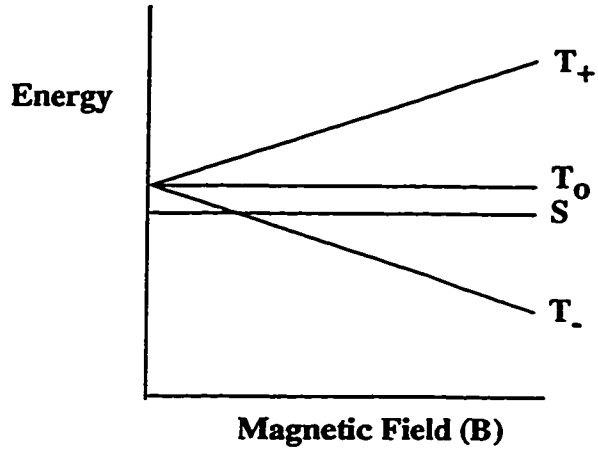

Figure 1.6: Splitting of electronic sublevels in a magnetic field

The difference in energy between a triplet level and the singlet level (E_{TS}) corresponds to the exchange integral (or exchange interaction, 2J). A positive 2J value (typical for singlet and triplet excited states where S is higher in energy than T in the absence of a magnetic field) arises from coulombic repulsion energies in instances where the orbitals containing the two electrons can possibly overlap. Biradicals and radical pairs usually have a negative exchange energy (-2J) because there will be a bonding/antibonding interaction in the singlet state that can ultimately correlate with the bonding/antibonding states of the singlet recombination products.[76] So, in addition to the case where the orbital wavefunction differs only in exchange energy (as for singlet and triplet excited states), the case of radical pairs involves both the exchange energy as well as further splitting of the energy levels via bonding/antibonding processes.

Intersystem crossing is exponentially proportional to the singlet-triplet energy gap (E_{TS}).[2] Therefore, as the magnetic field splits T_+ and T_- from the singlet energy level, the rate of ISC decreases. At high magnetic fields, the rate of ISC

from these two triplet levels will be essentially zero, assuming that there is no population interconversion between the triplet sublevels as is the case for many carbon-centered radicals. It is worth noting that at the point where the energies of T_- and S are equal, the rate of ISC is enhanced relative to that obtained at all other fields.

1.7.4 Distance Dependence of the Exchange Interaction

The exchange interaction depends on the distance between two electrons. This point is crucial to understand in terms of covalently linked biradicals, but also for caged radical pairs where the micelle or vesicle represents the maximal separation distance at short times (*i.e.* when there is no escape).

Figure 1.7 demonstrates that the energy of the triplet radical pair decreases as the distance between the two radicals increases and reaches an asymptotic value.[76,80] For singlet radical pairs, the energy decreases into a well which occurs because of the attractive force between the two electrons and this is where recombination of the two radicals occurs. At larger inter-radical distances, the energy begins to rise until it reaches an asymptotic level. At infinite distance, the energy level of the triplet radical pair and the singlet radical pair will be equal because the electrons can no longer interact with each other. At this point, free radicals (doublets) exist because the spins are no longer correlated.

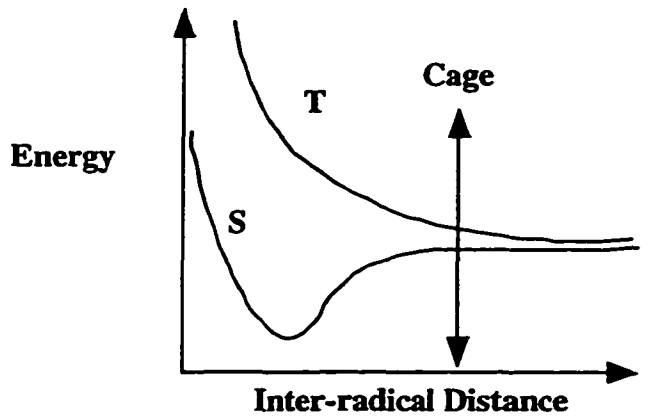

Figure 1.7: Distance dependence of energies for singlet and triplet radical pairs.

1.7.5 Roots of Magnetic Field Effects

In a radical pair, the spin Hamiltonian (H_{rp}) can be represented as the sum of exchange (H_{ex}), Zeeman (H_{zs}), electron spin-spin (H_{ss}) and hyperfine coupling (H_{hfc}) interactions.[81]

$$H_{rp} = H_{ex} + H_{zs} + H_{ss} + H_{hfc} \qquad (1.14)$$

On their own, each term has a negligible energy, but each can switch the reaction from a spin forbidden to a spin allowed process, thus altering the reactivity of the reaction intermediates.[82] H_{ex} depends on the exchange integral (J) and on the electron spin for both radicals (*i.e.* depends on E_{TS} and the spin multiplicity). The Zeeman splitting parameter is dependent on the g values (relates orbital angular momentum and electron spin) for each radical as well as the magnetic field strength. The spin-spin interaction term is derived from the g values and the spin of the unpaired electrons, but most importantly is inversely proportional to the distance

between the two radicals (αR^{-3}). H_{hfc} is defined by the hyperfine coupling between the electron and nuclear spin magnetic moments.[81] All these parameters can influence the mechanism through which magnetic fields can interact with electronic and nuclear spins and hence alter the course of a chemical reaction.

1.7.5.1 The Radical Pair Mechanism

A transition from a singlet multiplicity to a triplet state (intersystem crossing) for a radical pair can occur by the Δg mechanism, hyperfine interaction mechanism, level crossing mechanism and the (spin orientation or spin-lattice) relaxation mechanism.[83-85] Each of these mechanisms relies on the electronic (and nuclear) elements described in the previous section. In addition, other mechanisms such as the triplet mechanism and radical-triplet pair mechanism are known to contribute to observed magnetic field effects on chemical reactions and will be discussed in section 1.7.5.2.

1.7.5.1.1 Δg Mechanism

In the case where J=0, the hyperfine coupling constant is 0 and the difference in the g-values are not equal to 0 (*i.e.* different electron spin and orbital angular momenta for each radical), the mixing element between the singlet and triplet states can be shown to be equal to $\Delta g \mu_B B/2$. Thus, as the difference in g-values increases and as the magnetic field increases, the amount of mixing between the S and T_o also increases. This leads to the magnetic field dependence shown below[81] (Figure 1.8):

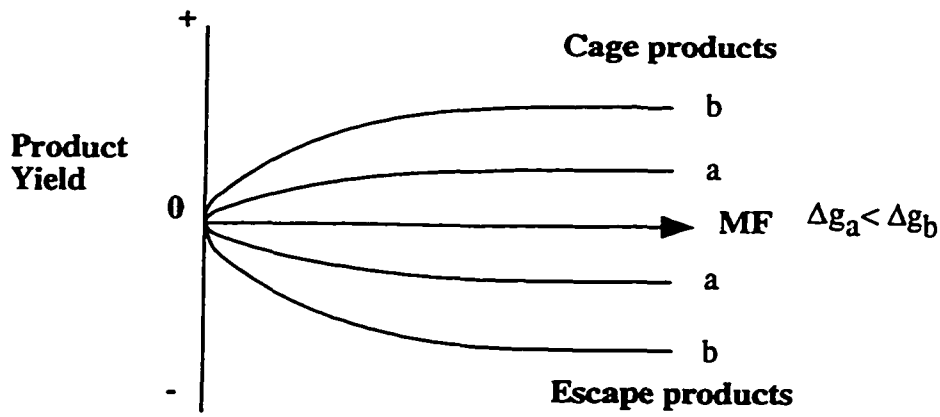

Figure 1.8: Effect of magnetic fields on the formation of cage and escape products from triplet precursors in the Δg mechanism.

The rate of S-T_0 conversion increases with increasing MF, but there is no interconversion between S-$T_{\pm}$ because of Zeeman splitting. Figure 1.8 demonstrates that there is an increase in the amount of cage products with increasing magnetic field, with a concomitant decrease in the amount of escape products when the products are derived from a triplet radical pair. Note that for a singlet precursor, the situation is reversed so that an increase in the escape products should be observed as the magnetic field is increased.

1.7.5.1.2 Hyperfine Interaction Mechanism

At zero magnetic field, interconversion between all triplet states is possible under conditions where J=0, Δg=0, but hyperfine coupling occurs. However, at higher magnetic fields, only ISC between S and T_0 can occur because the Zeeman splitting component becomes much larger than the hfc term. Thus, the rate of the S-T conversion decreases with increasing magnetic field (at low fields) and is

saturated at high fields (where interconversion to $T_{\pm}$ is completely cut off). The yield of cage products decreases with application of a magnetic field, with a concomitant increase in products derived from escape processes (Figure 1.9). The expected observations at high field are opposite to that observed for the Δg mechanism. Calculations also reveal that the effect of MF's on the product distribution based on this mechanism are half completed by 100 G for most carbon-centered radicals and the effects are saturated below 1 kG.[81]

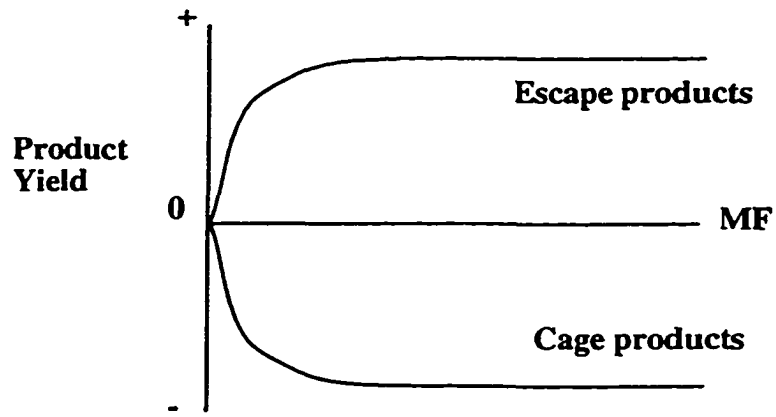

Figure 1.9: Effect of magnetic fields on the formation of cage and escape products from triplet precursors in the hfc mechanism.

1.7.5.1.3 Combined Δg and hfc Mechanisms

In the scenario where in the absence of a field, J=0, $\Delta g \neq 0$ and the hfc constant $\neq 0$, both the Δg and hfc mechanisms can operate. The rate of S-T conversion decreases with increasing magnetic field at low MF's (hfc mechanism) and then increases again at higher MF's (Δg mechanism). In this case, escape

products derived from a triplet precursor increase at low fields, but then decrease at higher fields (Figure 1.10). Note that most experiments are conducted under 5 kG, so typically the hfc mechanism predominates and the Δg mechanism plays no role.

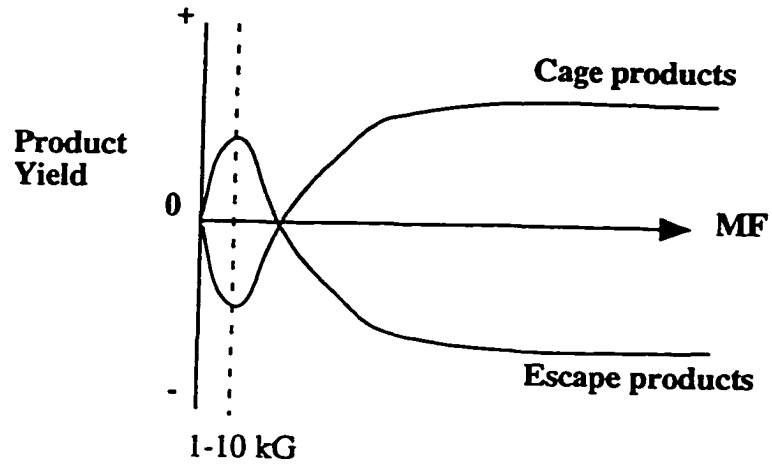

Figure 1.10: Effect of magnetic fields on the formation of cage and escape products from triplet precursors in the combined hfc and Δg mechanism.

1.7.5.1.4 Level Crossing Mechanism

If the value of 2J (E_{TS}) is much larger than that of the hfc constant, then the level crossing mechanism may predominate. Its characteristics include no interconversion between any triplet level when B=0, but at higher fields, where the energy of T_- is substantially reduced by the Zeeman splitting term, intersystem crossing can occur and reaches a maximum at $2J/g\mu_B$. Thus, when the magnetic field reaches the point where T_- crosses S, a sharp increase in the amount of cage product is expected (Figure 1.11).

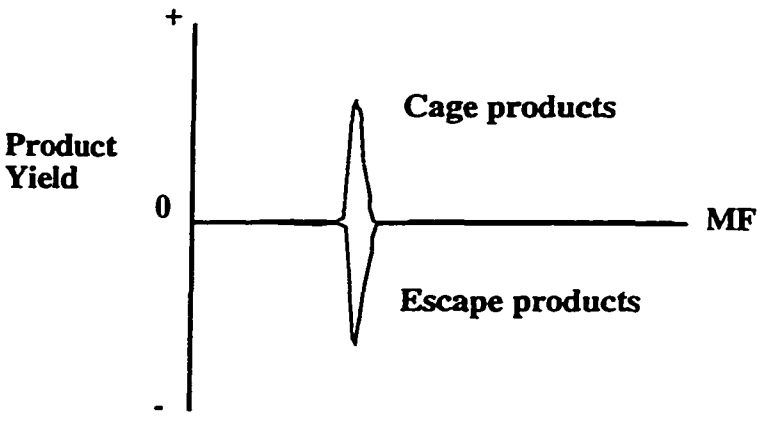

Figure 1.11: Effect of magnetic fields on the formation of cage and escape products from triplet precursors in the level crossing mechanism.

1.7.5.1.5 (Electron Spin Orientation or Spin-Lattice) Relaxation Mechanism

The relaxation of electronic spin due to the interaction between the electron point charge dipole and that of the electron spin is also possible. As the magnetic field increases the splitting between the triplet sublevels, the lifetime of the radical pair increases and as such the possibility of a spin flip can also increase. The MF effect is related to the distance ($\alpha\ r^{-6}$) and the lifetime of the radical pair. So, as the interactions between the unpaired electrons increase (short distances) and as they are exposed to each other for longer periods, relaxation may occur.[83] For organic molecules in constrained media, the lifetime of the pair is sufficiently short that this mechanism contributes little, if at all. This mechanism does become important when dealing with paramagnetic complex ions and other triplet excited states.[83]

1.7.5.1.6 Other MF Dependent Radical Pair Mechanisms

Other mechanisms exist that can induce intersystem crossing and are dependent on the strength of magnetic fields. Paramagnetic interactions of molecules between a radical pair and other unpaired electrons can lead to interactions that induce ISC. An investigation involving the interaction between a triplet excited species and a triplet radical pair has been carried out. The observation that Gd^{3+} (7 unpaired electrons) quenches geminate benzyl radical pairs in SDS micelles better than other heavier elements in the lanthanide series[86] suggests that it is the extent of paramagneticity that is important in quenching in this type of mechanism. In a similar manner, interactions of stable free radicals (doublets) have been shown to induce ISC in singlet[87] and triplet excited states.[88-91]

1.7.5.2 The Triplet Mechanism

This mechanism is related to magnetic effects based on interactions between the triplet sublevels. In contrast to the radical pair mechanism, it is symmetry selection rules that govern the rate of intersystem crossing.[76,77] If population of only one sublevel of the triplet manifold occurs, the possible processes include depopulating that state so as to distribute the population among all sublevels or to decay by product formation. If only one sublevel is depopulated, then a magnetic field can influence the decay kinetics. However, in the case where all three levels are equally populated and decay in an identical manner, no MFE is expected.

1.7.5.3 ISC by Spin-Orbit Coupling

The interaction between the angular momenta of the electron spin and that of its orbital is called spin-orbit coupling (SOC). It is a magnetic field independent process and will thus not contribute to any magnetic field effects. The heavy-atom effect is proportional to Z^4 and so the presence of heavy elements has to be

safeguarded against in MF dependence studies. SOC is also very dependent on the distance between the two interacting states.[92]

1.7.5.4 Mechanistic Implications for the DBK/Micelle System

The strength of magnetic fields used in this study are under 3 kG, therefore the Δg mechanism plays no role. Assuming that the three triplet states are populated equally, spin-lattice relaxation will not occur. In the case of DBK, the triplet-singlet energy gap is comparable to the hyperfine interaction, so the level crossing mechanism is also inoperative. Thus, of all the submechanisms, hyperfine interactions play the largest role in determining the magnetic field effects for DBK derived radical pairs.

1.8 Magnetic Isotope Effects (MIE)

In 1976, Buchachenko *et al.* reported the enrichment of magnetic isotopes in chemical reactions.[93] The recovery of ketone after photolysis of unlabelled dibenzyl ketone (DBK) in benzene showed a remarkable increase in the ^{13}C in the carbonyl carbon. At almost full conversion, there was an increase of 17% according to mass spectrometry. It was reasoned that the presence of a larger hyperfine coupling constant for the radical pair containing a ^{13}C carbonyl moiety relative to those with ^{12}C increased the amount of ISC and hence induced recombination. The enhancement of ^{13}C at the carbonyl carbon occurs because its hfc constant exceeds all other hyperfine interactions in any given radical pair. In addition, the application of small magnetic fields reduced the ^{13}C enrichment.[93] This can be rationalized by the decreased amount of hfc induced ISC thereby leading to less "(solvent)cage" products.[94] The presence of a magnetic field effect

on the isotope enrichment is a valuable tool since it can eliminate the possibility of a classical kinetic isotope effect which is based solely on mass.[95]

In the late 1970's, Turro *et al.* reported that photolysis of DBK in benzene yields isotopically enriched products and photolysis in CTAC micelles produces an even larger amount of ^{13}C enriched ketone.[96] In fact, the isotope enrichment only begins to occur above the cmc.[97] Moreover, application of a 15 kG magnetic field can decrease the isotope enhancement by reducing the hfc induced ISC pathway to yield escaped products rather than cage products.[96,98] Photolysis of DBK in both benzene or CTAC micelles yielded the largest enrichment at small fields (150 G - 300 G). The isotope enrichment increased and then began to decrease above 300 G.[99] Photolysis of ^{13}C enriched starting material generated products with no enrichment when exposed to very high magnetic fields (100 000 G)[98] because the hyperfine interaction no longer limits intersystem crossing. This is exactly what one expects when probing the combined hyperfine interaction and Δg mechanisms of ISC (*cf.* Figure 1.10).

By raising the temperature of DBK photolysis in micelles, the amount of isotope enrichment decreases while the quantum yield of DBK loss increases.[65] This indicates that less of the primary radical pair is recombining and more escaped products are being formed. The main reason for the lack of primary radical recombination is the fact that the quantum yield of decarbonylation (in CTAC) increases from 0.38 to 0.81 when the temperature is increased from 27°C to 70°C.

Studying the results in micelles begs the question whether the additional isotope enrichment when the photolysis is performed in micelles is caused by size of the micelle or viscosity considerations. Using DBK, a decrease in size (C_{16}TAC to C_{12}TAC) of the micelle had little effect on the enrichment of ^{13}C in the

ketone.[100,101] In addition, solvents with viscosities from 0.6 cP to 60 cP were used for the photolysis and also had little effect on the MIE. This shows that both viscosity and size of the micellar interior plays a small role in the enrichment of ^{13}C while demonstrating that it is the cage structure that is important in enhancing primary geminate recombination.[100,101] In fact, photolysis in porous glass and polymer films have also led to isotope enrichments.[63]

1.9 Magnetic Field Dependence of the Cage Effect

While micelles have a pronounced effect on the cage effect,[67] it is also clear that there should be a pronounced magnetic field effect on the amount of radicals that recombine within the cage. Assuming a hyperfine coupling based ISC mechanism, there should be a decrease of geminate (cage) products from triplet radical pairs as the magnitude of the magnetic field is increased. Using the quenching methodology to determine the cage effect as explained above, photolysis of DBK in CTAC micelles gave a smaller observed cage effect in the presence of magnetic fields compared to the Earth's MF. For ^{12}C-DBK, the cage effect in CTAC was found to be 32% and 18% at 0.0 and 7 kG, respectively. The cage effect was identical for ^{13}C-DBK (enriched in the carbonyl), but was significantly larger for di-^{13}C-DBK (substitution at both benzyl positions).[66] This is caused by the enhanced ISC rate within the micelle due to the presence of a relatively large amount of magnetic ^{13}C.[66] At very high MF's (145 kG), an increase in the cage effect is observed as the Δg mechanism overcomes the hfc and Zeeman interactions.[102]

1.10 Magnetic Field Effects on Kinetic Measurements

As explained previously, there have been a number of groups working with MF experiments using LFP to study the photolysis of DBK in micelles.[69,70,72] The presence of a fast decay with first order kinetics is followed by a second order decay. Interpretations differ between the groups with regard to the cause of each of the decays, and instead of dealing with discrepancies, this section will serve to provide a more unified approach to magnetic field effects on the decay of radical pairs derived from dibenzyl ketone and its derivatives in micelles.

1.10.1 Magnetic Field Effect on the Fast Decay

Initially, it was reported that the rate constant for the fast process for DBK in CTAC micelles was 2.5×10^6 s^{-1} which was reduced to 1.4×10^6 at 400 G.[69] These rate constant are probably within experimental error and do not represent a slow down of any kind due to external magnetic field. In addition, other reports[70] also mentioned that the decay was reduced in the presence of an applied field, however neither rate constants nor the decay kinetics were evident in the published work. Another account[72] suggests that at low fields (100 G), the rate constant decreases and then increases as the MF is increased to 1.5 kG. The authors' reasoning is that the Δg mechanism is at work on the benzyl-phenylacetyl radical pair. However, by their own admission, the errors in the rate constants are 5%-10% and the entire range for the rate constant of the fast process is only ~15%,[72] so the observed effect is close to experimental error.

The fast decay (k_{fast}) corresponds predominately to the recombination of the primary radical pair[72] and those radicals that do not react on the fast time scale appear as a residual absorbance (ΔA_{-}).[49,50] The value of ΔA_{-} is magnetic field

dependent showing that fewer radicals recombine in the presence of an external magnetic field (Figure 1.12).[69,70,72]

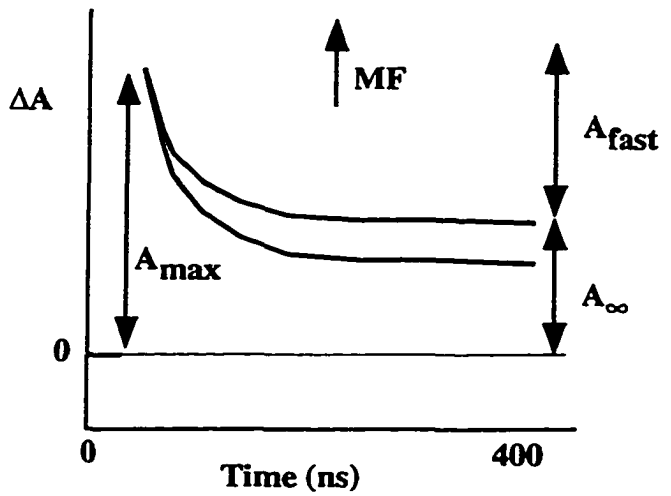

Figure 1.12: Illustration of the fast decay process for DBK in micelles. The decay of the fast process is termed k_{fast}, the maximum ΔA and residual ΔA are abbreviated as ΔA_{max}, ΔA_{∞}, respectively.

1.10.2 Decarbonylation of DBK in Micelles

There is no expected or observed magnetic field effect on the rate constant for decarbonylation. In fact, the growth due to the formation of benzyl radicals was found only by Cozens *et al.*[72] Due to this step, it is very hard to calculate the exact magnetic field dependence of the residual absorbance (ΔA_{∞}) of the fast process as the absorbance due to the newly formed benzyl radicals interferes with the measurement between 0.4-2 μs.

1.10.3 Magnetic Field Dependence of the Slow Process for DBK in Micelles

The slow decay was found to be a first order decay and magnetic field independent by some investigators,[2,10,69] but others have found a MF dependence[71,72] on second order decay kinetics.[71,72] The fact that first order decays were considered may be due to the poor signal to noise ratio in the experiments. The second order decay kinetics are expected for a bimolecular recombination and so the decay is attributed to the decay of random radical pairs that have exited from the micelle. The presence of a magnetic field effect also alludes to the idea that the random encounters are occurring after re-entry into a micelle - not in the bulk aqueous solution. The second order kinetics were fit to a plot of the dependence of $1/\Delta A$ with time. The linearity of the fit provides additional proof of a second order decay.[103] By ensuring that the ΔA_{max} was the same for all kinetic traces, it was found that the rate constant decreased by almost a factor of 2 at 1 500 G relative to the Earth's magnetic field (~0.5 G).[72]

1.10.4 Dynamics

1.10.4.1 Geminate and Exit Rate Constants in Micelles

As shown for the benzophenone/1,4-cyclohexadiene/SDS system,[49,50] the overall fast decay of the ketyl radical is the sum of the rate constants for exit (k_-) and intersystem crossing (k_{ISC}).[72] The same treatment can also aid in the discrimination of k_- from the geminate recombination rate constant of the primary radical pair, k_{gem}, because k_{gem} is dependent on k_{ISC}.[49,50]

$$\%\ \text{escaped} = 100\left(\frac{k_-}{k_{gem} + k_-}\right) = 100\left(\frac{\Delta A_\infty}{\Delta A_{max}}\right) \qquad (1.15)$$

In SDS, it was reported that k_{gem} for DBK is ~ 1.2×10^7 s^{-1} and $k_- = 8 \times 10^6$ s^{-1}. The exit rate constant for benzyl radical has also been determined to be $(1.4 \pm 0.3) \times 10^6$ s^{-1} by chemically induced dynamic nuclear polarization and LFP studies.[30,74] The 4-methylbenzyl radical has a slower exit rate constant of 2.6×10^5 s^{-1} [74] while the phenylacetyl radical has $k_- = \sim 6.6 \times 10^6$ s^{-1}.[72] The exit rate constants are similar to those determined by phosphorescence studies using neutral arenes where the entry rate constant, k_+, was assumed to be diffusion controlled.[75]

1.10.4.2 Effect of Micelle Size on Triplet Radical Pairs

Hydrogen abstraction by the n,π^* triplet excited state of butyrophenone from Vitamin E (α-tocopherol) was studied in SDS micelles. The formation of this radical pair occurs within the laser pulse and a key attribute is that the hydrophobicity of the Vitamin E element prevents it from exiting the micelle on the LFP timescale, so the dynamic diffusional behaviour of the radical pair comes from the butyrophenone ketyl radical alone (Scheme 1.7).

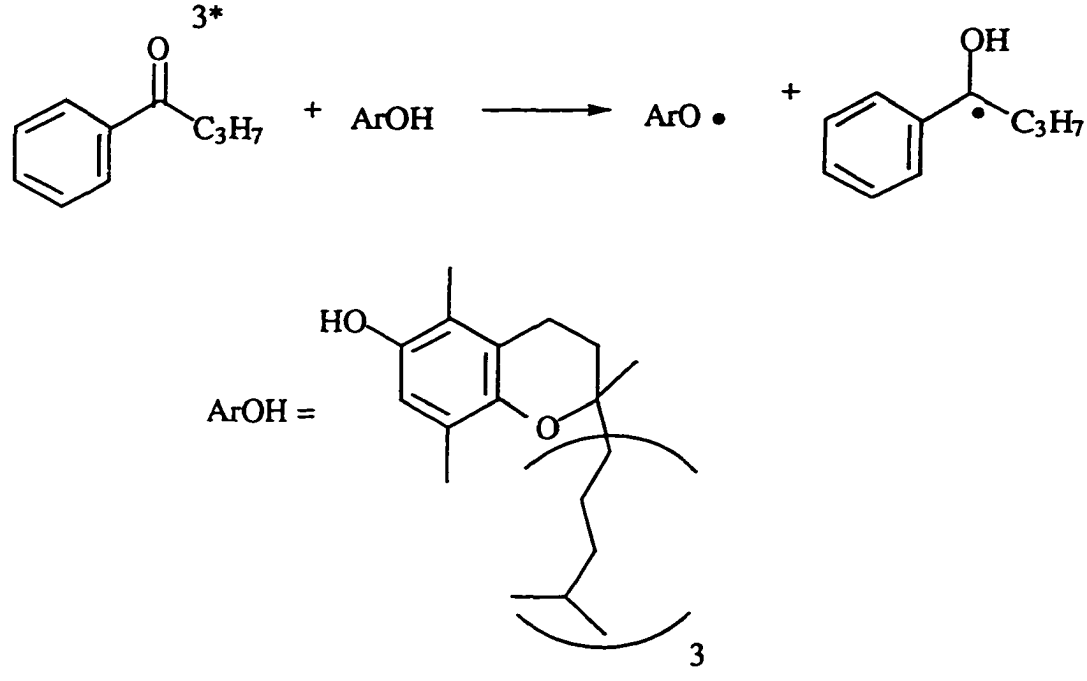

Scheme 1.7 Formation of a radical pair using triplet butyrophenone and Vitamin E as precursors.

It was determined that in SDS micelles, k_{gem} for the radical pair in Scheme 1.7 is equal to 2.5×10^6 s^{-1} at 20°C and increases to 5.6×10^6 s^{-1} at 80°C.[104] Under the same conditions, the exit rate constant increases from 0.72×10^6 s^{-1} to 5.2×10^6 s^{-1}. The micelle size is known to be smaller at higher temperatures and although the rate constant for geminate recombination increases as the micelle size decreases, the enhancement in the exit rate constant controls the rate of decay of the fast component in the smaller micelles.[104] The same feature was monitored in micelles where the size was varied using different chain lengths and/or in the presence of up to 0.5 M NaCl. This change in the exit and geminate rate constants

as well as their temperature dependence led the authors to propose that exit is associated with a decrease in entropy where water molecules must organize to solubilize the newly exited hydrophobic radical.[104] The disruption in the hydrogen bonding nature of water inflicts an increasingly organized assembly around the solutes.

1.10.4.3 Singlet Encounter Frequency

The temperature effect discussed above also demonstrates that the competition between geminate recombination and exit is related to the frequency of encounters between the radicals.[104] Of prime importance is that geminate recombination can only take place when the radical pair possesses a singlet multiplicity. It has been proposed that the geminate rate constant is proportional to both the frequency of encounters in a micelle (k_e) and the probability of the radical pair to be in a singlet state (f_s).[105] In the case of benzylic radicals in micelles, it has been proposed that the geminate decay (in the absence of a magnetic field) is limited by both the diffusional motion of the radicals within the micelle and the hyperfine interactions.[106] When a magnetic field is applied so that the exchange interaction is greater than the hyperfine interaction (in the absence of other ISC mechanisms), recombination is limited by the frequency of encounters. When the radical pair separates, the hyperfine interaction decreases making ISC more likely and f_s larger. The importance of the two terms (k_e and f_s) is that at larger separations where the frequency of encounter is small, the probability of the radical pair being in the singlet state is increased. If a micelle acts as a cage, then, as the micelle size increases, the frequency of encounter decreases. Moreover, magnetic field effects on micellized radical pairs originate from the f_s term because of the MF dependence of the hyperfine interactions.

1.11 Behaviour of Benzyl and Diphenylmethyl Radical Pairs in Non-Micellar Systems

DBK and its derivatives have been studied on porous silica, in zeolites and in cyclodextrin cavities. Other ketone probes that yield diphenylmethyl radicals such as 1,1-diphenylacetone (DPA) and 1,1,3,3-tetraphenylacetone (TPA) have been used in vesicles.

1.11.1 Diphenylmethyl Radicals in Vesicles

Upon photolysis of 1,1,3,3-tetraphenylacetone (TPA), α-cleavage occurs to yield a triplet radical pair consisting of a diphenylacetyl radical and a diphenylmethyl radical.[107] The decarbonylation of the diphenylacetyl radical to yield a second diphenylmethyl radical occurs rapidly.[73,108] For 1,1-diphenylacetone (DPA), diphenylmethyl radical is formed along with an acetyl radical that decarbonylates slowly and is invisible to absorbance type measurements at wavelengths where the diphenylmethyl radical is monitored (330 nm).[109]

1.11.1.1 Small DODAC Vesicles

Diphenylmethyl radicals were formed from TPA by laser flash photolysis in small DODAC vesicles and observed to decay by first order kinetics (with some deviation) with a lifetime of ~5 μs.[109] In micelles, the lifetime of the geminate process is about 0.2 μs, and since no exit process is observed in micelles,[110] the fast process in vesicles is attributed to geminate recombination occurring in a restricted environment.[109] As a deviation in the first order kinetics was observed and since 5 μs is a long time for a geminate process, it may be interesting to point

out that this decay may actually involve second order kinetics that reveal the existence of random processes. Elevating the temperature above the phase transition of the vesicles had little effect on the kinetics.[109] This is puzzling as the vesicle should become more fluid and if the recombination is truly geminate, then the kinetics should be dramatically altered. A magnetic field effect was observed for the radical pairs generated from the photolysis of TPA, but saturation occurred above 4 kG, so no mechanistic implications could be drawn.

For DPA generated diphenylmethyl radicals, an exceptionally long lifetime (>40 μs) was attributed to arise from fast separation from the acetyl radical, so that recombination is a very slow process. The acetyl radical is expected to exit fast due to the polarity of the carbonyl moiety.

1.11.1.2 Large DODAC Vesicles

Laser flash photolysis with diffuse reflectance detection was used to monitor the diphenylmethyl radical in the turbid solutions consisting of 500 nm vesicles. The decay derived from the photolysis of DPA was found to be very long lived (>150 μs) and was attributed to the random recombination pathway.[109] For TPA, no fast transient was observed and only a long-lived decay was seen. Thus, in contrast to the small vesicles, in large vesicles, the decay for TPA was attributed to random encounters.[109] No magnetic field effect was observed in large vesicles for either photolysis. An increase in temperature (above the phase transition) led to a significant increase the decay kinetics.

The work completed in vesicles is very complex and is difficult to analyze. The use of a simpler and more thoroughly studied system such as DBK will probably shed some insight onto the problem.

1.11.2 Cage Effects in the Solid State

Cyclodextrin (bucket shaped molecules with holes at both ends consisting of glucose monomers) complexes with DBK in the solid state. Isolation of the photoproducts following photolysis of these complexes demonstrates that constrained environments can influence the distribution of products.[111]

Silica gel has a chemical composition of SiO_2 $(H_2O)_x$ and can act as a cage for radical pairs. The photolysis of 4-MeDBK directly on porous silica indicated that as the pore size increases, there is less geminate recombination. Pore sizes of 22 Å and 95 Å gave cage effects of 21% and 7% at higher occupation levels, respectively.[112] Magnetic isotope enrichments of ^{13}C were also found[113] to be independent of the pore size.[114] Furthermore, ^{17}O enriched ketone was also recovered from photolysis on silica gel.[114,115] In summary, porous silica can bind the ketone and create a suitable environment for the observation of magnetic field effects.

1.11.3 DBK in Zeolites

Zeolites are crystalline aluminosilicates whose internal structure contains cages or channels filled with exchangeable cations.[116] The cage effect was found to decrease from Silicalite (no cavities) to NaX zeolites (13Å diameter with 8Å windows to create channels) and NaA (11Å diameter with 4Å windows to create supercages). NaA has windows that are too small to allow DBK or 4-MeDBK inside the zeolite.[117] The cage effect of 0% demonstrates that all reactions are random encounters.[116] For 4-MeDBK, a cage effect of 18% was observed on NaX. Surprisingly, when DBK is used, the major product is the *ortho* coupling product (1-*o*-tolyl-2-phenylethanone). Even more striking is that for zeolite NaY,

the major product from DBK photolysis is dimethylbenzophenone![118] These results show the remarkable effect of host structure on chemical reactions. Just as outstanding was the fact that *o*-methylDBK was adsorbed only on to the exterior of the zeolite whereas 4-methylDBK (*para* derivative) was inaccessible to the quencher (2,2,6,6-tetramethylpiperidin-1-oxyl, TEMPO) and consequently inside the zeolite framework.[119] In the presence of a radical scavenger, no coupling products are formed from the starting *o*-methylDBK. However, in the absence of radical traps, the yields of the symmetric products (bibenzyl and the di-*o*-methylbibenzyl) are increased such that they are both greater than the asymmetric product by 2.5 times.[119] This was rationalized by the sieving of the benzyl radical. The *o*-methylbenzyl radical cannot enter into the zeolite, whereas the *p*-methylbenzyl radical can. Thus, the probability for symmetric recombination is enhanced.[119]

The work in zeolites has direct application to the work carried out in micelles because zeolites can alter the chemical reactivity based on structure. Thus far, it has been shown that micelles are also capable of fine-tuning radical reactivity. The issue of molecular sieving may also have application to micelles.

1.12 Biological Implications of Magnetic Field Effects on Radical Pairs

There are many paramagnetic materials in biological systems that can be affected by the application of magnetic fields. These may be substrate-enzyme complexes involving radical pairs or radical ion pairs,[120] co-factors,[121,122] or magnetite particles that are used as biological compasses in migratory animals.[123] There is a vast public interest in the possible harmful effects of power lines and other electronic items such as computer screens and cellular phones on biological organisms.[124-128] For this reason, there have been studies on both whole

organisms (humans[129] and mice[130]) as well as on radical pairs in biological media such as proteins and DNA.[131]

From the studies above,[122,123,131] it is clear that as long as *binding* of a radical pair precursor occurs in a *constrained* or *restricted* environment, an externally applied magnetic field may alter the fate of chemical reactions. The use of static and dynamic magnetic fields was also studied to test for fluctuations due to the variations in magnetic fields. It was determined that AC magnetic fields have effects identical to those of DC MF's.[132-135] The similarity in both situations results from the fact that the electronic spin "feels" essentially the same magnetic field because 60 Hz oscillations are still slow relative to the kinetics of the radical reactions.

From the work presented in earlier sections, it is clear that there are many ways to restrict the mobility of radical pairs (*e.g.* structural rigidity (zeolites), differential binding sites (porous silica), micro-organization and curvature (vesicles) as well as hydrophobicity (micelles). All of these characteristics can be found in biological systems whether it be at an active site of an enzyme, in a cell membrane or cell wall, or within a DNA helix. It is believed that the radical pair mechanism will provide the answer to better understand electromagnetic field effects.[133,135-137]

1.13 Project Proposal

There is a wealth of information regarding the probing of microheterogeneous media using radical pairs - especially those derived from dibenzyl ketone derivatives. Most of the previous work has been carried out in simple self-aggregating systems such as micelles and host-guest complexes such as cyclodextrin, zeolites and porous silica. In an effort to further investigate the behaviour of radical pairs in biological systems, vesicles will be studied. The use of these large aggregates as models for cell membranes is well established and conclusions derived from this work should be more applicable to cell membranes than those obtained from micelles. The use of DBK derivatives to yield triplet radical pairs can be fertile when both product studies and time-resolved LFP studies can be completed. Thus, both techniques will be used to understand the mobility of radical pairs in biomimetic systems.

Structural rigidity, differential binding sites, micro-organization and curvature as well as the hydrophobicity of the aggregates can be investigated using micelles and vesicles. The often studied micelles can be used as a starting point to understand the behaviour of radicals in vesicles. Furthermore, the phase transition in vesicles can be probed to examine the effects of microviscosity, whereas temperature effects in micelles can lead to a better understanding of the effects of size on the dynamics of radical pairs.

CHAPTER 2: MATERIALS AND METHODS

2.1 Common Laboratory Reagents and Equipment

2.1.1 Reagents

Dibenzyl ketone (DBK, Aldrich, 98%), diphenylmethane (Aldrich, 99+%), and 4,4'-dimethylbibenzyl (Lancaster, 90%) were purified by recrystallization from diethyl ether at -78°C, ethanol/water, and ethanol respectively. Sodium dodecylsulfate (SDS, Sigma, 99+%) was purified by Soxhlet extraction for 24 h with diethyl ether in the presence of lithium aluminum hydride, followed by at least three recrystallizations from 1:1 isopropanol/ethanol. Dioctadecyldimethylammonium chloride (DODAC, TCI) was similarly purified except that the recrystallizations were carried out by adding methanol to hot acetone containing the alkylammonium salt. Bibenzyl (Aldrich, 99%) was used without purification. Water was distilled and deionized (Sybron-Barnstead).

2.1.2 Equipment

2.1.2.1 UV-Vis Spectroscopy

UV-Vis absorption spectra were recorded on a Varian Cary 5 or Cary 1 at room temperature. The scan rate was usually 400 nm/min and the slits were set at 2 nm. The instrument was zeroed with air and baseline correction was employed.

2.1.2.2 Gas Chromatography

Gas chromatography (GC) was conducted using a Fisons 8000 Series gas chromatograph containing a 1 m guard column followed by a 15 m, 25 μm I.D. OV-1 column. The flame ionization detector (FID) was connected to a 486-33 MHz

PC-compatible computer. ChromCard™ software (Fisons Inc.) running under Windows 3.11 was used to capture the data and then to integrate the peaks. The GC injector and FID temperatures were 220°C and 280°C, respectively. The GC oven method began at 80°C and increased at 15°C/min up to 250°C where it was held at for 3 min.

2.1.2.3 Nuclear Magnetic Resonance and Mass Spectroscopy

Mass spectra (MS) were obtained on a Finnegan mass spectrometer (Finnegan 3300) and were run courtesy of Dr. D. McGillivray. Typically, chemical ionization (methane) was used in a glycerol matrix at 60°C. Low-resolution *m/z* data were obtained by observing the molecular ion peak as well as the signals at M + 1, M + 29 and M + 41.

Nuclear magnetic resonance (NMR) spectra were obtained on a Brüker (Model AC300) 300 MHz NMR equipped with an autosampler and connected to a Windows-based PC with Win-NMR™ (Brüker, version 5.1). Spectra were obtained in $CDCl_3$ and the spectrometer locked on the residual $CHCl_3$ signal.

2.2 Preparation of Ketone Derivatives

2.2.1 Synthesis of 4-Methyldibenzyl Ketone ((4-methyl)-1,3-diphenyl-2-propanone (4-MeDBK))

This synthesis is based on that of Turro *et al.*[68] where benzyl magnesium bromide was reacted with a 4-methylphenylacetyl chloride.

2.2.1.1 Preparation of Benzyl Cadmium Bromide

Activated magnesium turnings (1.12 g, 0.0459 mol) were placed in 20 mL dry diethyl ether. Following a pinch of I_2, benzyl bromide (7.78 g, 0.0455 mol in 20 mL diethyl ether) was added to a round bottom flask equipped with a condenser and magnetic stirring. Upon completion of the bromide addition, 15 mL of diethyl ether were added, after which the solution turned a turbid light gray-green. Solid $CdCl_2$ (8.41 g, 0.0459 mol) was added over 15 min to the reaction mixture after allowing the Grignard reagent to cool in an ice bath while stirring for 20 min. The solution turned greyish-blue and a further 90 mL diethyl ether were added. The reaction mixture became creamy and was allowed to stir for 120 min.

2.2.1.2 Preparation of 4-Methylphenyl Acetyl Chloride

Thionyl chloride (4.76 g, 0.040 mol) was added to 4-tolylacetic acid (2.93 g, 0.0195 mol). With gentle heating, the colour changed from a pale yellow to a dark orange. The ^1H NMR shift of the benzylic hydrogens changed from 3.58 ppm to 3.95 ppm as the reaction progressed. Removal of excess $SOCl_2$ was carried out under reduced pressure.

2.2.1.3 Preparation of 4-Methyldibenzyl Ketone

The acid chloride was added dropwise to the cadmium benzyl bromide reagent. The creamy solution turned varying shades of orange as the reaction was allowed to proceed over an ice bath. Two aliquots of 30 mL diethyl ether were added to the mixture and after 2.5 h from the beginning of the addition, the reaction was quenched by the addition of ice. The crude organic layer was extracted by three equivolume washes with water and then with saturated sodium chloride (aqueous). The reaction mixture was dried over anhydrous $MgSO_4$, filtered by gravity and then concentrated under reduced pressure. Flash column

chromatography using silica gel 60 (Merck) with a 3:1 hexanes:ethyl acetate eluent was used as the next purification step. A second gravity chromatography column with 20:1 hexanes:ethyl acetate eluent was used to extract almost pure ketone. The final step in the purification was column crystallization.[138] A test tube containing ketone in diethyl ether was slowly lowered into a dry ice/acetone bath until crystal formation was observed. The crystals were separated from the solution phase and then re-exposed to the procedure at least three times. The overall yield was 8%. 4-Methyldibenzyl ketone was pure as determined to be >99.9% by GC. ^{1}H NMR (300 MHz, $CDCl_3$): δ 7.0-7.4 (m, 9H, ArH), δ 3.78 (s, 2H, CH_2), δ 3.76 (s, 2H, CH_2), δ 2.30 (s, 3H, CH_3). ^{13}C NMR: δ 205.9 (C=O), δ 136.7, δ 134.2, δ 131.0, δ 129.6, δ 129.5, δ 129.4, δ 128.7, δ 127.0(Ar), δ 49.0 (CH_2), δ 48.8 (CH_2) and δ 21.0 (CH_3). The melting point was above 0°C and less than 30°C and could not be accurately determined. Low resolution mass spectroscopy (CI) yielded a molecular ion peak at *m/z* = 224. The spectral data agree with those previously published.[68]

2.2.2 Synthesis of 4-*t*-Butyldibenzyl Ketone ((4-*t*-butyl)-1,3-diphenyl-2-propanone (4-*t*-butylDBK))

This preparation involves addition of phenylacetyl chloride to the alkylated Grignard reagent to form the ketone.

2.2.2.1 Preparation of 4-t-Butylbenzyl Magnesium Bromide

Activated magnesium turnings (1.46 g, 0.06 mol) were placed in 50 mL dry tetrahydrofuran (THF). Following a pinch of I_2, 4-*t*-butylbenzyl bromide (9.09 g, 0.04 mol in 15 mL THF) was added dropwise to the round bottom flask equipped

with a condenser and magnetic stirring. Upon completion of the bromide addition, 10 mL of THF was added. The solution turned turbid and gray and was allowed to stir for 2 h. The Grignard reagent was cannula transferred to another dry round bottom flask to await further reaction.

2.2.2.2 Preparation of *4-t*-Butyldibenzyl Ketone

Phenyl acetyl chloride (Aldrich, 6.18 g, 0.04 mol) in 100 mL THF was placed on an ice bath and added to the Grignard reagent at 4°C in a dropwise manner. The reaction mixture became yellow and was allowed to stir for 1.5 h. The reaction was quenched by the addition of ice cooled water containing a few drops of conc. H_2SO_4. Diethyl ether was added to the mixture and the organic layer was thrice extracted with water, a 1:1 mixture of Na_2CO_3 (saturated aqueous solution):water and finally NaCl (saturated aqueous solution). The organic layer was dried over $MgSO_4$, filtered and concentrated under reduced pressure. At this point the crude mixture contained a precipitate and an oil. After filtration, the solid was determined to be 4,4'-di-*t*-butylbibenzyl by NMR and mass spectroscopy (see below).

Flash column chromatography using silica gel 60 with a 10:1 hexanes:ethyl acetate eluent was used as the next purification step. A second column run by gravity with 20:1 hexanes:ethyl acetate eluent followed by a third column with a 40:1 ratio of the co-eluents were used to extract almost pure ketone. The final step in the purification was column crystallization as described in the synthesis of 4-methyldibenzyl ketone. ^{1}H NMR (300 MHz, $CDCl_3$): δ 6.90-7.25 (m, 9H, ArH), δ 3.62 (s, 2H, CH_2), δ 3.58 (s, 2H, CH_2), δ 1.25 (s, 9H, CH_3). ^{13}C NMR: δ 205.9 (C=O), δ 150.0, δ 134.2, δ 131.0, δ 129.6, δ 129.2, δ 128.7, δ 127.1, 125.7 (Ar), δ 49.1 (CH_2), δ 48.7 (CH_2) and δ 24.5 (C) and δ 31.4 (CH_3). The

melting point was above 0°C and less than 30°C and could not be accurately determined. Low resolution mass spectroscopy (CI) yielded a molecular ion peak at $m/z = 266$.

2.2.3 Characterization of 4,4'-di-*t*-Butylbibenzyl

The white solid was filtered from the concentrated extract derived from the synthesis of 4-*t*-butyldibenzyl ketone. The filtrate was washed with cold diethyl ether. Recrystallization from ethanol yielded white crystals with a melting point of 143-144°C. ^{1}H NMR (300 MHz, $CDCl_3$) signals: δ 7.20 and δ 7.30 (AB pattern, 9H, ArH, $^3J_{AB}$ = 10 Hz) with δ 2.84 (s, 4H, CH_2), and δ 1.30 (s, 9H, CH_3). ^{13}C NMR: δ 148.7, δ 139.0, δ 128.0, δ 125.2 (Ar), δ 37.4 (CH_2) and δ 34.4 (C) and δ 31.4 (CH_3). Low resolution mass spectroscopy (CI) yielded a molecular ion peak at $m/z = 294$.

2.3 Preparation of Solutions Containing Microheterogeneous Systems

2.3.1 Preparation of Micellar Solutions

Typically, SDS solutions contained 0.1 M surfactant (2.71 g/25 mL water). The solutions were allowed to stir overnight. Enough probe was added as a colourless oil (ρ = 1.065 g/mL, 10.5 μL/25 mL solution) to yield a 2 mM ketone solution. The surfactant/ketone solution was stirred while covered with aluminum foil overnight. Solutions were disposed of after a maximum of one week and no noticeable decomposition was observed by UV-Vis spectroscopy over this timeframe.

2.3.2 Preparation of Solutions Containing Small Vesicles

DODAC was solubilized in deionized water and was allowed to stir overnight to generate a 40 mM solution. Upon complete solubilization of the surfactant, the probe was added in the same fashion as for the SDS solutions. This solution was stirred while exposed to temperatures of 73-78°C using a water bath. The solution became less viscous and was allowed to stir for about 1 h.[38,39,41,109,139]

Sonication (Ultrasonic Processor Heat Systems-Ultrasonic Inc., Model 385) of the surfactant/ketone solution using a microtip probe immersed in the turbid solution was carried out in a 70°C water bath. Five repetitions with settings of 50% duty cycle and continuous sonication at a power level of 4.5 for 3 min followed by a 2 min rest period were carried out to achieve a homogeneous vesicle solution.[109] The solution was transferred to two or more 25 mL centrifuge tubes and centrifuged using an Adams Dynac centrifuge at a speed rating of 7.5 for more than 1 h. The solutions were decanted, cooled down to ambient temperature and kept protected from light until use the following day.

2.3.3 Preparation of Solutions Containing Large Vesicles

A 25 mL solution of 20 mM DODAC in $CHCl_3$ was prepared. Enough ketone was added to make a 2 mM solution. Large vesicle preparations were performed in a modified condenser with a GC septum held on by a thermometer adapter at one end (Figure 2.1).

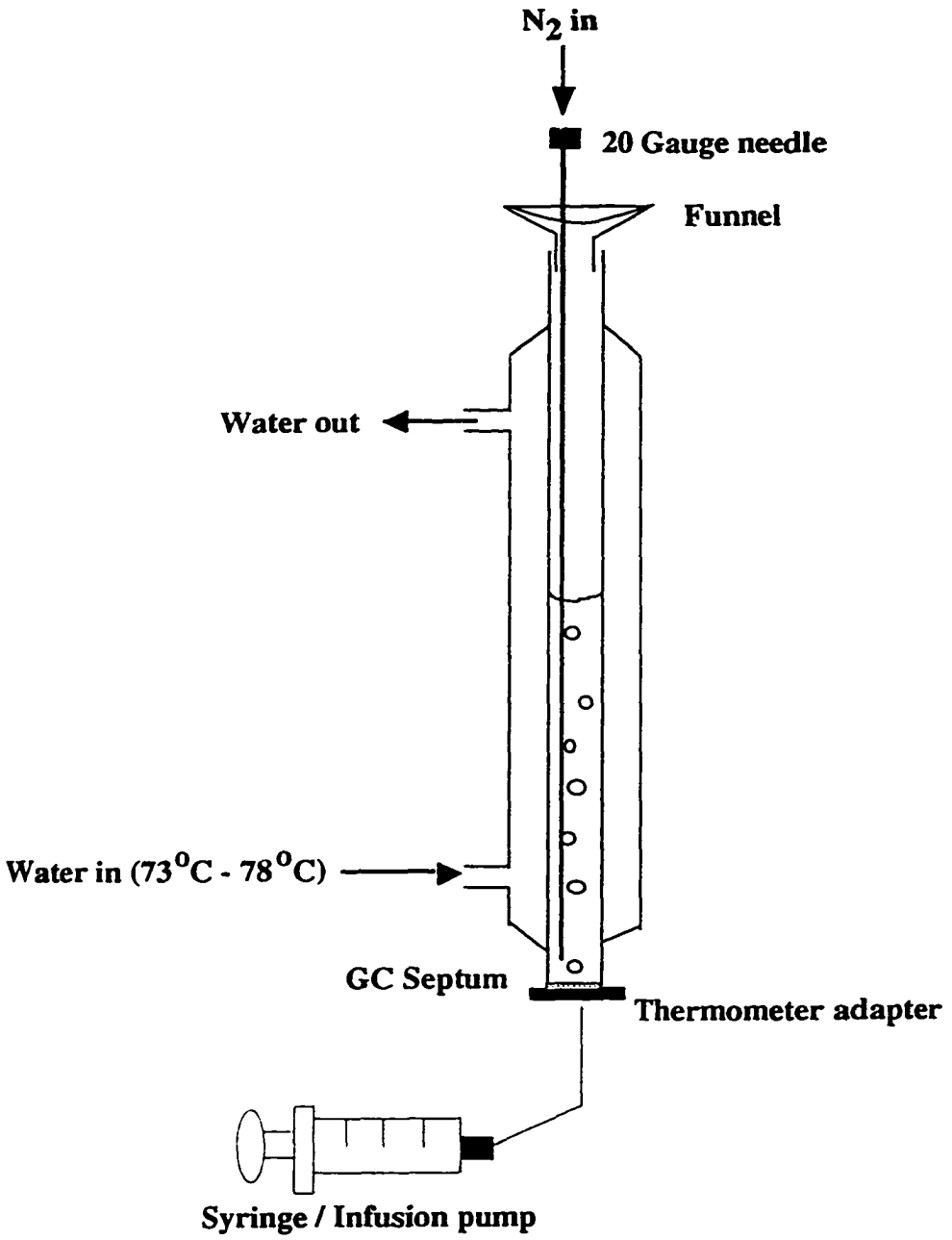

Figure 2.1: Setup for preparation of large vesicles by infusion

Deionized water (10 mL) was heated up to 73-78°C inside the condenser for at least 25 min prior to injection, and was kept at this temperature during the infusion process using a Haake D1 circulating water bath. A 5 mL aliquot of the ketone/DODAC solution was injected into the heated water using a 5 mL glass B-D (ID = 11.72 mm) syringe and a syringe pump (Harvard Instruments, Model 11) at 16.8 mL/h. The final DODAC and ketone concentrations were 10 mM and 1 mM, respectively. Infusion occurred with a constant stream of nitrogen being evolved from a 20 gauge syringe needle about 1 cm above the GC septum. A small funnel was placed on top of the condenser to ensure that all of the aqueous solution remained inside the condenser system as the evaporation of chloroform produced vigorous bubbling. In order to ensure that all of the chloroform had evaporated, the 20 gauge needle was lowered to the septum and the nitrogen was left flowing for an additional 20 min after complete infusion. The turbid vesicle solution was transferred to a sample vial and allowed to cool prior to being characterized.

2.3.4 Characterization of Vesicle Solutions

A NICOMP submicron particle sizer (model 370) was utilized to determine the distribution of vesicle sizes. A HeNe laser irradiates the sample and the angles of the scattered radiation are monitored. Particles of different sizes scatter light in different manners due to their varied diffusional motions. In this manner, aggregate sizes can be determined by analyzing the angle and magnitude of scattered light. These measurements were done at 20°C and depend on the viscosity (1.002 cP) and the refractive index (1.333) of the bulk solution (water). To obtain statistically relevant results, it was necessary to dilute the vesicle solution with water to achieve an initial intensity between 200 and 400 counts. A minimum of 1×10^6 counts was

accumulated and in most cases, over 5×10^6 were obtained prior to fitting the data by either Gaussian or NICOMP distributions.

Gaussian fits yielded suitable χ^2 values (a measure of goodness of fit) for the large vesicles. For small vesicles, Gaussian fits could be used only under conditions where a small (non-statistical) number of counts ($< 1 \times 10^6$) were obtained. For this reason, prolonged analysis and NICOMP fits were deemed reasonable. NICOMP fits recognize the possibility of discrete sizes of vesicles rather than overall distributions. Using a NICOMP fit, in all experiments, the solutions containing small vesicles were determined to have >98% of 30±2 nm sized vesicles. The remaining <2% were sized to be 115±15 nm. The large vesicles were determined to be 150±65 nm using a Gaussian distribution in single experiments. All trials involving large vesicles yielded identical results. The solutions containing small vesicles were stable from anywhere between 3 - 5 days as determined by light scattering. The solutions of large vesicles were stable for at least 1 week, however fresh solutions were employed for all experiments.

2.4 Steady-State Photolysis

2.4.1 Experimental Setup

Figure 2.2 illustrates the setup for steady-state irradiation of the dibenzyl ketone derivatives using a 75 W xenon lamp (1). The light passes through a 280 nm cut-off filter (3) and through two focusing lenses (3" (5) and 6" (6)). The sample holder (7) sits in the middle of a home built electromagnet (8, MF_{max} = 3.0 kG, 10 mm × 10 mm poles, Chris Kaputa; Dr. M. Stuchly, Department of Electrical Engineering, University of Victoria) that is controlled by a power supply

(9, Anatek 6030). Calibration of the magnet was performed with a gaussmeter (Walker Scientific, model MG-50). Due to the constrained environment around the magnet the temperature is varied by placing a paint stripper (10, Super Stripper 1200, model LW-128) at suitable distances from the sample holder and the temperature is monitored with a thermocouple (Omegameter, model DP 2000) placed in the solution away from the irradiated area. Since the magnet is slightly heated, the calibration was checked at the highest temperature employed and did not vary by more than 2%. Two shutters (mechanical and electronic) control the exposure of the sample to the irradiation light and are controlled by a program (Dr. L. Netter) written with LabView software (version 4.0, National Instruments) on a Macintosh IIci so that each sample can be irradiated for 110±1 s for micelles and 140±1 for vesicles.

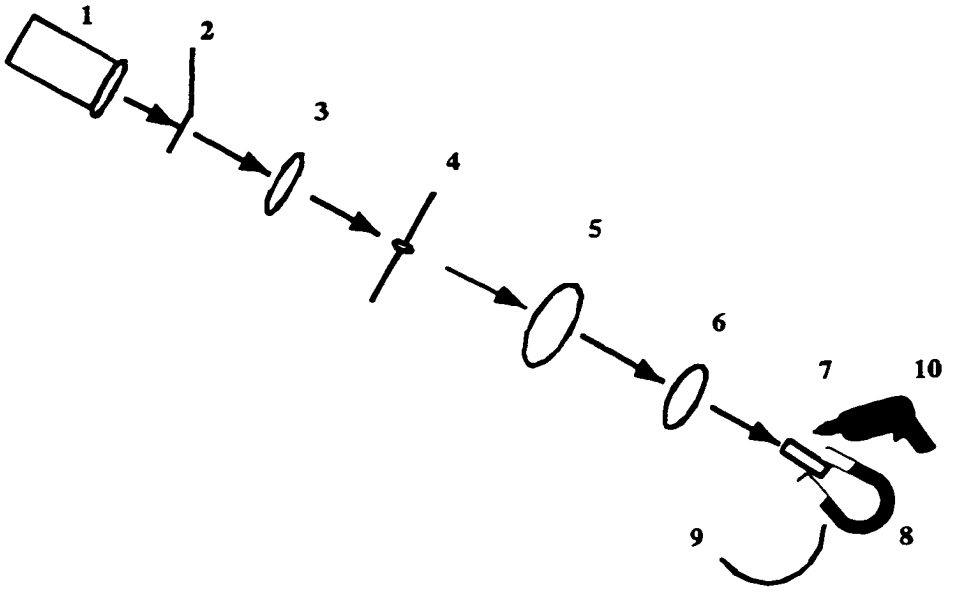

Figure 2.2: Setup for steady-state irradiation of ketones in microheterogeneous systems (2) and (4) are mechanical and electronic shutters, respectively. See text for more details.

2.4.2 Irradiation of Ketones and Workup of Photoreaction

After stirring overnight, 2.20 mL of the probe-micelle (or vesicle) solution was transferred to 7 mm × 7 mm quartz cells. The cells were deoxygenated using either a single 20 gauge stainless steel needle or two needles (one extended down into the cell, the other above the solution surface to diminish bubbling). The cells were deoxygenated for 20 min with nitrogen flow and then placed consecutively in the sample holder. In all cases, a blank which contained ketone within the supramolecular assemblies was run, but not exposed to photolytic light. Less than 20% of the ketone was converted to photoproducts.

Following photolysis, the photoproducts were extracted using an organic mix (4:1 mixture of ethyl acetate:chloroform).[140] A volume of 1.50 mL was taken from the irradiation cell and placed in a (10 mm × 75 mm) centrifuge tube to which 1.00 mL organic mix, 0.25 mL diphenylmethane (internal standard, 1 mM stock in organic mix) and 0.25 mL saturated NaCl in water were added. The centrifuge tube was capped, inverted and shaken. A needle was used to vent the closed system and the solutions were centrifuged for a minimum of 10-15 min. The supernatant (organic layer) was removed and placed in another centrifuge tube. Another 1.25 mL organic mix was added to the initial tube that contained the aqueous layer, mixed, vented and subjected to another 10-15 min centrifugation. The organic layer from this extraction was combined with the organic layer from the first extraction. This process of double extractions ensured that over 90% of the material was extracted from the aqueous solution. In order to eliminate any remaining surfactant from the organic solution, a reverse extraction (adding 0.90 mL of deionized water and 0.10 mL saturated NaCl to the combined organic layer, centrifuging and removal as above) was performed. The organic (top) layer was removed and dried over $MgSO_4$ and filtered by vacuum into a 10 mL round bottom flask. The organic solution was run through a 3 cm^3 silica gel column (in a 5 mL disposable B-D syringe). At least 6 mL of diethyl ether was added to the column to ensure complete elution. The column was run dry and then the solvent was removed under reduced pressure until only 50-100 μL remained. To ensure that measurements were carried out above the detection limit of the GC, 2 μL injections were made. All peaks in the chromatogram were assigned based on retention times of authentic samples with the exception of the asymmetric photoproducts. The GC oven program listed above was used (*cf.* 2.1.2.2) and when the temperature was allowed to increase until 300°C, no significant product peaks eluted.

2.4.3 Standardization of GC and Mass Balance Determination

In order to ensure proper quantification of product distribution, diphenyl methane (DPM) was used as an internal standard. Plots of the dependence of the area ratio on concentration ratio between the authentic photoproducts and DPM were determined at least twice. Errors derived from the calibration curves were less than 2%.

No authentic samples of the asymmetric photoproducts (4-MBB and 4-tbBB) were obtained. For this reason, an average of the BB curve and the disubstituted photoproduct curve was taken since the response function of the flame ionization detector should be similar for all three photoproducts. The mass balance of the reaction could be checked by comparing the amount of starting material found in the blank (relative to the internal standard) and the amount of products produced (relative to the internal standard). In all cases, the mass balance was greater than 90%.

2.5 Time-Resolved Laser Flash Photolysis

2.5.1 Experimental Setup

The basic laser flash photolysis setup is shown in Figure 2.3. In the current studies, the excitation source is a Lumonics Excimer laser (1, model EX-510) operated with a Xe/HCl gas mixture (308 nm, $\leq$ 40 mJ/pulse). Typically, the laser pulse energies are attenuated to less than 20 mJ/pulse through the use of neutral density filters ((6), 63%, 40%, 25% and 10% are available). The laser beam is reoriented using a mirror (3) and then concentrated, but not focused using a spherical lens (7). A prism (5) is used to alter the course of the laser beam so that it

strikes the sample holder (15), after being further concentrated by a spherical lens (8), at 90° relative to the monitoring beam.

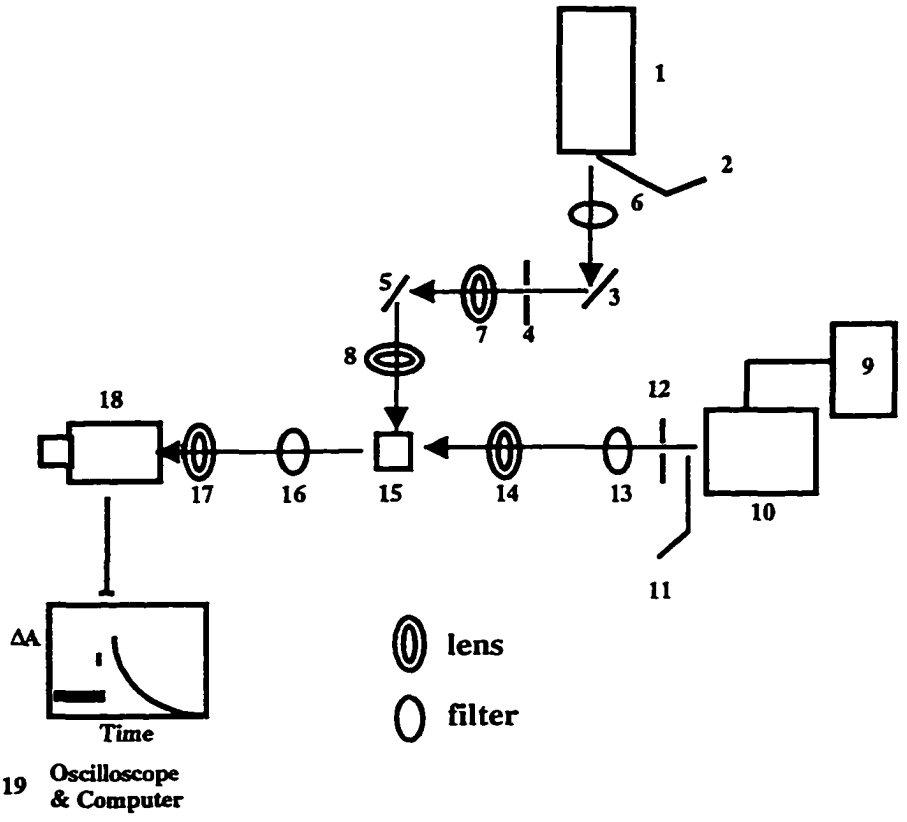

Figure 2.3: Schematic setup of the laser flash photolysis apparatus. (2) and (11) are mechanical shutters, (4) and (12) are electronic shutters. See text for more details.

A 150 W xenon lamp ((10), Oriel housing model 66057, PTI power supply model LPS-220) is used as the light source for the monitoring beam. The pulser ((9), custom built, University of Victoria) can create high intensity light for a period of 4 ms upon triggering and is connected to the xenon lamp. The analyzing beam passes through a cut-off filter ((13), no filter, 320 nm, 375 nm, 435 nm or 590 nm) to ensure that little degradation of the sample takes place due to constant irradiation by the xenon lamp during the period of data accumulation. The beam is focused (14) so that the focal point lies just behind the sample. The beam passes through a pinhole on the sample holder. After passing through the sample, the monitoring beam proceeds through another cut-off filter (16) to ensure that the detection system does not observe overtones of the wavelength being monitored and scattered laser light. The beam then proceeds through a focusing lens (17) to collimate the beam. Both filters are set by the computer (see below) so that the wavelength being monitored is no less than 20 nm above the set cut-off wavelength.

For the studies involving magnetic fields, where the magnet (21) does not provide access for the laser beam at 90° to the monitoring beam, another prism (20) is aligned at an angle of ~20°C with respect to the sample holder (Figure 2.4). This setup induces the formation of reflections that can be easily detected by the photomultiplier tube. In addition, the pinhole is no longer able to be part of the metal sample holder because the metal backing reflects the laser light directly towards the detector. The cell holder used for magnetic field studies has no back wall and so the pinhole normally located on the backside (relative to the new laser alignment) has to be situated ~ 2 cm from the sample holder. The beam through the cell has a diameter between 3 and 5 mm and the laser beam is always larger than the monitoring beam. To further reduce the number of reflections from the laser flash, an iris (22) is positioned before the collimating lens.

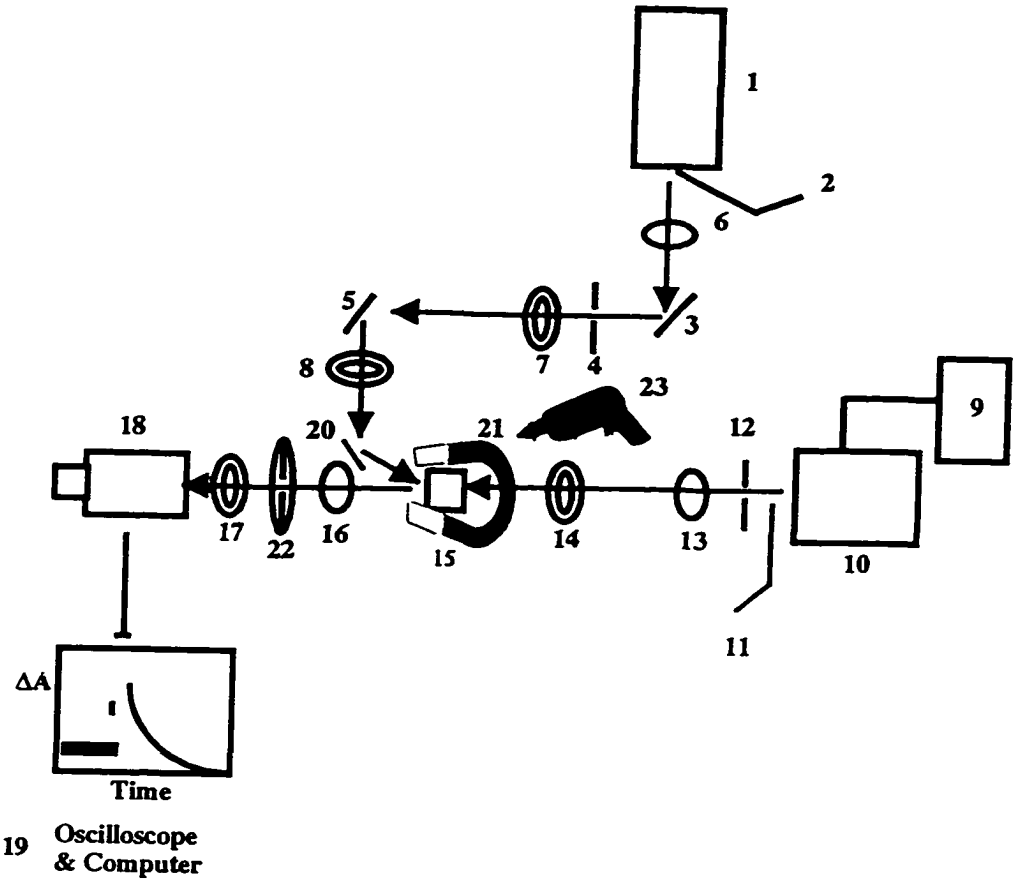

Figure 2.4: Schematic setup of the laser flash photolysis apparatus for magnetic field experiments. See text for more details.

A photomultiplier ((18), Hamamatsu R446) coupled to a monochromator (CVI Digikrom 240) is used to monitor light intensities at fixed wavelengths. Signals from the photomultiplier tube are directed to a baseline compensation unit[12]

that offsets the light intensity before the laser pulse. The signal is transferred to a digital oscilloscope ((19), Tektronix, TDS 520) and to the computer.

2.5.2 Timing and Experimental Measurements in LFP

The system is set up so that the laser fires during the stable region of the lamp pulse (1.6 ms after the start of the lamp pulse). When a transient is being monitored over a time scale greater than 20 μs, a baseline shift due to the profile of the lamp pulse is observed and must be corrected for. The baseline correction shot is performed immediately following the signal shot and is a new signal collected in the absence of a laser pulse. The correction is carried out after data transfer to the computer. This corrected signal corresponds to the subtraction of the baseline from the signal for each pair of sequences, *i.e.* signal shot and baseline shot.

Software written on the Labview 4.0 platform (National Instruments, Dr. L. Netter) controls all the experimental settings, subtracts correction shots, transforms voltage data tracked from the oscilloscope into absorbance values ($\Delta A = -\log (1 - ((V_t)_{corrected}/V_o))$), averages sets of measurements and also allows for storage of the data. The relationship between voltage and absorbance as shown above is derived from the fact that the measured voltage is obtained directly from the photomultiplier tube voltage output. This output corresponds to the amount of light being transmitted through the sample. As the response of the PMT is not linear, and the relationship described above requires a linear response function, only small changes in light intensity (*e.g.* small voltage changes, corresponding to $\Delta A \leq 0.2$) are measured.

2.5.3 LFP Data Analysis

The decay curves are fit with a program written in C by Dr. A.D. Kirk (University of Victoria) based on Levenberg-Marquardt algorithms that was interfaced into Labview. Alternatively, Kaleidagraph™ (Synergy Software version 3.08) was used to fit the data.

2.5.4 Experimental Methods

Samples (7 mm × 7 mm Suprasil quartz cells) were deoxygenated prior to irradiation by bubbling nitrogen through the solution for at least 20 min. Samples utilized in kinetic studies had ground state absorbances of ~0.3 in 7 mm × 7 mm cells at the wavelength of excitation and contained ~2 mM ketone in the solution. If required, samples were brought to the requisite temperature in a water bath prior to being subjected to the laser flashes. As ketone photoionization is known to be a problem at high laser energies,[141] the absorption in LFP experiments due to solvated electrons (usually monitored at 680 nm) was minimized by attenuating the laser energy. Typically, each cell was flashed with fewer than 20 shots so that sample decomposition was minimized. Transient kinetic traces were averaged for 5-10 shots. Unless otherwise specified, experiments were conducted at 20±2°C. In LFP experiments, the same paint stripper used in the steady-state state studies was used to heat the samples. The hot air blower was placed at suitable distances from the sample holder and the temperature was monitored with a thermocouple placed in the solution away from the irradiated (or monitored) area.

The benzyl radical decay was monitored at 317 nm for DBK and 4-MeDBK and 320 nm for 4-*t*-butylDBK. The random recombination reaction corresponds to a bimolecular process, and the decay kinetics depends on the benzyl radical concentration. Since the value for the molar absorptivity of the benzyl radical and

the pathlength (5-7 mm) for a front face alignment of the laser are uncertain, second order rate constants were measured as $2k/\varepsilon l$ values. In order to be able to quantify the small changes observed for $2k/\varepsilon l$ in the presence of a magnetic field, the initial ΔA values for the benzyl radical were matched by adjusting the delivered laser energy with neutral density filters. No significant decomposition of DBK, 4-MeDBK or 4-*t*-butylDBK (checked by UV-Vis absorption spectroscopy) occurred during the experiment due to the limited irradiation of each sample.

CHAPTER 3: MICELLES - RESULTS AND DISCUSSION

3.0.1 Behaviour of Radicals in Micelles

Micelles are spherical, fairly disordered aggregates that are made up of amphiphilic surfactant monomers. They possess a hydrophobic core, so apolar molecules have a tendency to be solubilized by these macroassemblies. The ketone probes employed here probably reside at the interface between the micelle and water phases. Our primary goal was to use these "simple" systems to understand work completed in vesicles (Chapter 4). Typically, the dynamics and reactivity of radicals in these systems has been ascribed to structural ramifications such as rigidity, organization and shape. The combination of steady-state and time-resolved experiments discussed in this Chapter reveal that although the structure plays a large role under certain system conditions, there are other factors which must be taken into account in order to explain radical mobility in organized systems. Results obtained using magnetic field and temperature effects on the dynamics of radical pairs are discussed in this section.

3.1 Steady-State Photolysis

As discussed in Chapter 1, photolysis of asymmetric dibenzyl ketone derivatives leads to product distributions that are dependent on the existence of a supramolecular cage and the magnitude of an applied magnetic field. In this section, the quantification of photoproducts under various experimental conditions is considered.

3.1.1 4-Methyldibenzyl Ketone

The use of an asymmetric dibenzyl ketone derivative is imperative for direct product analysis, because photolysis of DBK (and other symmetric derivatives)

primarily leads to the formation of a single photoproduct. The study began with 4-methyldibenzyl ketone as its photochemistry has been established for some time.[62,68,142,143] All of the results obtained at room temperature are identical to those obtained by others.[68,144] Upon exposure to UV light, the ketone yields three products as shown in Scheme 1.

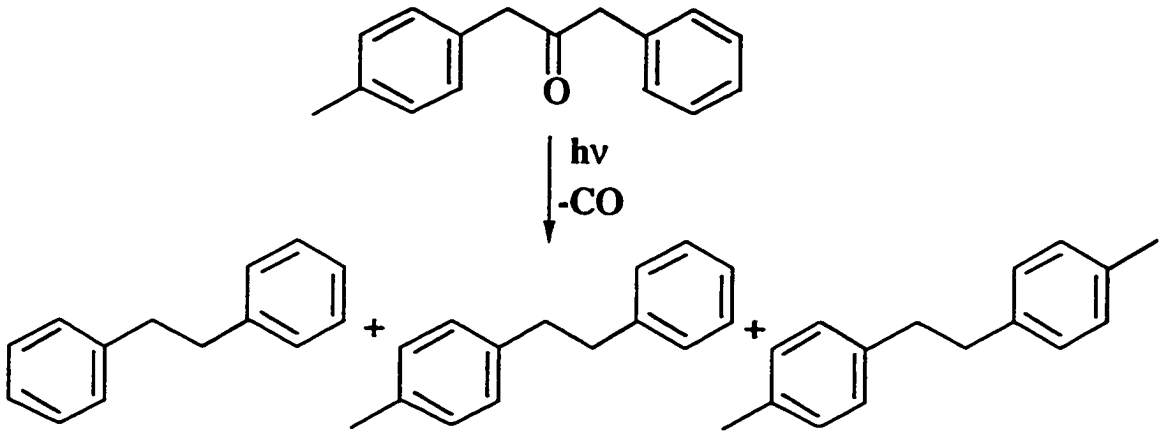

Scheme 3.1: Formation of products from the photolysis of 4-methyldibenzyl ketone

Gas chromatography allows quantitative determination of the photoproducts following extraction of the products from SDS micelles. The cage effect (Equation 1.11) relates the excess of the asymmetric product to the total amount of diarylethanes formed. For comparison, it was necessary to determine the observed cage effect in homogeneous solution. Photolysis of a 2 mM 4-MeDBK/n-hexane solution at 0 kG led to a cage effect of (0±1)% (3 experiments) as expected. A typical chromatogram is shown in Figure 3.1.

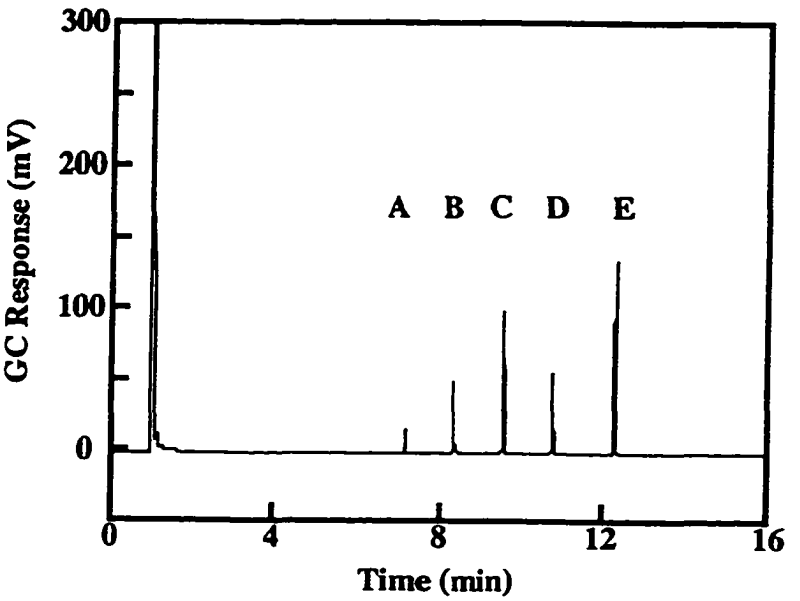

Figure 3.1: Gas chromatogram obtained after photolysis of 4-MeDBK in n-hexane at 20°C. Peaks labeled A, B, C, D and E are diphenylmethane, bibenzyl, 4-methylbibenzyl, 4,4'-dimethylbibenzyl and 4-MeDBK, respectively. The retention times are slightly different on this run from those presented below due to a slightly different initial oven temperature (110°C).

3.1.1.1 4-Methyldibenzyl Ketone in SDS Micelles

More geminate product is expected to form in the presence of supramolecular cages. SDS micelles increased the cage effect value thereby showing that more asymmetric product was formed relative to photolysis in homogeneous solution. A characteristic gas chromatogram is shown in Figure 3.2.

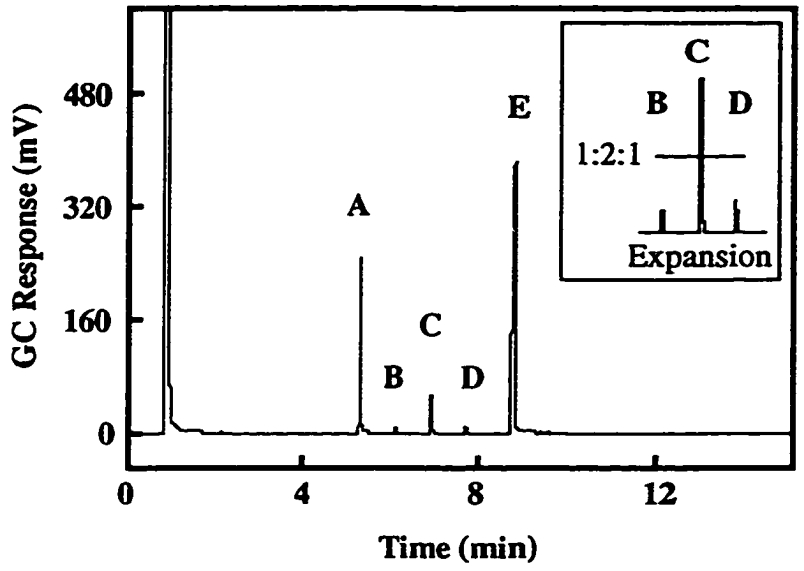

Figure 3.2: Gas chromatogram obtained after photolysis of 4-MeDBK in 0.1 M SDS at 20°C. Peaks labeled A, B, C, D and E are diphenylmethane, bibenzyl, 4-methylbibenzyl, 4,4'-dimethylbibenzyl and 4-MeDBK, respectively. The inset is an expansion of peaks B, C and D. The horizontal line shows the level of peak C if there was a 1:2:1 ratio for B:C:D.

3.1.1.2 Effect of Applied Magnetic Fields and Temperature

Figure 3.3 highlights the effect of applied external magnetic fields on the formation of products in SDS micelles. The application of a magnetic field decreases the cage effect. This was anticipated because magnetic fields reduce the rate of intersystem crossing which consequently increases the amount of products derived from escape pathways (*cf.* 1.7.5). For comparison, the photolysis of a 2 mM 4-MeDBK/n-hexane solution at 2.7 kG led to a cage effect of (0.0±0.5)% (3 experiments).

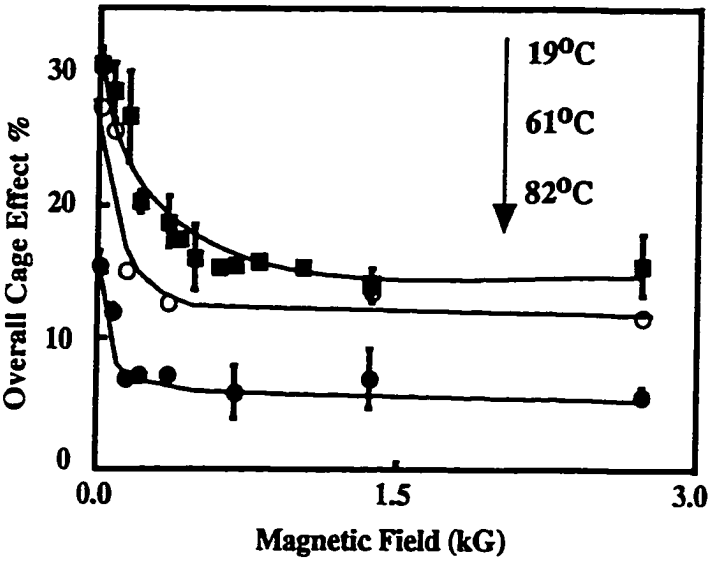

Figure 3.3: Effect of applied magnetic fields and temperature on the formation of photoproducts from 4-MeDBK in SDS.

In the Earth's magnetic field, a cage effect of 31%, 27% and 16% was observed for the photolysis of 4-MeDBK in the presence of 0.1 M SDS at 19°C, 60°C and 80°C, respectively. Table 3.1 lists the pertinent data, their associated errors and the number of times the cage effect was measured at the specific magnetic field.

Table 3.1: Cage effect data for 4-MeDBK in SDS micelles The errors represent average deviations for all trials. The number of experiments is listed in parentheses and blank entries refer to unattempted experiments.

MF (kG)	Cage Effect % (19 ± 2) °C	Cage Effect % (60 ± 2) °C	Cage Effect % (80 ± 2) °C
0.00	31 ± 1 (6)	28 ± 1 (3)	16 ± 1 (4)
0.07	29 ± 2 (6)	26 ± 1 (3)	15 ± 1 (4)
0.14	27 ± 3 (5)	15 ± 1 (3)	7 ± 1 (4)
0.20	21 ± 1 (6)		7 ± 1 (4)
0.34	19 ± 2 (5)	13 ± 1 (3)	7 ± 2 (4)
0.40	18 ± 1 (1)		
0.47	16 ± 3 (5)		
0.60	16 ± 1 (1)		
0.68	16 ± 1 (4)		6 ± 2 (4)
0.80	16 ± 1 (1)		
1.02	16 ± 1 (3)		
1.36	14 ± 1 (4)	14 ± 1 (3)	7 ± 2 (4)
2.71	16 ± 2 (7)	12 ± 1 (3)	6 ± 1 (4)

The results at the lowest temperature are similar to those reported earlier.[68,145] The effect of Zeeman splitting (*cf.* Figure 1.6) implies that at higher magnetic fields interconversion between $T_{\pm}$ and S_0 is almost completely shut down. At this point, it is wise to remember, that at low field strengths in this study, it is the hyperfine interactions that are controlling the amount of ISC, but at larger fields Zeeman splitting determines the rate of intersystem crossing.

The $H_{1/2}$ value is defined as the magnetic field at which an experimental observable is decreased by half. This parameter displays the sensitivity of this observable to magnetic fields. As the reaction becomes more susceptible to magnetic fields, the $H_{1/2}$ value decreases. This decrease would suggest that a smaller magnetic field can bring about the same change in the observed rate constant or product distribution when one compares the reaction under two sets of experimental conditions.

As the temperature is raised, the $H_{1/2}$ value decreases, suggesting that at higher temperatures the cage effect is more sensitive to the application of a magnetic field. Table 3.2 lists the approximate $H_{1/2}$ values for 4-methyldibenzyl ketone photolysis in SDS micelles. Although the errors in Table 3.2 are fairly large, experiments completed at 20°C always had a larger $H_{1/2}$ value than those done at 80°C.

Table 3.2: Sensitivity of the cage effect to magnetic fields at different temperatures for 4-MeDBK. The values shown are averages, errors are estimates. The number of experiments is shown in parentheses.

Temperature (±2°C)	$H_{1/2}$ (G)
19	200 ± 60 (5)
61	80 ± 30 (3)
82	40 ± 30 (4)

3.1.2 4-*t*-Butyldibenzyl Ketone

Upon photolysis, 4-*t*-butyldibenzyl ketone (4-*t*-butylDBK) yields three primary photoproducts in a similar manner as for 4-MeDBK. The 4-*t*-butylDBK photolysis products were analyzed in an identical manner to that for the 4-methyl derivative of DBK. A point of interest is that the signals obtained from gas chromatography differed in retention times. Due to the additional size and contribution to boiling point of the *t*-butyl moiety relative to methyl, 4,4'-di-*t*-butylbibenzyl (4,4'-dtBB) has a retention time even longer than the starting ketone (Figure 3.4).

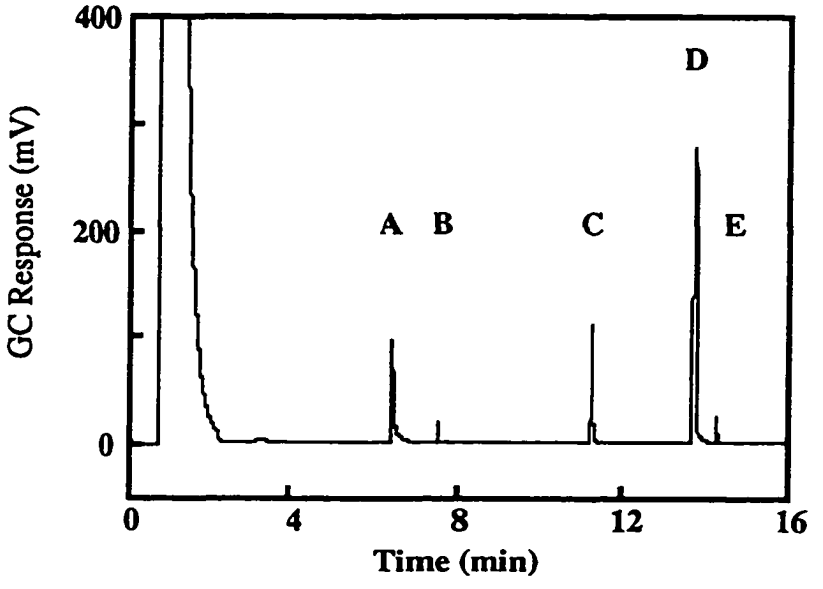

Figure 3.4: Gas chromatogram obtained upon photolysis of 4-*t*-butylDBK in SDS micelles. Labels A through E represent diphenylmethane, bibenzyl, 4-*t*-butylbibenzyl, 4-*t*-butylDBK and 4,4'-di-*t*-butylbibenzyl, respectively.

3.1.2.1 Effect of Applied Magnetic Field and Temperature

Upon photolysis of *t*-butylDBK in n-hexane, a cage effect of 1±1% (2 exp) was obtained. This is expected because it represents a 1:2:1 product distribution. The presence of micelles increased the cage effect, whereas the application of magnetic fields decreased this value in the presence of micelles. The absolute magnitude of the cage effect value strongly increases with an increase in probe hydrophobicity.[68] This was dramatically witnessed as the cage effect for 4,4'-di-*t*-butyldibenzyl ketone was determined to be 95% in cetyltrimethylammonium micelles.[68] In our case, the mono *t*-butyl derivative had a cage effect of 75% thereby suggesting that the increased hydrophobicity leads to a greater enhancement of asymmetric product. Figure 3.5 demonstrates the effect of magnetic field and temperature on the product enhancement (Table 3.3).

Table 3.3: Sensitivity of the cage effect to magnetic fields at different temperatures for 4-*t*-butylDBK. The values shown are averages, errors are average deviations between runs. The number of experiments is shown in parentheses. The blank entry represents an unattempted experiment.

MF (kG)	Cage Effect % (20±2) °C	Cage Effect % (80±2) °C
0.00	75 ± 3 (3)	63 ± 4 (3)
0.07	76 ± 2 (3)	54 ± 6 (3)
0.14	71 ± 4 (3)	52 ± 5 (3)
0.20		51 ± 6 (3)
0.34	73 ± 3 (3)	53 ± 7 (3)
0.47	70 ± 2 (3)	50 ± 5 (3)
0.68	66 ± 4 (3)	48 ± 7 (3)
1.35	61 ± 2 (3)	41 ± 2 (3)
2.71	56 ± 2 (3)	47 ±1 (3)

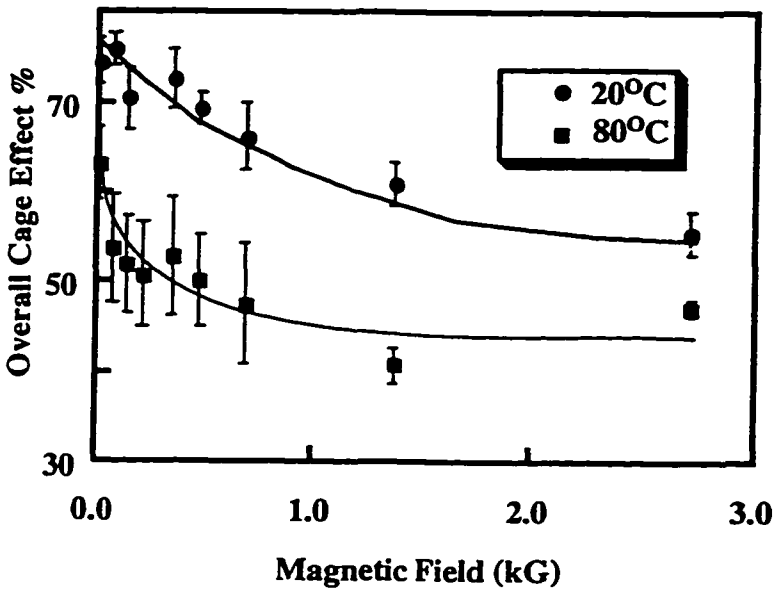

Figure 3.5: Effect of applied magnetic fields and temperature on the photolysis of 4-*t*-butylDBK in SDS micelles. Errors are average deviations.

Upon perusal of Figure 3.5, it is apparent that the $H_{1/2}$ values decrease as the temperature increases. In a similar manner to 4-MeDBK, this implies that the reaction is more sensitive to magnetic fields at higher temperature. The fact that the $H_{1/2}$ values are significantly higher than those observed for 4-MeDBK is also noteworthy.

Table 3.4: $H_{1/2}$ values for 4-*t*-butylDBK photolysis in SDS micelles. The number of experiments is in parentheses

Temperature (±2°C)	$H_{1/2}$(G)
20	≥450 ± 100 (3)
80	200 ± 40 (3)

3.2 Time-Resolved Laser Flash Photolysis

3.2.1 4-Methyldibenzyl Ketone

3.2.1.1 4-Methyldibenzyl Ketone in Homogeneous Solution

Laser flash photolysis allows us to observe transients on a nanosecond to microsecond time scale. It is well known that benzyl radicals have absorptions in the UV, and the tolyl (*p*-methylbenzyl) radical is no exception.[146-148] Figure 3.6 illustrates the transient spectrum derived from 308 nm excitation laser flash photolysis of 4-MeDBK. The absorption maximum occurs at 317 nm, which is in accord with previous reports.[148]

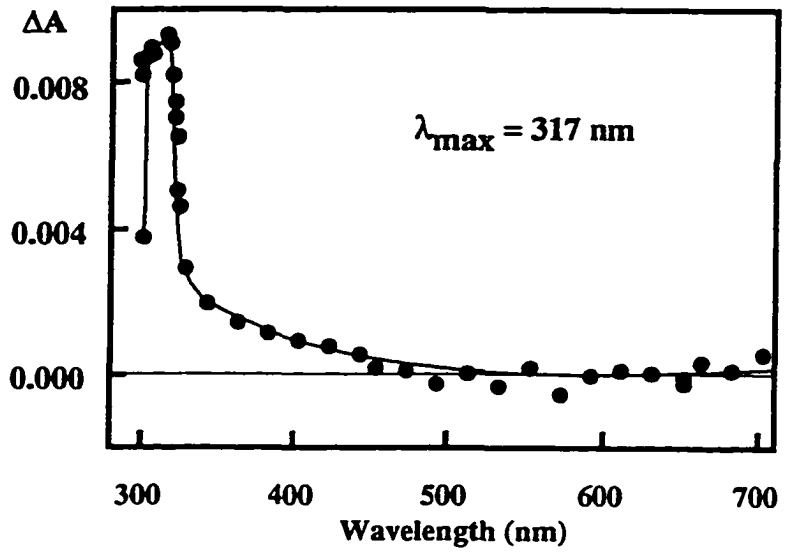

Figure 3.6: Transient spectrum of 4-MeDBK in n-hexane. The spectrum was taken 2.6 μs after the 308 nm laser pulse.

Most of the radicals are formed within the laser pulse (~10 ns). However, there is some delayed formation of the transient monitored at 317 nm (Figure 3.7A). This is followed by a slow, second order decay (Figure 3.7B). This behaviour is identical to that observed for DBK.[58,59] The fast growth in the photolysis of DBK corresponds to the decarbonylation of the phenylacetyl radical to form a benzyl radical, while the second order decay is ascribed to the recombination of two benzyl radicals. The decay of the radical monitored at 317 nm proceeds to the baseline over the experimental time scale indicating that all of the benzyl radical has reacted. In the absence of O_2 and at room temperature in methanol, the rate constant for the decarbonylation process is 4×10^6 s^{-1}. The value of $2k/\varepsilon l$ for the slow recombination process is 3×10^6 s^{-1} (*cf.* section 2.5.4 and 3.2.1.4).

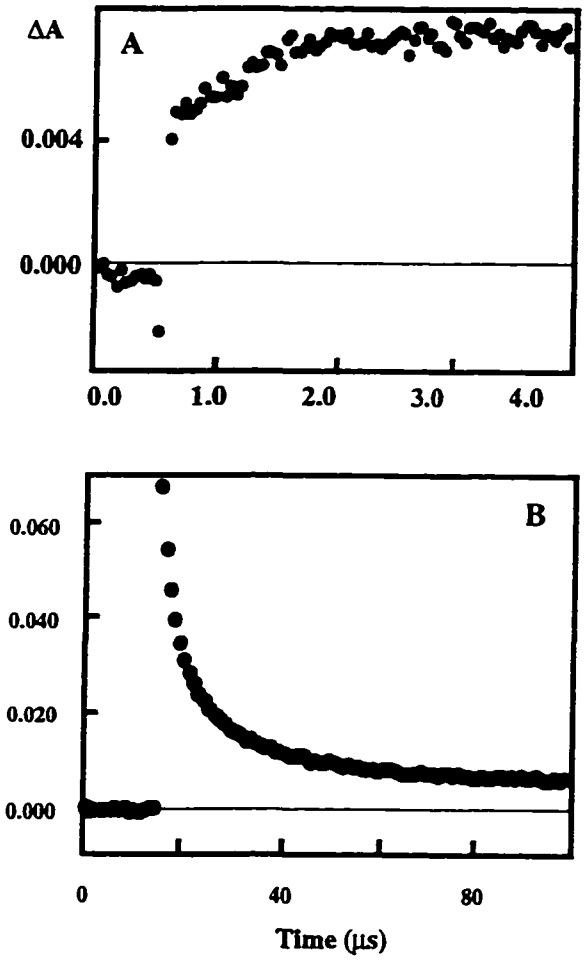

Figure 3.7: Kinetics of 4-MeDBK monitored at 317 nm in methanol at (A) fast and (B) slow time scales.

The kinetics observed for 4-MeDBK are qualitatively identical as that observed for DBK in both homogeneous solution[58,59,146-148] and in SDS micelles.[69,72,74] The laser energy was attenuated so that photoionization (as is

common for many aromatic ketones)[141] does not occur. Specifically, this is a requirement in polar solvents such as methanol as well as in anionic micelles.[141] The rate constants for decarbonylation and random encounters are identical for DBK and 4-MeDBK within experimental error.

3.2.1.2 4-MeDBK in SDS Micelles - Geminate Processes

The spectral absorption maximum shown in Figure 3.6 is unchanged in aqueous solutions of SDS micelles. However, the kinetics monitored at 317 nm are remarkably different. Initially, there is a fast, first order decay (k_{fast}) with a lifetime of 70 ± 5 ns (50 ± 5 ns for DBK) that accounts for ~ 60% of the benzyl radicals formed within the laser pulse. For DBK, this decay has been attributed *principally* to the recombination of the primary geminate radical pair (benzyl and phenylacetyl radicals (*cf.* 1.6.3).[72] Figure 3.8 illustrates that the decay does not extend all the way down to the baseline ($\Delta A_{\infty} \neq 0$). This indicates that long-lived benzyl radicals are present after the geminate reaction is complete. This fact was seen as evidence for escape of a radical from a micelle in the benzophenone-SDS system[49,50] and others have already extrapolated this notion to the DBK/SDS system.[72,74]

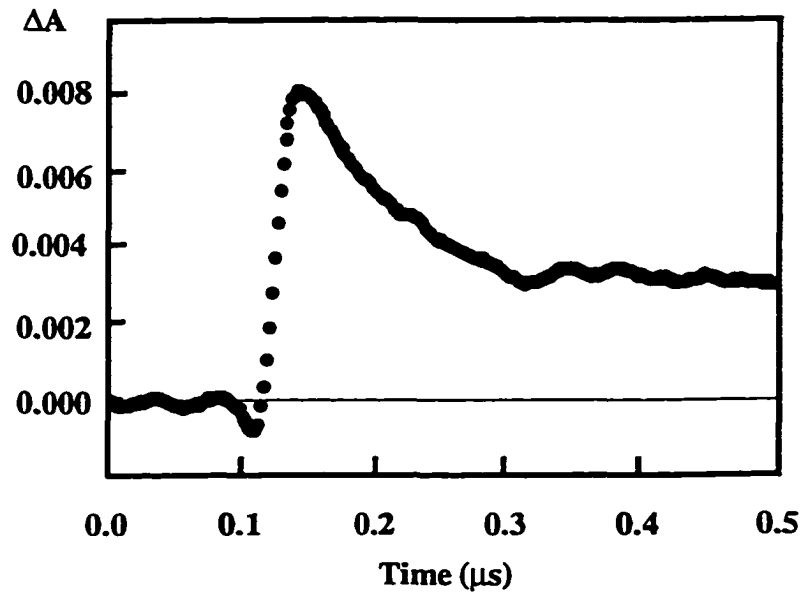

Figure 3.8: Decay of the primary geminate radical pair derived from 4-MeDBK in SDS micelles.

3.2.1.2.1 Effect of an Applied Magnetic Field on the Kinetics of the Geminate Processes

As the applied field strength increases, one expects that more radicals are able to escape from the micelle. This can be seen in Figure 3.9 where as the external field strength was increased so did the amount of residual absorbance that existed at the end of the fast time scale. Also, no significant effect due to magnetic fields was observed on k_{fast}. As noted in section 1.6.3, others reported[69,72] small effects of magnetic fields on k_{fast} that may have been within their experimental error. Note that the same concentration of radicals was formed (same ΔA_{max}) upon laser excitation.

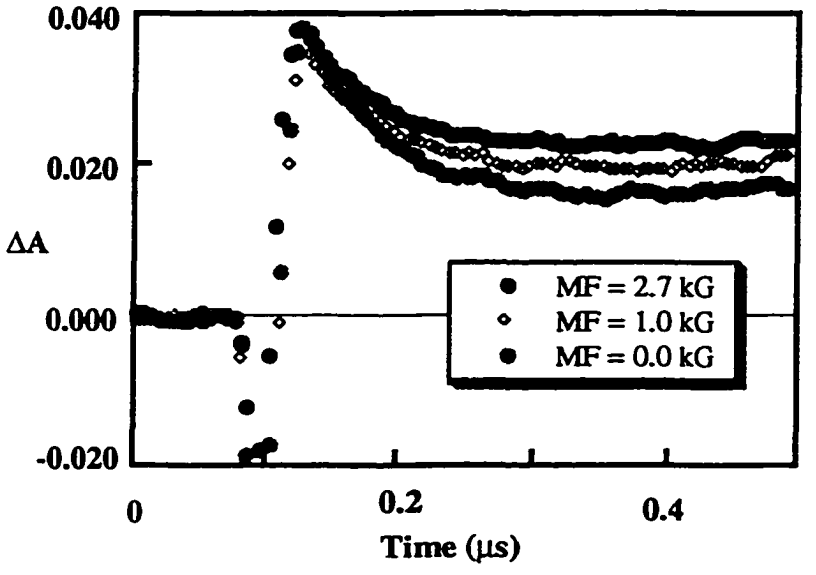

Figure 3.9: Effect of magnetic fields on the decay of the geminate radical pairs derived from 4-MeDBK in SDS micelles. The negative ΔA values immediately following the laser pulse are caused by scattered light entering the detector because of the geometric arrangement of the laser and sample holder (*cf.* section 2.5.1).

3.2.1.2.2 Effect of Temperature on the Kinetics of the Geminate Processes

Figure 3.10 displays the effect of temperature on the decay of the fast process. The initial ΔA_{max} increases as the temperature is raised. This implies that there are more radicals being formed at higher temperatures within the laser pulse. As this fast decay mostly corresponds to the recombination of the PRP, the fact that more radicals are formed before the decay (*i.e.* within in the laser pulse) shows that there is an increase in the amount of α-cleavage leading to the PRP. In fact, in a

study pertaining to DBK, the α–cleavage rate constant increased with a corresponding increase in temperature.[65]

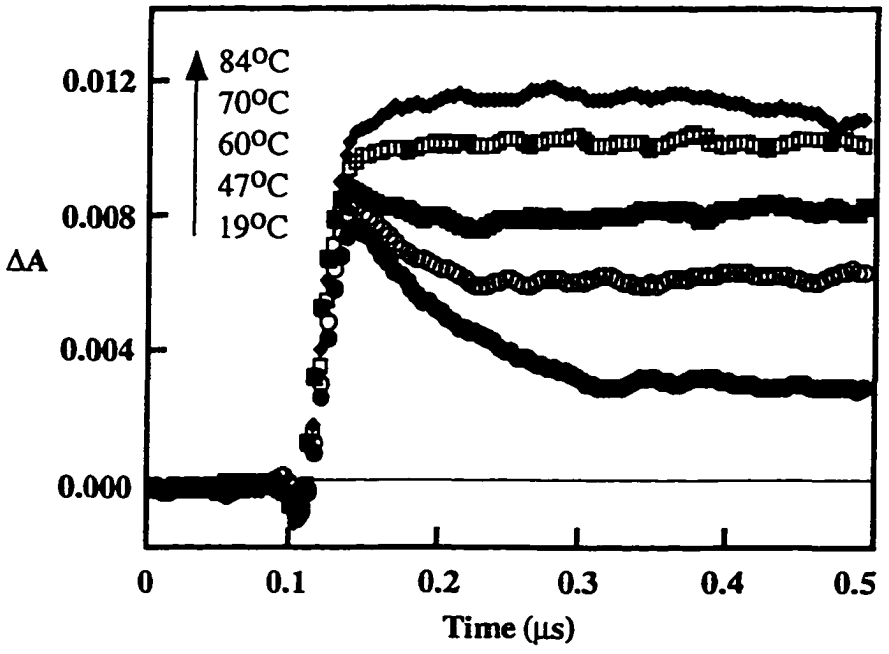

Figure 3.10: Effect of temperature on the decay of the fast process derived from 4-MeDBK in SDS micelles.

The above figure also provides evidence of faster decay rate constants for the fast component (k_{fast}) as the temperature is raised. Although the rate constant increases, the overall contribution to the decay diminishes. The decay kinetics are too fast to be detected above the 60-70°C range. Arrhenius treatment (Figure 3.11) yielded an activation energy of 4.6±0.8 kcal/mol (3 exp). From the dependence of k_{fast} with temperature (<70°C), the value of k_{fast} for 4-MeDBK at 80°C was

estimated to be 8.5×10^7 s^{-1} (~12 ns) which is beyond the time resolution of the equipment.

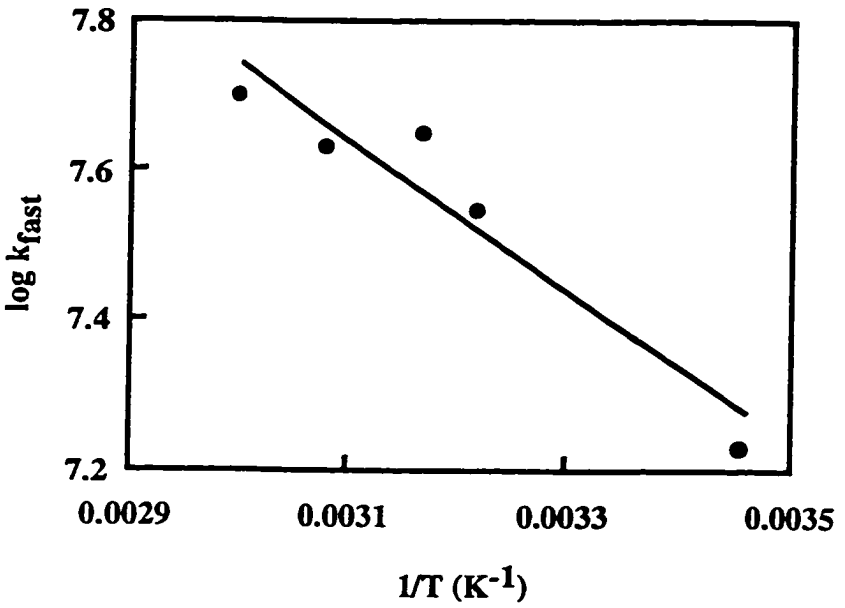

Figure 3.11: Arrhenius plot drawn to determine E_a of the fast process in SDS micelles. The plot shown is from a single experiment. Values from three experiments were obtained to yield the values quoted in the text.

In contrast to the increase of the overall benzyl radical yield, the contribution of the fast processes to the overall benzyl radical decay decreases when the temperature is raised. This contribution can be quantified by the ratio of $\Delta A_{fast}/\Delta A_{max}$, ($\Delta A_{fast}=\Delta A_{max}-\Delta A_{\infty}$, where ΔA_{∞} is the transient absorbance after completion of the fast process and ΔA_{max} is the absorbance at time=0). It is difficult to estimate ΔA_{∞} because of the contribution of the growth kinetics from the next step in the radical reaction (decarbonylation, see below), so there is considerable

amount of uncertainty in these absorbance values. The value for $\Delta A_{fast}/\Delta A_{max}$ decreases linearly with an increase in temperature up to 70 °C, above which no fast decay is observed (Figure 3.12).

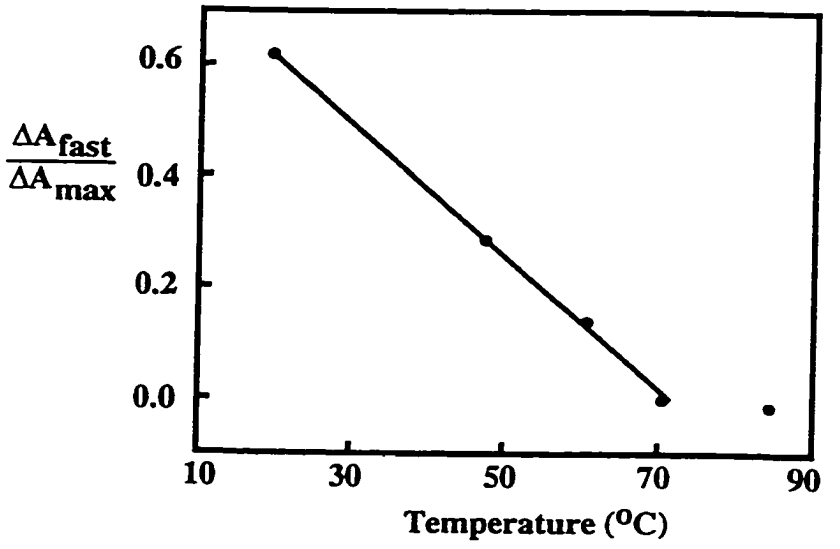

Figure 3.12: Effect of temperature on the proportion of radicals decaying by the fast process. This plot was taken from one experiment, but other experiments yielded similar results.

The sum of k_{gem} and the exit rate constant (k_{-}) is equal to k_{fast}. It is worth noting that an increase mainly in k_{gem} would have increased the $\Delta A_{fast}/\Delta A_{max}$ ratio (Figure 3.12) because more radicals would recombine via the geminate pathway. Therefore, the increase in k_{fast} is due to an increase in the exit rate constant as demonstrated by the decrease of the ratio of ΔA_{fast} with respect to ΔA_{max}.

3.2.1.3 4-MeDBK in SDS Micelles - Decarbonylation Process

At room temperature, the decay kinetics of the primary radical pair is followed by a modest first order growth (k_{-CO}) with a lifetime of 450 ± 20 ns (400 ± 20 ns for DBK) that for DBK was characterized to be the decarbonylation of the phenylacetyl radical.[72] Figure 3.13 shows the growth that follows the fast decay when the transient is monitored at 317 nm. This process does not involve a radical pair and so magnetic fields do not affect the rate of reaction.

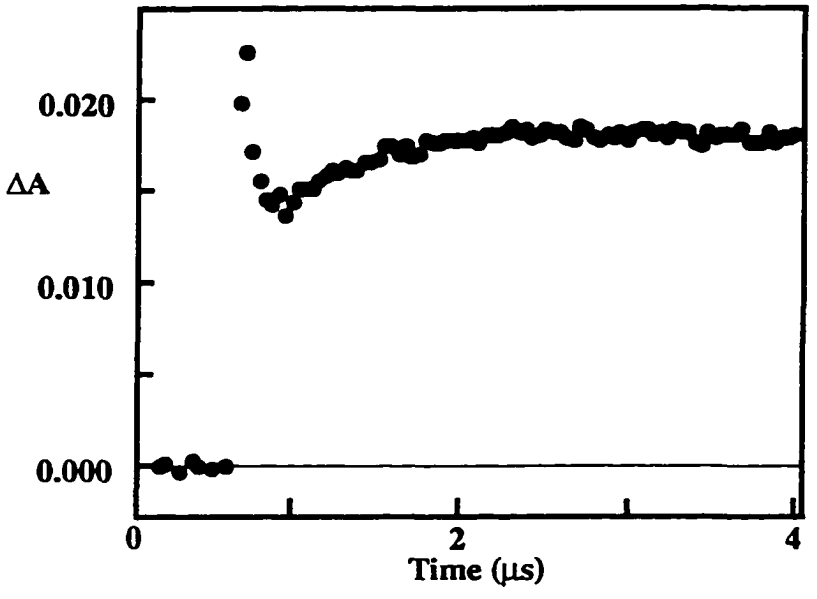

Figure 3.13: Growth due to the formation of the benzyl radical derived from the phenylacetyl radical upon photolysis of 4-MeDBK in SDS micelles.

3.2.1.3.1 Effect of Temperature on the Decarbonylation Process

As the temperature is increased above 20°C, the rate constant for decarbonylation increases. Above 60-70°C, an initial fast growth is the predominant process observed at the expense of the geminate decay component (Figure 3.10). At the higher temperatures, the kinetics are qualitatively similar to

those observed at room temperature in homogeneous solution such as hexane where no fast decay is seen.

3.2.1.3.2 Effect of Solvent Polarity on the Decarbonylation Process

Investigation into the dependence of the rate constant of decarbonylation after DBK cleavage on solvent polarity has been reported by others. It was determined that the rate constant for this unimolecular process decreases with solvent polarity.[58-60] In this work, the activation energy was ascertained by an Arrhenius treatment (T range = 292-353 K, r^2=0.992) to be 8.0 ± 0.9 kcal/mol with log A (s^{-1}) = 12 ± 2 in SDS micelles. The corresponding rate constant at 27°C (3.5×10^6 s^{-1}) is even slower than the rate constant in methanol. Thus, the result obtained here agrees well with that of Cozens *et al.* and suggests that the decarbonylation takes place in an environment more polar than methanol.[72] Due to the large discrepancy between k_{CO} in SDS micelles and that in methanol (5.2×10^6 s^{-1}), we propose that the decarbonylation occurs primarily in the aqueous phase.

3.2.1.4 4-MeDBK in SDS Micelles - Random Radical Recombination

At 20°C, slow, second order decay kinetics with a 2k/εl value of 1.4×10^6 s^{-1} (see below) follows the first order growth. For DBK, this was assigned to the random recombination of two benzyl radicals that occurs after exit from the micelle,[72-74] and its kinetics is similar to the latter part of the decay observed in homogeneous solution. The rate constant for the bimolecular random encounters is expressed as 2k/εl values (rate constant product), where k is the recombination rate constant, ε is the molar absorptivity of the benzyl radical and l is the cell pathlength.

The rate constant must be expressed as this product because neither the pathlength nor molar absorptivity is known. The analysis was carried out by plotting the dependence of the reciprocal absorbance and time. The slope of this straight line plot is equal to $2k/\varepsilon l$.

3.2.1.4.1 Temperature Effect on Random Radical Recombination

An increase in temperature generally decreases the viscosity of solutions which consequently increases diffusional rates. The value for $2k/\varepsilon l$ increases from $1.4 \times 10^6\ s^{-1}$ to $5.0 \times 10^6\ s^{-1}$ when the temperature is raised from 19°C to 80°C (Figure 3.14), which is consistent with a decrease of the solvent viscosity as demonstrated by others.[146,149]

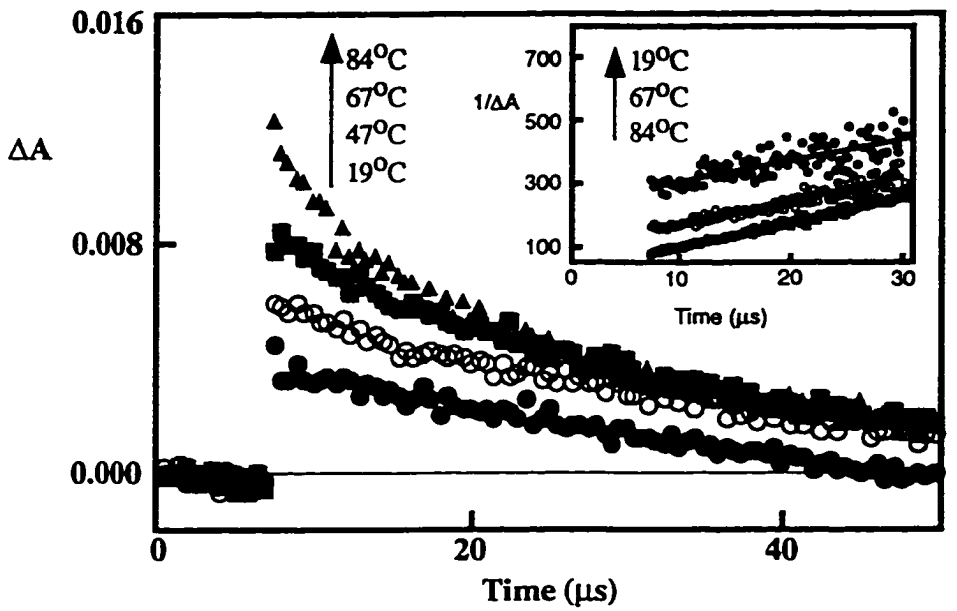

Figure 3.14: Effect of temperature on the random radical encounters derived from the photolysis of 4-MeDBK in SDS. The inset reveals the linear plots of reciprocal absorbance vs. time for 19°C, 67°C and 84°C. All $2k/\varepsilon l$ values were obtained from similar plots.

On these timescales, a significant increase is observed for the initial absorbance (ΔA_{max}) when the temperature is raised. It is important to note that this increase is larger than that observed for the value of ΔA_{max} of the fast component (due to faster α-cleavage, Fig. 3.10). This shows that most of the increase of benzyl radical yield is due to a more efficient decarbonylation and exit process. Hence, in terms of ΔA values, the higher photo-α-cleavage yield is related to a smaller contribution of the recombination from the primary radical pair.

3.2.1.4.2 Effect of Applied Magnetic Fields on Random Radical Recombination

The magnetic field effect on this process was studied in the same fashion as reported by Cozens and Scaiano,[72] and a decrease of the 2k/ϵl values with the application of an external magnetic field was observed at all temperatures (Figure 3.15, Table 3.5).

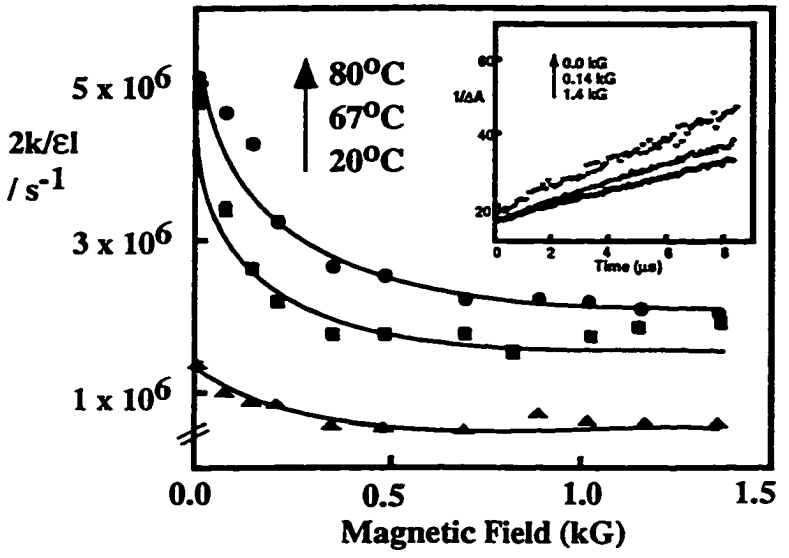

Figure 3.15: Effect of temperature on the rate constant product 2k/εl. The inset shows typical experimental data at 67°C to yield the value of 2k/εl. The main plots are derived from a single experiment and the value of 2k/εl varied by as much as 15% between experiments.

Table 3.5: Effect of magnetic field and temperature on the second order rate constant product ($2k/\varepsilon l$). The values are from a single experiment and varied by as much as 15% between experiments. Errors are derived from the best-fit straight line ($1/A = 1/A_{max} + 2kt/\varepsilon l$).

Magnetic Field (kG)	$2k/\varepsilon l$ /10^6 s^{-1} (20 ± 2) °C	$2k/\varepsilon l$ /10^6 s^{-1} (67 ± 2) °C	$2k/\varepsilon l$ /10^6 s^{-1} (80 ± 2) °C
0.0	1.4 ± 0.1	3.8 ± 0.1	5.0 ± 0.1
0.07	1.0 ± 0.1	3.4 ± 0.1	4.7 ± 0.1
0.14	0.9 ± 0.1	2.7 ± 0.1	4.3 ± 0.1
0.20	0.9 ± 0.1	2.2 ± 0.1	3.3 ± 0.1
0.34	0.5 ± 0.1	1.8 ± 0.1	2.7 ± 0.1
0.47	0.5 ± 0.1	1.8 ± 0.1	2.6 ± 0.1
0.68	0.5 ± 0.1	1.8 ± 0.1	2.2 ± 0.1
0.88	0.7 ± 0.1	1.5 ± 0.1	2.3 ± 0.1
1.02	0.7 ± 0.1	1.8 ± 0.1	2.2 ± 0.1
1.15	0.7 ± 0.1	1.9 ± 0.1	2.1 ± 0.1
1.36	0.6 ± 0.1	1.9 ± 0.1	2.1 ± 0.1

As judged by the $H_{1/2}$ value, the sensitivity of the second order rate constant product decreased as the temperature was raised in an analogous manner as observed for the cage effect. The $H_{1/2}$ values shown in Table 3.6 are similar to those determined in the steady-state experiments. The errors are quite large, but the trend of increasing sensitivity with temperature is always observed.

Table 3.6: Sensitivity of 2k/εl to applied magnetic fields. The errors are estimates. The number of experiments is listed in parentheses.

Temperature (±2°C)	$H_{1/2}$ (G)
20	220 ± 50 (3)
60	120 ± 50 (3)
80	70 ± 30 (3)

3.2.1.5 Reversibility of the Temperature Effect

In a single sample, the kinetics may be obtained at room temperature and at elevated temperature. If one obtains kinetics before raising the temperature and then applies heat to the sample while taking kinetics at different temperatures, one observes the changes described above. The expected, but nevertheless good to see, aspect of this experiment is that the same kinetics are recovered at 20°C even after repeated heating and then cooling with a single sample. The thermal aspects of this reaction are entirely reversible. This description follows at all experimental time scales (*e.g.* geminate, decarbonylation or random encounter time scales).

3.2.2 4-*t*-Butyldibenzyl Ketone

Qualitatively, the *t*-butyl derivative of DBK behaves exactly the same way as the parent compound in homogeneous and microheterogeneous media. The spectral characteristics of the benzyl/*t*-butylbenzyl radical pair are very similar to that of the parent ketone and has a maximum absorption at 320 nm (Figure 3.16).

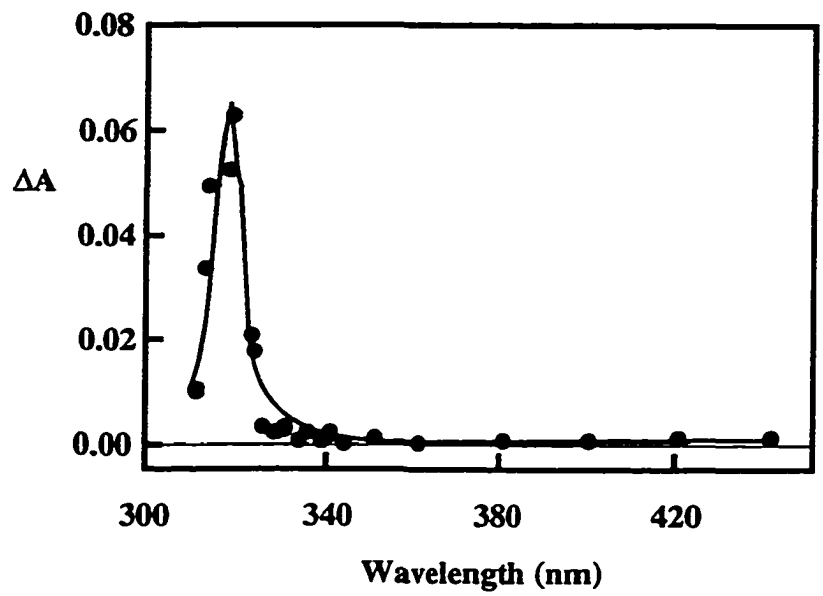

Figure 3.16: Transient spectrum of the benzyl/*t*-butylbenzyl radical pair taken 2.0 μs after the laser pulse in hexane.

3.2.2.1 4-*t*-Butyldibenzyl Ketone in Homogeneous Solution

In hexane, *t*-butylDBK has a fast growth that is followed by a slow, second order decay. It is assumed that this growth corresponds to the decarbonylation of the phenylacetyl or substituted phenylacetyl radical and that the slow, second order process is characteristic of random radical recombinations. The decarbonylation rate constant in hexane was $(1.2 \pm 0.2) \times 10^7$ s^{-1} (1 exp) and the subsequent decay ($2k/\varepsilon l$) was determined to be $(4.8 \pm 0.3) \times 10^6$ s^{-1} (1 exp).

3.2.2.2 4-*t*-Butyldibenzyl Ketone in SDS Micelles - Geminate Processes

The spectral characteristics of the transient observed in SDS micelles resembles that in n-hexane with the exception that photoionization readily occurs. In the experiments described, the formation of the hydrated electron was minimized by attenuating the laser energy. It is quite possible that the additional electron donating ability of the *t*-butyl group relative to the methyl group helps to stabilize the radical cation product of the photoionization process.

At fast time scales, the primary radical pair recombines with a rate constant of 78 ± 3 ns (2 exp). The rate constant for fast recombination and the percentage of radicals that decays at fast times is similar to that of 4-MeDBK.

3.2.2.2.1 Effect of Magnetic Field on Geminate Processes

When an external magnetic field is applied, k_{fast} remains unchanged, but the residual absorption (A_∞) increases. At all magnetic fields, the kinetics can be fit to a first order decay with a shift in the baseline (due to unreacted benzyl radicals). As for DBK and 4-MeDBK, the increase in the residual absorption implies that more radicals are escaping the micelle as the MF is increased.

3.2.2.2.2 Effect of Temperature on Geminate Processes

Figure 3.17 illustrates the effect of temperature on the geminate decay processes.

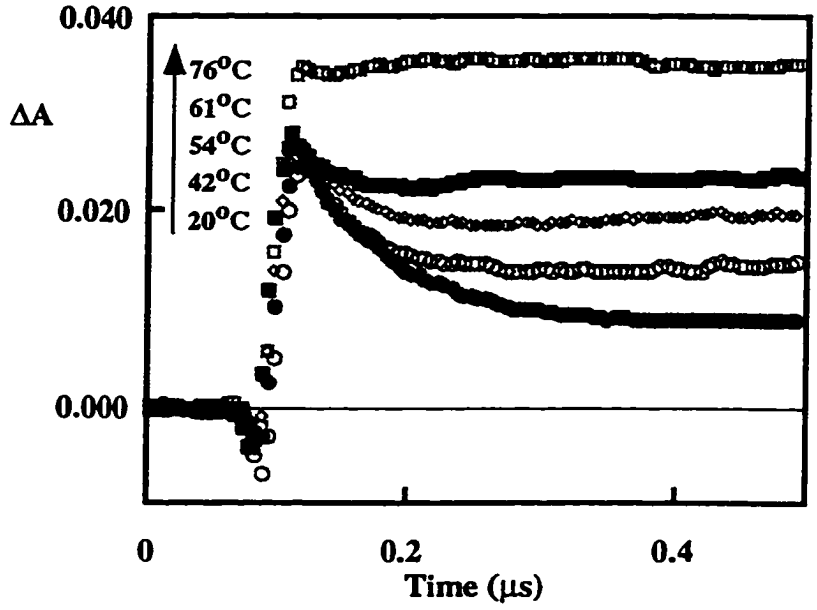

Figure 3.17: Effect of temperature on the geminate processes derived from the photolysis of 4-*t*-butylDBK.

In the above Figure, there is a small increase in the initial absorbance from 20°C to 61°C, and a large enhancement as the temperature is increased further. As seen for 4-MeDBK, the plot above may be transformed into Figure 3.18 where the dependence of the relative absorption due to the geminate processes is compared to the total absorption.

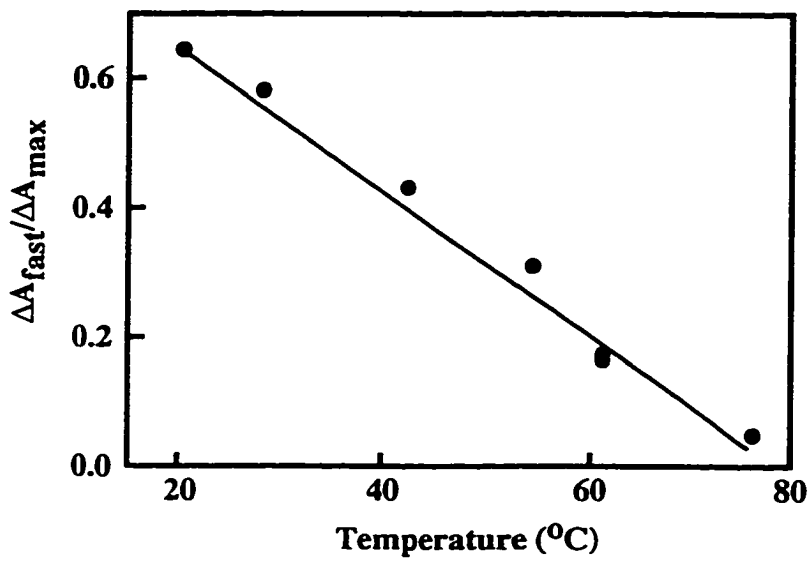

Figure 3.18: Effect of temperature on the amount of geminate recombination for 4-*t*-butylDBK in SDS micelles. This plot is derived from a single experiment. Whereas the absorbance values <70°C have an error of ~15% between experiments, the ratio of absorbances (> 75°C) was 0.03 ± 0.02 (2 exp).

This result shows that more radicals are escaping as the temperature is increased and that above 75°C either none or only a minute amount of the geminate processes are proceeding. The ΔA_{max} values increase (Figure 3.17) with temperature also demonstrating that the underlying kinetics (competitive rates of geminate recombination and decarbonylation) of 4-*t*-butylDBK operates in a similar manner to that of 4-MeDBK.

Arrhenius parameters for the fast process were determined to be log A (s^{-1}) = 10.3 ± 1.2 and E_a = 4.4±1.0 kcal/mol (293-343 K, r^2 = 0.989). Upon comparison to DBK and 4-MeDBK, these parameters remain within experimental error.

3.2.2.3 4-*t*-butylDBK in SDS Micelles - Decarbonylation

At room temperature a modest first order growth (k_{-CO}) with a lifetime of 1500 ± 270 ns (2 exp) follows the geminate decay process. This lifetime is unaffected by magnetic fields. This is over three times longer than the lifetime observed for 4-MeDBK.

3.2.2.3.1 Effect of Temperature on the Decarbonylation Process

The rate constant for decarbonylation increases as the temperature is raised. Above 74°C, an initial fast growth is the predominant process observed at the expense of the geminate decay component. Studies of the temperature dependence (293-343 K, $r^2 = 0.991$) lead to values of E_a = 10.5 ± 0.4 kcal/mol (log A (s^{-1}) = 13.5 ± 0.5, 2 exp) for the decarbonylation of *t*-butylDBK in SDS. The activation energy is larger by about 2 kcal/mol relative to 4-MeDBK and DBK.

3.2.2.4 4-t-Butyldibenzyl Ketone in SDS Micelles - Random Radical Recombination

In SDS micellar solution, the random radical recombination occurs with a 2k/εl value of $(1.5 \pm 0.1) \times 10^5\ s^{-1}$. This rate constant product is slower by over an order of magnitude compared to any of the other DBK derivatives. This implies that the radicals derived from the photolysis of 4-*t*-butylDBK do not recombine as readily as those where half of the radical pair is less hydrophobic. It is not possible to determine the magnetic field dependence of this decay because the decay is completed beyond the time resolution of the apparatus.

3.3 Discussion

In order to understand of the micelle/ketone system one must investigate all of the processes that may be occurring for all three of the probes (DBK, 4-MeDBK and 4-*t*-butylDBK) simultaneously. The initial results of a magnetic field effect on radical pair dynamics are not new,[62,64] but the temperature effects are both novel and exciting as they reveal some key attributes of radical mobility in supramolecular assemblies. In addition, the combined use of LFP and steady-state product studies in the same study enabled us to observe both the time-resolved dynamics as well as the overall reactivity of the radical pair.

With this in mind, the key observation that yields vital information regarding radical dynamics in micellar system is that at high temperatures the fast process is not observed (*cf.* Fig 3.10 and 3.17), but the cage effect derived from product studies is still significant (*cf.* Fig 3.3 and 3.5). If the fast decay process corresponds to geminate behaviour (primary and secondary), then these results cannot be reconciled by the models put forth until now, in which the cage effect was exclusively assigned to the geminate recombination process. There are two possible explanations for the observations at high temperatures: (*i*) there is a significant contribution of random encounters to the cage effect, and (*ii*) the geminate process occurs, but is faster than the time resolution of our equipment. The next section will address these issues. After reviewing these results and their ramifications, a new model will be proposed that features outcomes that are not based on structural considerations as discussed throughout Chapter 1.

3.3.1 The Geminate Process and the Cage Effect

The fast decay process has been attributed to contributions from both the primary radical pair (PRP) as well as the secondary radical pair (SRP) recombination reactions.[72] The commonality is that in both of these radical pairs,

recombination may take place before escape. It is important to realize that the cage effect determined by product studies considers *only* the products caused by recombination of the SRP.

The contribution of PRP recombination can be investigated by looking at the quantum yield of DBK disappearance. Work done by Turro *et al.* showed that this quantum yield in CTAC micelles increases from 0.30 to 0.75 when the temperature is raised from 27°C to 70°C.[65] This suggests that the contribution of primary geminate recombination to the overall photoprocesses diminishes since this reaction regenerates DBK. This is consistent with the increased benzyl yield (for 4-MeDBK and 4-*t*-butylDBK) observed as the increase in ΔA_{max} at short timescales (Figures 3.10 and 3.17). As the increase was observed for both derivatives, we can assume that the reactivity of all benzyl or substituted benzyl radicals in this study are similar to those reported in homogeneous solution.[146-148] Thus, an increase in temperature diminishes the amount of PRP recombination which in turn leads to more secondary radical pairs or escaped radicals.

In the LFP experiments, the cage effect may correspond to the excess amount of benzyl radicals that react before exit from the micelle. In this respect, the cage effect may be correlated with $\Delta A_{fast}/\Delta A_{max}$ (Figures 3.12 and 3.18) assuming that the fast decay is comprised of contributions from the SRP and PRP. As the cage effect determined by product studies measures only recombination for the SRP and the kinetics show the benzyl radicals involved in the recombination of both the PRP and the SRP, the observed cage effect for product studies is expected to be smaller or equal to $\Delta A_{fast}/\Delta A_{max} \times 100\%$. Figure 3.12 and 3.18 illustrates that above ~75°C, the amount of absorption due to the geminate process is negligible. At 80°C, there is a stark contrast between the lack of a fast process in LFP and the

product studies derived cage effect values of 16% and 63% for 4-MeDBK and 4-*t*-butylDBK. Furthermore, according to LFP, throughout the entire temperature range, the approximate number of radicals derived from the photolysis of 4-MeDBK and 4-*t*-butylDBK reacting within the fast kinetic pathway is similar (*cf.* Figures 3.12 and 3.18). This type of behaviour has been reported previously such that in micelles at room temperature, the ΔA_{fast} values for DBK and 4,4'-di-*t*-butyldibenzylketone are the same.[69] If there was a relationship between the fast decay and the cage effect from product studies, the ratio of $\Delta A_{fast}/\Delta A_{max}$ would be expected to increase as the hydrophobicity of the probe increased. Moreover, the lifetime of the fast process for 4-MeDBK (70 ± 5 ns) and 4-*t*-butylDBK (78 ± 3 ns) were the same within experimental error. This adds further proof that the primary recombination is not influenced to a large extent by hydrophobicity.

3.3.2 The Competition Between Geminate and Exit Processes

The rate constant for the fast process observed by LFP increases as the temperature is raised. This observation can be related to the decrease in micelle size as has been proposed in the butyrophenone-Vitamin E/SDS system by other investigators.[104] The rate constant for the fast process is the sum of k_{gem} and $k_.$ which can be estimated from the ratio of ΔA values for the fast and slow components:[72]

$$\frac{\Delta A_{fast}}{\Delta A_{max}} = \frac{k_{gem}}{k_{gem} + k_.} = \frac{k_{gem}}{k_{fast}} \qquad (3.1)$$

It is important to note that this equation only leads to estimates for k_{gem} and k_-, since the value of ΔA_- (*i.e.* end of the fast decay) is not easily determined due to the contribution of the growth related to the decarbonylation step. The results from calculations at two temperatures using Equation 3.1 are summarized in Table 3.7.

Table 3.7: Estimates of k_- and k_{gem} derived from ΔA_{max} and ΔA_{fast} for 4-MeDBK and 4-*t*-butylDBK. The values of k_{gem} and k_- are calculated.

Starting Ketone	Temp (°C)	$\Delta A_{fast}/\Delta A_{max}$	k_{fast} /10^7 s^{-1}	k_{gem} /10^6 s^{-1} (calc.)	k_- /10^6 s^{-1} (calc.)
4-MeDBK	20	0.60	1.5	9.0	6.0
4-MeDBK	60	0.15	4.4	6.6	37
4-*t*butylDBK	20	0.65	1.3	8.5	4.5
4-*t*butylDBK	60	0.18	3.4	6.1	28

For 4-*t*-butylDBK and 4-MeDBK, the results show a decline in $\Delta A_{fast}/\Delta A_{max}$ and an increase in k_{fast} as the temperature is raised. These observations indicate an increase in k_- as opposed to a faster k_{gem}. The estimates of k_{gem} and k_- corroborate this point and indicate that most of the increase in the rate constant for the fast processes is due to an increase in the exit rate constant. The difference between the k_{gem} values at different temperatures could be within the errors associated with the estimates.

3.3.2.1 The Exit Process

The exit process has a faster rate constant at higher temperatures (Table 3.7). Equation 3.1 indicates that as the exit rate is enhanced so are the amount of radicals that do not decay via the fast pathway. The faster exit rate constant demonstrates that as the micelles size shrinks, the rate of exit is increased over the rate of geminate recombination.

The exit rate constant for the radicals derived from 4-*t*-butylDBK is smaller than that for 4-MeDBK at the temperatures for which the calculations were carried out. This reduction of $k_.$ is due to the increased hydrophobicity of the *t*-butylbenzyl radical compared to the benzyl radical. In addition, at higher temperatures, the difference in the exit rate constants for both ketones at 20°C and 60°C differs by over a factor of 6. This observed increase for the exit rate constant with temperature is in line with the observed increase for the exit of the butyrophenone ketyl radical from SDS micelles.[104] As the increase in the exit rate constant far outweighs any change in k_{gem}, this analysis *eliminates a fast geminate process that occurs within the laser pulse* as the cause for the excess cage effect observed at high temperatures. Unfortunately, an equivalent analysis is not possible for the radical dynamics at 80°C, since no fast component is observed at this temperature.

3.3.2.2 The Geminate Process

The value of k_{gem} is related to the frequency of encounters (k_e) and the probability of the radical pair being in the singlet state, f_s. As the temperature is elevated, the frequency of encounters within the smaller micelle should also increase due to greater diffusional rates. Intuitively, more radicals should encounter each other in smaller micelles. If this was the sole effect of the thermal energy, then k_{gem} would increase. So, if the decrease in k_{gem} shown in Table 3.7 is real (and not

due to experimental error), it would indicate that f_s is affected to a larger extent than k_e by the decrease of the micelle size (*cf.* 1.10.4.3).

According to the points above, the geminate rate constant is dependent on the temperature and the decrease observed is due to a decrease in f_s. It is known that the singlet-triplet energy gap (2J or E_{TS}) in biradicals gets larger as the temperature is increased.[150] The rate constant for intersystem crossing is dependent on the electron exchange interaction and hence on the triplet-singlet energy gap. Applying the same reasoning as for biradicals, the rate of ISC from a triplet to singlet level would also decrease as the temperature increases. Fewer of the radical pairs with correlated electron spins can intersystem cross at higher temperatures to achieve singlet encounter complexes leading to smaller f_s values.

3.3.3 Random Radical Encounters and Magnetic Field Effects

The magnetic field effect which was reported for the bimolecular recombination reactions is due to the fact that 75% of any encounter of two radicals will have triplet multiplicity. When this encounter occurs in a micelle in the presence of a magnetic field, the yield for escape from the micelle is enhanced (due to splitting of the $T_{\pm}$ levels from T_0) compared to the recombination reaction.[72] If product formation is primarily due to the recombination of random encounters and radicals are evenly distributed in the micelles, the same statistical distribution (1:2:1) as observed in homogeneous solution and no cage effect should be expected.

Let us assume at this point that the cage effect observed in product studies is due (at least partially) to random encounters. Whatever pathway causes the magnetic field dependence of the cage effect in the product studies must itself be dependent on MF's as well. Magnetic field effects were observed for the random encounters under LFP conditions. Special notice should be taken that this characteristic was also seen at high temperatures where no fast, geminate reactions

occur. It is now evident that the fast decay is not correlated to the cage effect and that in order to explain the cage effect observed in the product studies at high temperatures, a kinetic pathway other than the fast decay process must be sought. The similarity of the $H_{1/2}$ values shown in Table 3.2 and 3.6 (for 4-MeDBK) for the sensitivity of the random radical encounters and the product distribution to magnetic fields may be indicative of a link between random encounters and the cage effect.

3.3.3.1 Temperature Effects on Random Radical Reactions and the Cage Effect

At room temperature, a large majority of the random recombination reactions take place within the confines of micelles (*cf.* section 3.3.3). It is believed that the small decrease in the cage effect at higher temperatures mainly reflects a contribution of random encounters in the aqueous phase which occurs because of the augmented exit rate constant. These random encounters which occur in the bulk water are expected to behave as free radicals, so magnetic fields do not have any effect because of the fast nature of encounter and recombination.

3.3.4 Effect of Micelle Size on the Cage Effect

Micellar structure is known to undergo structural modifications with an increase in temperature.[24,26,151] The aggregation number decreases as the temperature increases until the micelle no longer shrinks in size (>65°C).[36] Whereas this behavior explains Figure 3.12 and 3.18 derived from the kinetic experiments, it does not provide a rationale for the findings of a cage effect for the product studies. Thus, while conventional models can be used to corroborate micelle size changes and the kinetic behavior in the transient studies, no cage effect should have been observed at high temperatures.

3.3.5 A New Model to Explain Radical Pair Dynamics in Micelles

3.3.5.1 Ingold-Fischer "Persistent Radical Effect"

Radicals may be divided into categories that are described as persistent, stabilized, or transient.[51] These distinctions are somewhat arbitrary, but can nevertheless be used as guides. A persistent radical has a long lifetime relative to a methyl radical and contains a stabilized radical center. The "persistence" of a radical depends upon its environment. Under conditions where radical traps (*i.e.* oxygen) are excluded, these radicals have long lifetimes. A stabilized radical has a stabilized radical center, but cannot endure for long periods of time under typical conditions. The significance of this theory become apparent when more than one radical intermediate is formed during the course of the reaction. If these radicals are generated with equal rates and one of the radicals has a longer lifetime (*i.e.* more persistent) due to either the intrinsic nature of the radical or to system conditions, then the buildup of the more stable radical will favour a certain pathway. This condition will ultimately yield different product ratios when compared to a mechanism where both radicals have the same lifetime.[152] Typically, it is the cross-termination product (CTP) that is enhanced.[153]

This effect has been observed for certain systems in homogeneous solution. An enhancement has been observed for the cross-termination product over the self-termination products for reactions involving hydroperoxides in homogeneous solution.[154-156] A more closely related example to our study is that of benzyl radical formed from a benzyl-coenzyme B_{12} model compound, where the CTP was formed by a factor of 10^5 in excess over the bibenzyl coupling product.[153]

3.3.5.2 Application of the "Persistent Radical Effect" to the Dibenzyl Ketone (and Derivatives)/Micelle System

The "persistent radical" concept can be applied to our micellar system if the self-termination reaction for 4-alkylbenzyl and benzyl radicals are different. Scheme 3.2 represents a simplified description of the dynamics of radical pairs at high temperature, which shows the essential features for the mechanism being proposed.

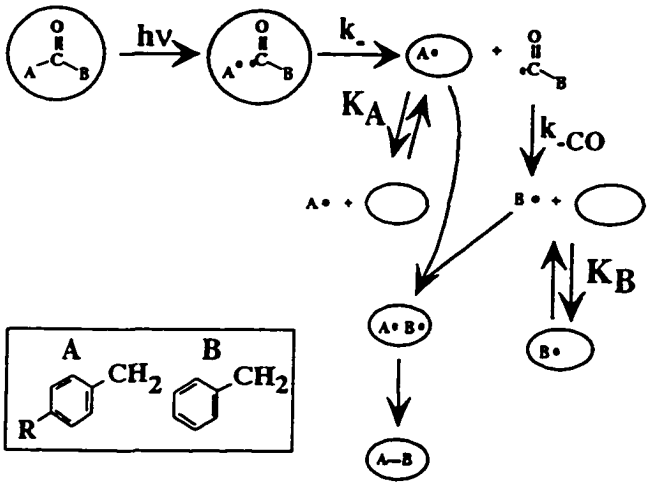

Scheme 3.2: Mechanism for radical pair dynamics in SDS micelles at elevated temperatures. Only the pathway for formation of the cross-termination product is shown.

Upon excitation, the alkylated derivative of DBK fragments so that 60% (for 4-MeDBK) of all α-cleavage yields the phenylacetyl and alkylbenzyl radicals.[142,143] The fraction of α-cleavage reactions that yield the substituted benzyl radicals increases as the substituent becomes increasingly capable of electron

donation.[142,143] Only one α-cleavage process is shown, but as will be evident below the contribution of the other cleavage (yielding alkylated phenylacetyl and benzyl radicals) does not invalidate the mechanism. Regardless of the cleavage patterns, ˙ACO and ˙BCO are more likely to escape into the aqueous phase than their partners. This is due to a higher solubility in water when compared to any of the radicals that do not contain a carbonyl group (4-alkylbenzyl (A) or benzyl (B)). It has been previously reported that there is almost a 5-fold difference in the escape rate constants for benzyl and phenylacetyl radicals.[72] For benzylic radicals, this difference in k_{-} determines the partition coefficient under steady-state (product study) conditions. Chemical equilibria develop and ultimately the more hydrophobic radical will have a greater residency time in micelles relative to the non-alkylated partner.

3.3.5.2.1 4-MeDBK Partitioning Between Aqueous and Micellar Phases

The conclusion that decarbonylation occurs mainly in the aqueous phase is supported by both the solvent and temperature dependence studies for the decarbonylation of DBK. After escape and decarbonylation, the radicals in the aqueous phase will either enter another micelle or will react with another radical to form product. Both these reactions are bimolecular processes with rate constants close to the diffusion controlled limit. The radical concentration (< 3 μM, based on a ε of 7200 M^{-1} cm^{-1} and l=0.7 cm)[72] is much smaller than the micelle concentration (1.7 mM) so that a radical will enter a micelle before encountering another radical in the aqueous phase. This indicates that all "random" radical recombination reactions will occur within the micelle and should therefore depend on the partitioning of the radicals between the phases. The association rate constant of solutes with micelles

is generally diffusion controlled[75] and differences in equilibrium constants are generally related to differences in the exit rate constants. Although the equilibrium constants for the benzyl and 4-alkylbenzyl radicals are not known, for the case of 4-MeDBK, the ratio of these constants will parallel the ratio of 3 observed for xylene and toluene.[157] This means that the residence time of each radical in water will be the same since association to the micelles is diffusion controlled, but the residence time of benzyl within the micelles will be three times shorter than for *p*-methylbenzyl. On average, relative to *p*-methylbenzyl radicals, more benzyl radicals will be in the aqueous phase and each benzyl radical will be able to explore a larger number of micelles.

Both the intramicellar and intermicellar mobility of the radicals is important to consider. Since radical recombination reactions occur only in micelles, the higher mobility of the benzyl radicals has three consequences: (i) enhanced formation of the CTP (AB) occurs since more micelles visited by benzyl radicals will have more alkylbenzyl radicals than benzylic ones. (ii) smaller amounts of bibenzyl will be formed since on average a higher concentration of these radicals are in water where they do not react. (iii) smaller amounts of 4,4'-dimethylbibenzyl are formed since the alkylbenzyl radical is less mobile and does not have as much a chance to explore other micelles when compared to benzyl radicals. In conclusion, the enhancement of the CTP is a consequence of the different partitioning of each of the radicals between micelles and the aqueous phase, which leads to different effective rates for self-termination reactions.

3.3.5.2.2 4-*t*-ButylDBK Partitioning Between Aqueous and Micellar Phases

The difference between the micelle residence times for benzyl and 4-*t*-butylbenzyl should be much larger than that observed for the methyl derivative and benzyl radical above. No partition coefficient has been reported for *t*-butylbenzyl or for that matter, *t*-butyltoluene. In an effort to determine the binding constant of the *t*-butylbenzyl radical, a linear free solvation energy relationship will be used.[157] The solute parameters needed for the relationship are readily available from the literature[158,159] for some solutes, but not for 4-*t*-butyltoluene. The closest match found was that of n-butylbenzene. In order to see the effects of a *t*-butyl group, the partition coefficient can be calculated for n-butylbenzene based on Equation 3.2 and then extrapolated to the case of the *t*-butyl and additional methyl substituents.[157]

$$\log_{10} K_s = -0.62 - 0.08\Sigma\alpha_2 - 1.84\Sigma\beta_2 - 0.57\pi_2 + 0.32R_2 + 3.25\left(\frac{V_x}{100}\right) \quad (3.2)$$

where K is the partition coefficient (equilibrium constant)
defined as $[S]_{micelle}/[S]_{aqueous} \times ([D_{total}] - [D_{CMC}])$;
[S] is the solute concentration
[D] is the detergent concentration
cmc is the critical micelle concentration
$\Sigma\alpha_2$ is the hydrogen bond acidity of the solute
$\Sigma\beta_2$ is the hydrogen bond basicity of the solute
π_2 is the solute dipolarity
R_2 is the solute excess molar refraction
V_x is the solute molar volume

Table 3.8 lists the values of the solvent parameters used for the calculation and the resulting partition coefficients with SDS micelles.

Table 3.8: Solvent parameters and equilibrium constants for solutes in SDS micelles. All parameters except for V_x were reported by Abraham *et al.*[159] V_x values were calculated algebraically.[158]

Solute	K (M^{-1})	$\Sigma\alpha_2$	$\Sigma\beta_2$	$\Sigma\pi_2$	R_2	$V_x/100$ (cm^3/mol)
Toluene	65	0	0.14	0.52	0.601	0.857
p-Xylene	170	0	0.16	0.52	0.613	0.998
Ethylbenzene	180	0	0.15	0.51	0.613	0.998
n-Propylbenzene	520	0	0.15	0.50	0.604	1.139
n-Butylbenzene	1460	0	0.15	0.51	0.600	1.280
t-butyltoluene*	4200	0	0.15	0.51	0.600	1.421

* Values for parameters (except for V_x) are estimated from those of n-butylbenzene

The values calculated for toluene and *p*-xylene are both within 15% of the experimental mean partition coefficient,[157] so a large degree of confidence can be placed on the statements regarding the *t*-butyl derivatives below. For both toluene and *p*-xylene, it is the V_x term which predominates in the calculation and so we feel that V_x is the solute parameter which must be regarded closely. Although no data could be found for *t*-butyltoluene, the parameters are available for n-butylbenzene for which all but V_x are similar to toluene and *p*-xylene. The calculation of V_x is based on the type of atoms and the number of bonds in a molecule.[158] As the calculation does not differentiate between the location or type (single, double, triple) of bond, structural isomers have the same V_x, so n-butylbenzene and *t*-butylbenzene as well as *p*-xylene and ethylbenzene possess the same V_x value. According to calculations, each subsequent addition of a methyl group to toluene also increases the partition coefficient by a factor of 3 because of the coefficient in front of the V_x term. Assuming that the other parameters remain identical to those

for n-butylbenzene, the partition coefficient for 4-*t*-butyltoluene yields a partition coefficient of 4200 M^{-1}.

3.3.5.3 Hydrophobicity and the "Persistent Radical Effect"

In earlier sections, it was noted that in a qualitative manner, *t*-butylDBK behaved like DBK or 4-MeDBK in micelles. As the temperature was elevated from 20°C to 80°C, a cage effect between 75% to 63% was observed. In the time-resolved experiments, kinetics that demonstrated the lack of a fast process at 74°C was observed. In this case, the dilemma of a high steady-state cage effect and negligible amounts of geminate processes is heightened. We now expect the Ingold-Fischer "persistent radical effect" to explain these observations.

The calculated binding constant of *t*-butyltoluene is almost a factor 25 times larger than for *p*-xylene. Comparing the equilibrium processes between the micelle and the water phases for both of these molecules indicates that the *t*-butyl derivative will reside in the micellar environment to a greater extent and infers that the residence time of a *t*-butylbenzyl radical in the micelle will be over 65 times that for the unsubstituted benzyl radical. If a radical persists in a micelle (at low occupancy) for a greater amount of time, then the self-termination rate constant will be quite small relative to the cross-termination rate constant and a much larger enhancement of the cross-termination product is observed. The overall cage effect detected by product studies for the photolysis of 4-*t*-butylDBK in SDS was increased by over 40% relative to the cage effect derived from 4-MeDBK. This increase has to be manifested in some manner in LFP experiments.

The second order decay rate constant of the *t*-butylbenzyl/benzyl random radicals is too long to accurately measure it by LFP ($>1 \times 10^4$ $M^{-1}s^{-1}$ in SDS) and is much longer than that in hexane ($(4.8 \pm 0.3) \times 10^6$ $M^{-1}s^{-1}$). For DBK and 4-

MeDBK, the difference in the rate constant (less than an order of magnitude) is not as drastic. The fact that the second order process is so slow suggests that if the radicals have the same reactivity then the radicals are not encountering one another. This system demonstrates that the radicals are being sorted by their equilibrium processes caused by different solubilities inside the micelle. In fact, if the random recombination reactions took place in the aqueous phase, no effect due to hydrophobicity on the lifetime would be seen. This is further direct evidence for the proposal that the random recombinations take place within micelles.

If 4-MeDBK is used as a standard, for *t*-butylDBK the cage effect is strongly enhanced, the lifetime of the fast kinetic process is identical and the rate constant of the slow process is also very different. The longer lifetimes of these *t*-butylbenzyl radicals allows for equilibration to occur to a greater extent and subsequent formation of the cross-termination product follows. This lack of reactivity demonstrates that the radicals possess a lower frequency of encounter. Hence, sorting of the radicals between the micellar pseudophase and that of the bulk water based on hydrophobicity is occurring.

The effect of increased hydrophobicity of the radicals in the radical pair has led to larger cage effects.[30,68] Going from DBK to 4,4'-dimethyl- and 4,4'-di-*t*-butyl-DBK, the cage effect in CTAC increased from 31 ± 1% to 59 ± 3% and 95 ± 5%, respectively.[68] The mono-*t*-butyl derivative studied here has an overall cage effect of 75% as determined by product studies and is in line with determinations for the range of ketones listed above. We believe that it is the partitioning of the radicals derived from the relative hydrophobicities of both the radical pair and the micelle that controls the observed geminate cage and partition effects.

3.3.5.4 The Partition Effect

A new term is necessary to describe the enhanced formation of the cross-termination product (AB) with respect to the self-termination products (AA and BB) in the absence of geminate reactions. The term *geminate cage effect* can be used to describe the enhancement of AB formation when this product arises from the reaction of radicals ($A^{\bullet}$ and $B^{\bullet}$) before any of these radicals escape the micelle. In this respect, the geminate cage effect is equivalent to the cage effect used by the previous models for radical pair dynamics in micelles. We define the overall cage effect as the sum of the *partition effect* and the geminate cage effect. The term partition effect is appropriate because some (most at high temperature) of the cross-termination product is ultimately formed via equilibrium processes. Under these conditions the radicals can be distributed by diffusive motion as described by their partition (binding) constants.

In the case of SDS micelles discussed here, at 20°C the cage effect is probably a combination of the geminate and partition effects, whereas at 60°C and 80°C the partition effect is primarily responsible for the enhancement in the observed CTP. The relative contribution of both the geminate cage effect and the partition effect is not easily evaluated. Steady-state quenching studies carried out by others demonstrate that the same value for the cage effect can be obtained in an indirect manner.[68] These quenching experiments can still be explained using the partition effect where the more hydrophobic radicals are less mobile, have a longer residency time in the micelle and therefore remain inaccessible to the quencher.

3.3.6 Extrapolation of the Partition Effect to Zeolites

The partitioning effect observed for micelles may be similar to the sieving mechanism discussed for zeolites (*cf.* 1.11.3) where it was assumed that size exclusion properties of zeolites altered the product distribution derived from the

photolysis of 1-MeDBK (the *ortho* derivative that resides outside the zeolite). In this case, the products bibenzyl and 1,1'-dimethylbibenzyl were enhanced relative to the asymmetric 1-methylbibenyzl.[119] This was rationalized by the fact that the stericly hindered methylbenzyl radical could not get inside the zeolite and thus could only recombine outside the zeolite. In terms of the partition effect, the methylbenzyl-benzyl radical complexes will encounter each other much less often due to their inherent distribution (inside vs. outside). Thus, the two radicals have a greater likelihood of encountering another 'like' radical. This leads to less cross-coupling product. This represents a case where the partitioning is not based on hydrophobicity, but rather on size exclusion. It also exemplifies the notion that as long as two radicals can partition (based on any characteristic), a change in the product distribution can be observed.

3.4 Conclusions: The Geminate Cage and Partition Effects

In summary, by working at high temperatures where the geminate and random radical encounters are decoupled, we have shown that the cage effect on the product distribution is due largely to the reaction of random encounters. We called this process the partition effect in order to differentiate it from the geminate cage effect previously proposed to be responsible for the enhancement of the cross-termination product with respect to the self-termination ones. These results demonstrate that geminate recombination is not a necessary requirement for the observation of a cage effect, nor are they required for magnetic field effects on radical reactions in the presence of an organized system. This scenario is directly applicable to biological systems due to their inherent microheterogeneity. In the following chapter, we will explore the ramifications of the geminate cage effect and the partition effect in vesicles.

CHAPTER 4: VESICLES - RESULTS AND DISCUSSION

4.0.1 Objectives

Vesicles are much more complex systems than micelles as they are larger, less dynamic in terms of both their organization and monomer exchange and are made up of a bilayer. For these reasons, vesicles are much better mimics for cell membranes. The work in micelles (Chapter 3) has yielded exceptionally relevant and interesting results and so in order to further understand the biological implications, liposomes are a prime target for study.

Although cell membranes are primarily composed of anionic phospholipids, the cost and difficulty in preparing and maintaining liposomes of specific sizes makes work with them troublesome. An investigation of small unilamellar vesicles (SUV) and large unilamellar vesicles (LUV) consisting of dioctadecyldimethylammonium chloride DODAC) was undertaken here. These vesicles can be made by sonication giving small, highly curved vesicles (SUV's), or by an infusion method to yield larger liposomes (LUV's). These cationic surfactant aggregates have been well characterized by others.[38-41,139] Both types of liposomes form stable bilayers with encapsulated water pools. As two different sizes of vesicles can be made, comparisons for different sized cages and their respective bilayer characteristics (*i.e.* packing arrangement and microviscosity) can be generated. In micelles there is no phase transition, but in Chapter 3, there was a marked changed in radical behaviour with an increase in temperature. Both sizes of vesicles have phase transitions that may be probed by observing radical product distributions in the two phases which have different degrees of organization.

As shown in Chapter 3, the product distribution studies in micelles led to the idea that under steady-state conditions, the radicals derived from the ketone precursor created a product distribution that is controlled by the magnitude of the

exit rates and binding constants between the different radicals and the micelle. Furthermore, the radicals may exit from the initial micelle and subsequently enter micelles until the point that a recombination reaction occurs. In combination with studies under time-resolved conditions, valuable insights regarding the behaviour of radicals in simple supramolecular systems were obtained. At low temperatures, the cage effect is determined partly by geminate processes, where the micelle serves as a cage. However, at higher temperatures, radicals can exit much faster and the observed cage effect is due to a partitioning of the radicals into regions of different hydrophobicities. A key aspect that must be kept in mind is that under conditions where the partition effect is operative, and assuming that the geometric structure does not affect the equilibrium constant, the structure of the aggregate plays only a very small role. Thus, the use of two systems consisting of the same monomer, but of different organization and size should help to further explain the implications of the partition effect. In this section, the quantification of photoproducts in small and large DODAC vesicles and LFP experiments in small vesicles under various system conditions is described.

4.1 Steady-State Photolysis in DODAC Vesicles

The cage effect (Equation 1.11) measures the enhanced formation of the cross-termination product (CTP). However, as discussed in Chapter 3, the original cage effect definition has been divided into two terms, the geminate cage effect and the partition effect. As in the case of micelles, it is difficult to separate the contributions from each of them and the analysis in this chapter will be similar to that found in the Chapter 3.

4.1.1 4-Methyldibenzyl Ketone

Gas chromatography allows a quantitative determination of the photoproducts following extraction of the products from small DODAC vesicles. The photoreactions had good mass balance (>90%) which indicates that the radicals do not react with the surfactant. The extraction was carried out in an identical manner to that for SDS. The results in homogeneous solution were discussed in Chapter 3. The gas chromatograms were similar to those observed in SDS micelles and no significant products other than the diarylethanes were observed at low conversions of the starting ketone.

4.1.2 Effect of Magnetic Fields and Temperature on the Overall Cage Effect in Small Vesicles

Solutions containing small DODAC vesicles contain aggregates where 98% of all macroassemblies are 30 ± 2 nm in diameter before and after photolysis. The dependence of the overall cage effect on magnetic fields was studied (Figure 4.1).

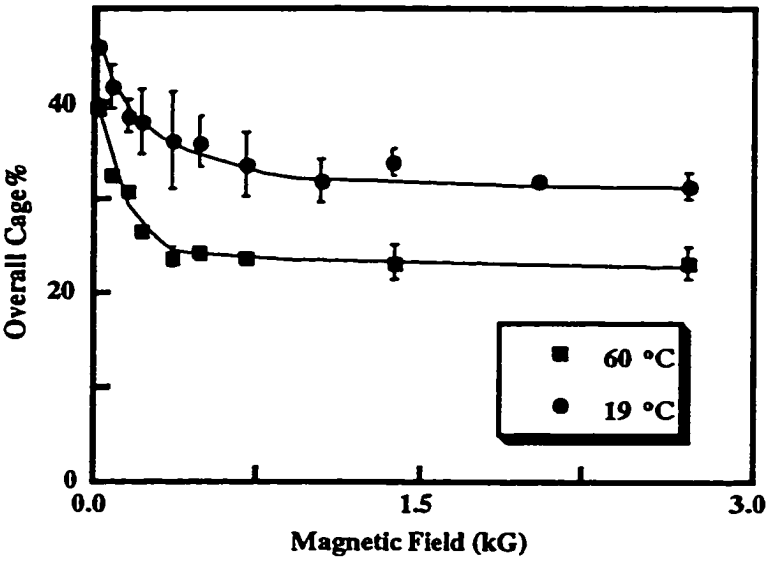

Figure 4.1: Dependence of the overall cage effect on magnetic fields and temperature for 4-MeDBK in small DODAC vesicles.

The Figure above shows that in the Earth's magnetic field, an overall cage effect of 47%, was observed at 19°C in small DODAC vesicles. As expected, the cage effect decreases with an increase in magnetic field to a limiting value of 32% (Table 4.1).

Table 4.1: Effect of temperature and magnetic field on the overall cage effect determined by product studies. Errors correspond to average deviations from the number of experiments listed in parentheses. Blank entries refer to experiments not completed.

Magnetic Field (kG)	Overall Cage Effect % (19 ± 2) °C	Overall Cage Effect % (60 ± 2) °C
0.00	47 ± 3 (6)	40 ± 1 (3)
0.07	42 ± 2 (5)	33 ± 1 (3)
0.14	39 ± 2 (5)	31 ± 1 (3)
0.20	38 ± 3 (5)	27 ± 1 (3)
0.34	36 ± 5 (2)	24 ± 1 (3)
0.47	36 ± 3 (4)	24 ± 1 (3)
0.68	34 ± 4 (4)	24 ± 1 (3)
1.02	32 ± 2 (2)	
1.36	34 ± 2 (4)	23 ± 2 (3)
2.03	32 ± 1 (5)	
2.71	31 ± 1 (5)	23 ± 2 (3)

The gel to liquid crystalline phase transition for the small vesicles was determined to be between 34-39°C.[38,39] This transition is a key aspect of biological membranes and alters the structural organization of the bilayer (*cf.* 1.4.2). For this reason, we investigated the behaviour of radical pairs below and above this critical temperature. Perusal of Figure 4.1 illustrates that the cage effect

in the absence of an applied, external magnetic field did not decrease by a large extent relative to the observations performed below the phase transition temperature (47% to 40%). At 20°C the microviscosity of the small vesicles is in the range of 144 cP[41] to 182 cP.[38] At higher temperatures, the bilayer becomes increasingly fluid and the microviscosity decreases to about 100 cP from 182 cP.[38] Clearly, the decrease in microviscosity and the decreased order in the bilayer had little consequence on the cage effect.

$H_{1/2}$ values (Table 4.2) demonstrate that the recombination reactions may be slightly more sensitive to external magnetic fields at higher temperatures, but the large errors associated with these values render such an analysis inconclusive.

Table 4.2: Sensitivity of overall recombination reactions in small vesicles to magnetic fields. The number of experiments is listed in parentheses. Errors are estimates.

Temperature (± 2 °C)	$H_{1/2}$ (G)
19	200 ± 40 (4)
60	120 ± 30 (3)

4.1.3 Effect of Magnetic Fields and Temperature on the Overall Cage Effect in Large Vesicles

Solutions of the LUV's consist of a Gaussian size distribution centered around 150 nm. Overall, the distribution spanned about 65 nm in either direction. All experiments were completed with vesicles of this size. Due to the fact that a distribution of sizes was utilized, caution must be used when interpreting the data exclusively based on size, however this does not change the ultimate conclusions.

The magnetic and thermal effects on the recombination of radicals in these large DODAC systems is shown in Figure 4.2 (also see Table 4.3).

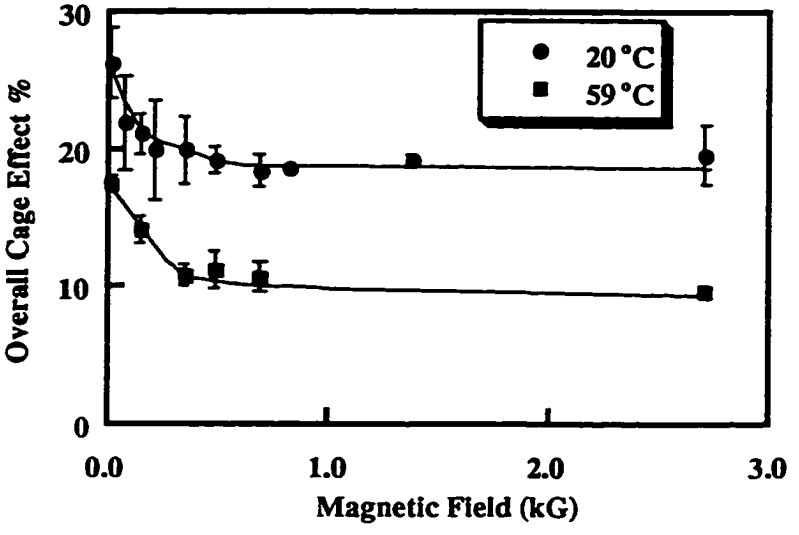

Figure 4.2: Effect of magnetic fields and temperature on the overall cage effect in DODAC LUV's

Table 4.3: Effect of magnetic fields and temperature on the overall cage effect in large DODAC vesicles. Errors correspond to average deviations from the number of experiments listed in parentheses. Blank entries refer to experiments not completed.

Magnetic Field (kG)	Overall Cage Effect % (20 ± 2) °C	Overall Cage Effect % (59 ± 2) °C
0	27 ± 3 (5)	18 ± 1 (2)
0.07	22 ± 3 (4)	
0.14	21 ± 2 (4)	14 ± 1 (2)
0.20	20 ± 4 (4)	
0.34	20 ± 3 (2)	11 ± 1 (2)
0.47	19 ± 1 (4)	11 ± 1 (2)
0.68	19 ± 1 (4)	11 ± 1 (2)
0.81	19 ± 1 (2)	
1.36	19 ± 1 (3)	
2.71	20 ± 2 (4)	10 ± 1 (2)

Figure 4.2 shows a decreasing trend in the cage effect as the external magnetic field increases in magnitude. In the Earth's magnetic field, the overall cage effect was determined to be 27% and 18% at 20°C and 59°C, respectively. These values are even smaller than those found in SDS micelles. It is important to note that the extent of the decrease with the application of a magnetic field is the same for both small and large vesicles.

The sensitivity of the reaction to magnetic fields measured as $H_{1/2}$ values were determined (Table 4.4) and are the same within experimental error. The overall magnitude of the $H_{1/2}$ values are similar to that determined in SDS micelles and in small DODAC vesicles.

Table 4.4: Sensitivity of radical recombination reactions to magnetic fields. Errors correspond to average deviations from the number of experiments listed in parentheses. Blank entries refer to experiments not completed.

Temperature (± 2 °C)	$H_{1/2}$ (G)
20	80 ± 30 (2)
59	110 ± 50 (2)

4.2 Time-Resolved Studies with Small DODAC Vesicles

The solutions containing small vesicles were always run less than 24 hours after being prepared. There was no change in the size of the vesicles (determined by particle sizing) after exposure to laser flashes.

4.2.1 DBK in Small DODAC Vesicles

All of the work discussed herein was conducted using the symmetric, parent derivative, dibenzyl ketone. In previous LFP work (Chapter 3), 4-MeDBK gave similar results to that obtained for DBK. The lifetime for the fast kinetic process in SDS micelles was enhanced by ~20 ns for the substituted ketone while the rate constant for the random encounters and decarbonylation were not markedly altered between 4-MeDBK and DBK. Therefore, comparisons between the kinetics of the methyl derivative and that of the parent ketone can be made. Moreover, the kinetics derived with DBK can be compared to the product studies investigated with 4-

MeDBK because it has been shown that the cage effect for DBK (by indirect quenching studies) and 4-MeDBK (direct observation) in SDS micelles is the same.[68,145] The transient spectrum derived from LFP of DBK in small DODAC vesicle solution had a maximum at λ_{max} = 317 nm (Figure 4.3).

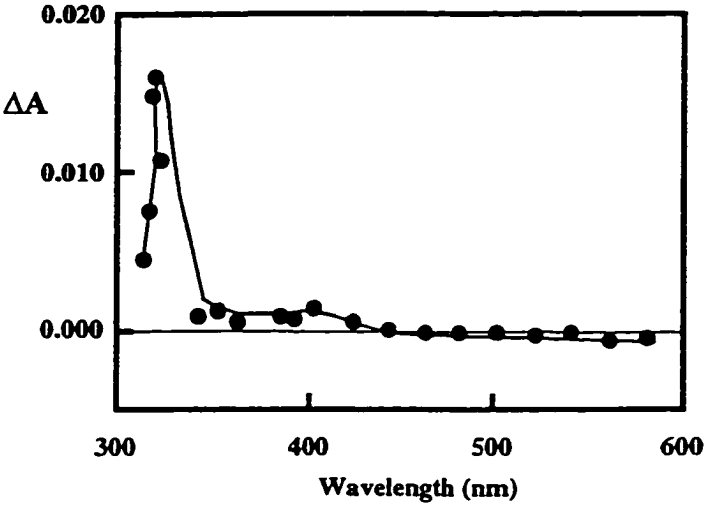

Figure 4.3: Transient spectrum obtained upon photolysis of 4-MeDBK in small DODAC vesicles. The spectrum was taken 2 μs after the 308 nm laser pulse.

A much higher laser power was required to photoionize DBK in DODAC vesicles in comparison to SDS micelles. This probably stems from the charge separation that can develop in micelles due to repulsive forces between the negatively charged SDS headgroup and the hydrated electron.[141] In the case of DODAC, the cationic head groups attract the hydrated electron, so it is still proximal to the photoionized ketone which enhances recombination to form the starting ketone.

4.2.2 DBK in Small DODAC Vesicles - Geminate Processes?

The transient was monitored at 317 nm and followed the kinetics shown below (Figure 4.4).

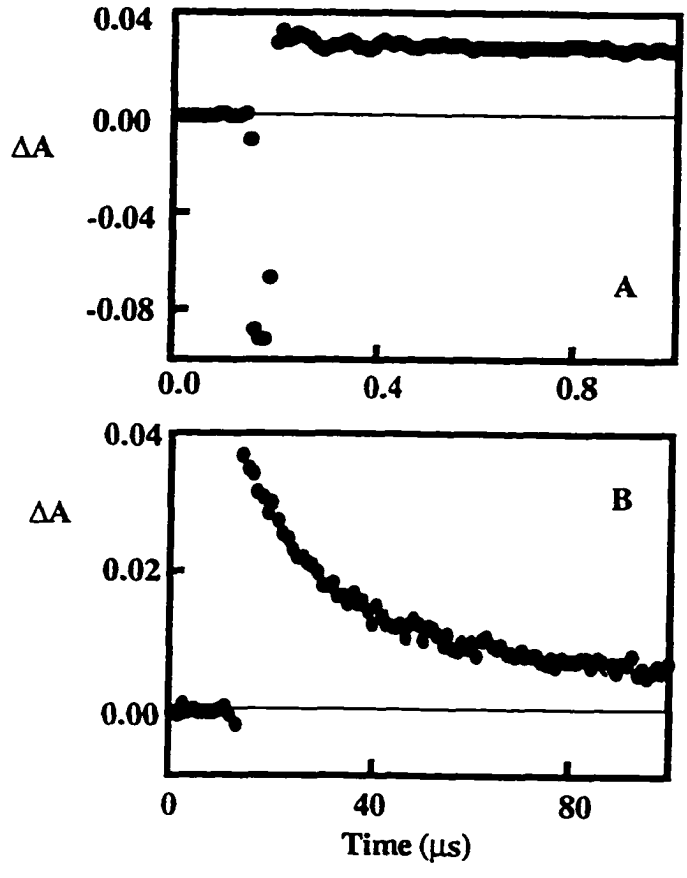

Figure 4.4: Decay kinetics observed at A) short and B) long time scales after laser flash photolysis of DBK in small DODAC vesicles using a 90° alignment for the laser with respect to the analyzing beam

On short time scales, there is a substantial amount of scattered light that arises because of solution turbidity. The detection of scattered light is enhanced in

the cloudy solutions because less light is being transmitted through the solution and consequently the photomultiplier voltage has to be increased to make it more sensitive. The magnitude of the ΔA values is not affected since it corresponds to a relative measurement. The large amount of scattered light stands out at early times of the trace and "hides" the initial part of the kinetic trace. For this reason, little information can be gathered in the first 100 ns. Due to the front face arrangement, when magnetic field experiments are performed, the scattering of the laser light also increases the amount of noise at the start of the kinetic trace (note that Figure 4.4 was taken at 90° where scattering is minimized), so MF experiments have even more noise associated with them). Regardless of the nature or magnitude of the scattered light, no fast process is observed in DODAC vesicles. Note that if the amplitude of a fast process similar to that observed in micelles (ΔA_{fast} = ~60%) was taking place in vesicles, then the overall decay would take place over 300 ns (*cf.* Figure 3.9) and some of the transient would indeed be observable. This analysis provides evidence that a fast, geminate process is not occurring in the experiment.

In fact, if there is a magnetic field sensitive geminate process that remains unobservable, then it is expected that the kinetic traces taken on time scales similar to that of Figure 4.4A would have MF dependent ΔA_{∞} values in the same fashion as micelles (*cf.* Figure 3.9). If the process was faster than the timescale that we can observe, the ΔA_{∞} of this unseen process would correspond to ΔA_{max} of the trace that we do observe. However, no such magnetic field dependence was observed. In short, we can assert that the fast, geminate process is not observed within the time resolution of the equipment for this experiment. This contrasts with the situation in SDS micelles where the fast recombination process is observed on these time scales.

4.2.3 DBK in Small DODAC Vesicles - Decarbonylation

Under experimental conditions where the amount of scattered light is low, it is not possible to make out a growth due to the decarbonylation process above the ringing noise. As shown in Figure 3.13, the magnitude of the growth due to decarbonylation is rather small (about 10% of the maximum absorbance) and for this reason, the process may get lost in the experimental noise.

4.2.4 DBK in Small DODAC Vesicles - Random Recombination

In the absence of oxygen, the slow decay followed second order decay kinetics and had a rate constant product ($2k/\varepsilon l$) of 4.8×10^6 s^{-1}. A detailed description of the kinetic analysis can be found in Chapter 3. In an analogous manner to the kinetics in SDS micelles, the decay shown in Figure 4.4B can be attributed to the recombination of radicals after the exit from the initial vesicle. However, at this point, it is important to note that random recombination *does not* have to occur after exit into the aqueous phase. Rather, radical escape may occur by (*i*) exit into the aqueous phase; (*ii*) separation of the radicals within the vesicle bilayer or (*iii*) escape into the interior water pool. Recall that the concept of escape stems from the idea that at the point where radicals no longer interact with each other they are considered to be free radicals, rather than a radical pair. In order to differentiate between the mechanism involving exit to the aqueous phase and those involving no diffusion outside the vesicle, quenching studies with $CuCl_2$ and CuCl were attempted, but the liposomal suspension precipitated out of solution. In fact, it has been reported that addition of any salt at concentrations greater than 0.1 M will precipitate the DODAC aggregates.[40,41]

4.2.5 Magnetic and Thermal Effects on Random Radical Recombination

In a parallel manner to SDS micelles, the analysis of the kinetic traces was accomplished by plotting the reciprocal transient absorbance vs. time. The slope of this plot yields the value of 2k/εl and is magnetic field dependent as shown in Figure 4.5.

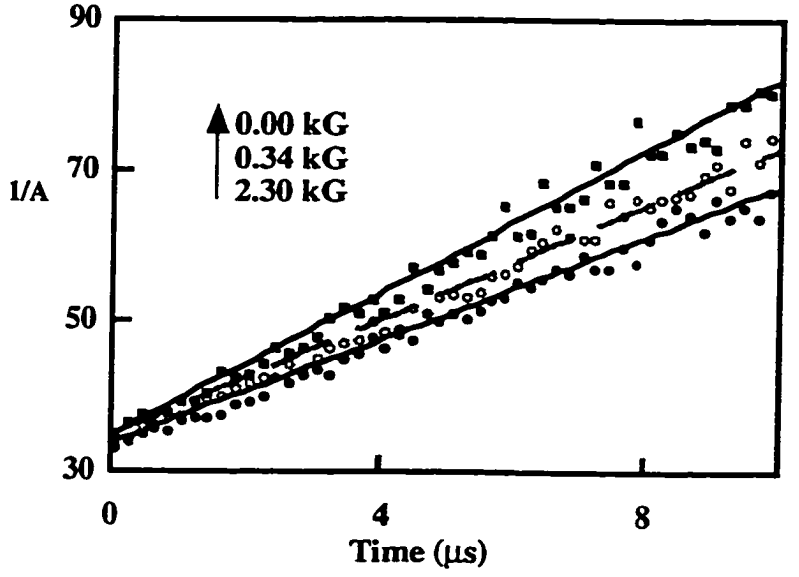

Figure 4.5: Determination of 2k/εl and observation of magnetic field effect in small DODAC vesicles.

The difference in the rate constant product at an external magnetic field strength of 0 kG compared to that at 2.7 kG at 20°C was routinely less than 20% (6 exp). However, in all cases, the value of 2k/εl decreased in the presence of a magnetic field (Figure 4.6).

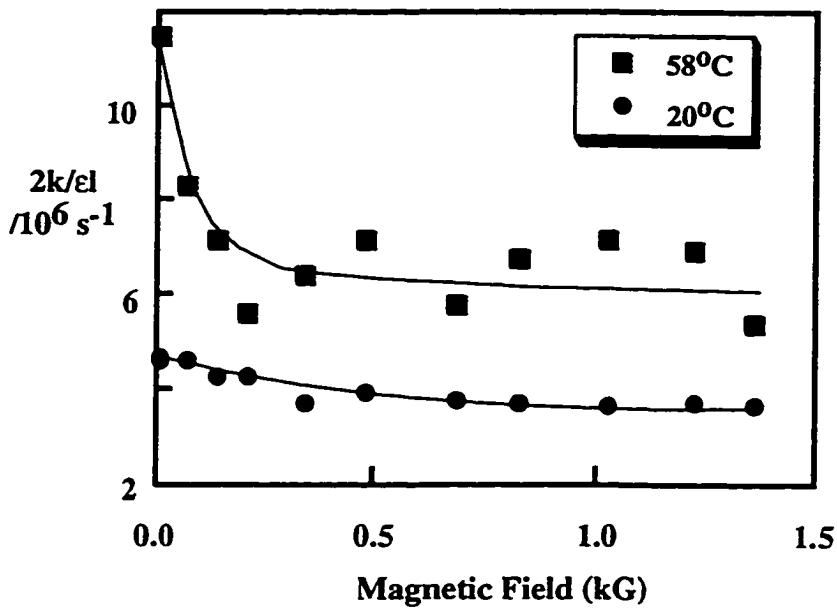

Figure 4.6: Effect of temperature and magnetic field on the value of 2k/εl. The values at 58° were determined only once, whereas those at 20°C were completed 5 times. At 20°C, the value of 2k/εl varied by ~15% between runs. Data from a single experiment are shown and the errors are derived from the fit of the best fit line (which are smaller than the data points) for the 1/ΔA vs. time plot.

Table 4.5 lists the data taken in the study of the effect of temperature and magnetic fields. The jump of 38°C increased the rate constant product by over a factor of 2.

Table 4.5: Magnetic field and temperature dependence of 2k/εl in DODAC SUV's. Errors come from statistical fits. The values at 58° were determined only once, whereas that at 20°C was completed 5 times. The data shown above are derived from a single, representative experiment, but all experiments at 20°C showed the same type of behaviour. Blank entries refer to uncompleted experiments.

Magnetic Field (kG)	2k/εl /10^6 s^{-1}@ (20 ± 2) °C	2k/εl /10^6 s^{-1}@ (58 ± 2) °C
0	4.8 ± 0.1	11.5 ± 0.2
0.07	4.7 ± 0.1	8.4 ± 0.1
0.14	4.4 ± 0.1	7.2 ± 0.1
0.20	4.4 ± 0.1	5.7 ± 0.1
0.34	3.8 ± 0.1	6.5 ± 0.1
0.47	4.0 ± 0.1	7.2 ± 0.1
0.68	3.9 ± 0.1	5.9 ± 0.1
0.81	3.8 ± 0.1	6.8 ± 0.1
1.02	3.7 ± 0.1	7.2 ± 0.1
1.22	3.8 ± 0.1	7.0 ± 0.1
1.36	3.8 ± 0.1	5.5 ± 0.1
1.56	3.7 ± 0.1	4.5 ± 0.1
1.69	3.5 ± 0.1	5.2 ± 0.1
1.83	3.4 ± 0.1	5.8 ± 0.1
2.03	3.7 ± 0.1	
2.30	3.4 ± 0.1	
2.51	3.5 ± 0.1	
2.71	3.5 ± 0.1	

As expressed in Table 4.5, it is easy to see that the magnitude of the rate constant product decreased by a factor of ~ 2 at 58°C between low and high MF's, and by about 1.3 at 20°C. This indicates that the recombination reactions are more sensitive to applied fields at higher temperatures (Table 4.6). This is similar to the observations made in micelles. This magnetic field dependence also implies that

there is a competition between radical pair separation and spin interconversion for random encounters.

Table 4.6: Sensitivity of the radical recombination reaction to magnetic fields at different temperatures in DODAC SUV's. The number of experiments is listed in parentheses. Errors are estimates.

Temperature (± 2 °C)	$H_{1/2}$ (G)
20	180 ± 20 (5)
58	100 ± 25 (1)

4.2.6 Time-Resolved Experiments in Large DODAC Vesicles

The large vesicles had an average diameter 5 times greater then the small vesicles. With aggregates of this size, it is impossible to transmit light through the sample, so it is impossible to use conventional laser flash photolysis. Kinetics of diphenylmethyl radicals in vesicles (~500 nm in diameter) have been studied using laser flash photolysis with diffuse reflectance detection.[109] This technique was pioneered by Wilkinson[160,161] and involves a measurement of the amount of diffusely reflected light from a sample. In principle, a laser pulse excites the sample, the monitoring beam strikes the sample and the amount of diffusely reflected light is acquired. The change in reflected light can be related to the concentration of transients by using the Kubelka-Munk function.[162] To our dismay, we found that our large vesicle solutions did not allow enough light to be transmitted to do LFP-transmittance measurements and were too clear (not enough diffusely reflected light) for LFP-diffuse reflectance measurements.

4.3 Discussion

In the absence of the results found in micelles (Chapter 3), we would be left with a perplexing problem. No fast process is observed in any of the time-resolved experiments, yet at 20°C and without the application of magnetic fields, a large cage effect is observed in the product studies in the small vesicles. These results are similar to those obtained in micelles at higher temperatures where we have ascertained that in addition to the geminate cage effect, the partition effect is operative. Moreover, in large vesicles, the cage effect at 20°C in the absence of a magnetic field is drastically reduced compared to small vesicles. We will first consider the time-resolved results derived from DBK photolysis in small DODAC vesicles.

4.3.1 Geminate Recombination in Vesicles

Laser flash photolysis experiments had a large amount of scattered light that blocked out the transient absorption at early times in the kinetic trace. No process that is faster than 4×10^7 s^{-1} (<25 ns) can be monitored and no fast decay (or growth) kinetics was observed in the small vesicles. Photolysis of DBK yielded a lifetime for the fast process of 50 ns in SDS micelles (Chapter 3). If the same amount of primary radical pair recombination occurred in DODAC vesicles, the geminate process would be observable because ~60% of the entire decay is caused by this process. However, no decay kinetics are observed experimentally thereby suggesting that no fast primary radical recombination occurs in small vesicles.

The rate of a geminate process depends on the probability of the radical pair being in a singlet multiplicity (f_s) as well as the frequency of encounters (k_e). If the structure of the vesicle is ultra-organized so that the radicals cannot efficiently separate, recombination should be very fast because the k_e term would be very large and it stands to reason that f_s should be affected by magnetic fields. The two

possibilities for MF effects are on (*i*) a fast unobserved process and (*ii*) a fast process that can be observed only close to the end of its lifetime. The first possibility should be seen as changes in ΔA_{max}, while the latter could be investigated through ΔA_{-}. No magnetic field dependence on the initial ΔA_{max} or on ΔA_{-} occurred on fast time scales. This lack of MF dependence rules out the possibility of a geminate process occurring beyond the time resolution of the experiment.

One of the possible reasons that no geminate process is occurring is that escape may constitute diffusion within the plane of the bilayer, an option that is not available for micelles. Diffusion coefficients of pyrene in egg lecithin vesicles were found to be 3×10^{-8} cm^2/s [163] and that of anthroyl-labelled phospholipids in dipalmitoylphosphatidylcholine was reported to be 1.6×10^{-8} cm^2/s.[164] Using the value of 2×10^{-8} cm^2/s as a guide, over a time scale of 100 ns, a radical could be displaced in an area of 2×10^{-15} cm^2. This two-dimensional area is large enough so that the radicals are no longer interacting with each other and thus can constitute an escape pathway. It should be noted that this analysis does not apply to micelles as the entire surface area of a micelle with a radius of 1.5 nm is 3×10^{-17} cm^2 and displacement in an area of 2×10^{-15} cm^2 will involve a radical-micelle/water interface encounter.

4.3.2 Decarbonylation

The growth due to the formation of benzyl radical from the phenylacetyl radical is not observed in small DODAC vesicles. If decarbonylation is taking place, it is either beyond the time-resolution of the experiment ($> 4 \times 10^7$ s^{-1}), or is not observed because the magnitude of the growth in terms of ΔA is small. Figure 4.4A demonstrates that at shorter time scales, neither decay nor growth kinetics is observed. The rate constants for decarbonylation of DBK are in the range of 5×10^6 s^{-1} (methanol) to 9×10^6 s^{-1} (isooctane).[58] The process is unimolecular, so no restriction due to vesicle structure or organization should play a role in the magnitude of the rate constant. Even, if the decarbonylation is occurring within the hydrophobic interior of the bilayer, it is unlikely that it would have a rate constant greater than that observed in isooctane. Consequently, the decarbonylation process is not seen due to its small magnitude. This view has precedence where in micelles the decarbonylation step was not observed in the LFP of DBK in micelles in initial LFP experiments[10,69] due to lower signal to noise ratios.

4.3.3 Random Encounters

Escape can occur by diffusion of a radical (*i*) into the bulk water; (*ii*) into the interior water pocket; or (*iii*) within the bilayer, but away from its partner (Scheme 4.1).

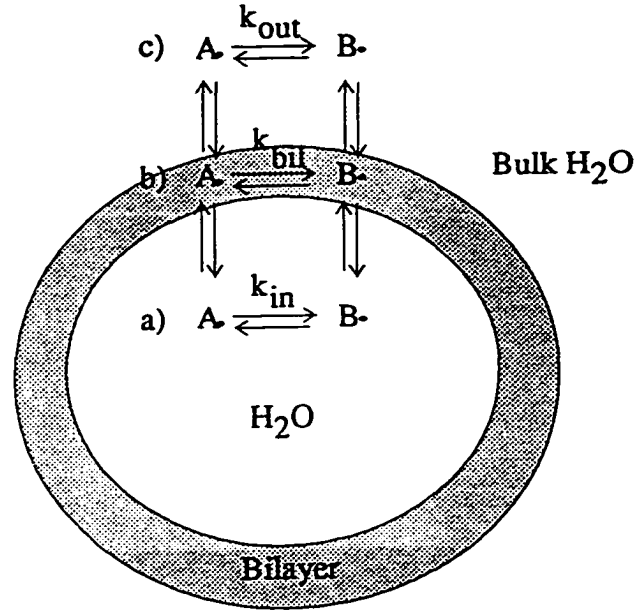

Scheme 4.1: Kinetic processes that involve recombination of radicals in vesicular systems. k_{out}, k_{bil} and k_{in} correspond to the recombination rate constants of two radicals in the bulk water, within the bilayer and inside the trapped water pool, respectively.

The picture shown above involves both diffusion of the radical species within the bilayer, and out of the bilayer. All of these processes may be termed escape processes. Bimolecular radical reactions are limited by diffusion and so are their respective recombination rate constants. Analysis of the LFP data and the subsequent conclusions regarding the location of the random radical reactions are important when ascertaining whether structure and organization plays a large role in determining the product distribution as well as the rates of random recombination.

4.3.3.1 Magnetic Field and Temperature Effects on Random Encounters

Time-resolved data for small vesicle solutions show that rate of radical recombination is slowed in the presence of magnetic fields (Figure 4.6). The difference between rate constant products is much larger (a factor of *ca.* 2) at higher temperatures. At higher temperatures, the bilayer is less ordered and less viscous,[38] so diffusional rates are faster. If we assume that the magnetic field effect (MFE) arises due to the competition between escape (k'$_{-}$, includes all processes that involve separation of the radical pair) and ISC/recombination (k_{gem}), then the MFE should be largest when the two rate constants are similar (k_{gem}~k'$_{-}$). From the reduction of the rate constant products by magnetic fields, it is possible to discern that this condition is satisfied to a greater extent at higher temperatures. Table 4.5 also demonstrates that the reaction in SUV's at higher temperatures is more sensitive to applied fields. The temperature and MF dependence provides evidence that the random radical recombination is occurring within the small vesicle. If the reactions happened in the aqueous regions, no temperature (or very small) temperature effects would be observed.

4.3.4 Product Studies in Small and Large Vesicles

In small DODAC vesicles in the Earth's magnetic field, a cage effect of 47% and 40% were determined at 20°C and 58°C, respectively. The DODAC vesicle phase transition temperature is situated at about 37°C, so a large difference in the cage effect was expected. As the temperature is elevated, the vesicle bilayer becomes less ordered and more fluid. This translates into a decrease in the microviscosity within the bilayer,[38] as well as increasing diffusional motion for a molecule situated in the bilayer.[38] Both of these points would lead to a decreased cage effect as the increased mobility of the radicals within the vesicle system would

allow an increased rate of exit. In fact, a decrease of only 7% over a temperature range that encompasses the phase transition demonstrates that the increased fluidity and disorder of the bilayer had minimal effect on the recombination of benzyl radicals. Analogous to micelles, another property aside from structure and organization is acting on the supramolecular system.

The large DODAC vesicles are approximately 5 times the size of the small vesicles. An increase in temperature from 20°C to 59°C decreased the cage effect from 28% to 18% in the Earth's magnetic field. The phase transition temperature was reported to be in the range of 35°C to 39°C (similar to that for the small vesicles)[39] and so the elevated temperature should have brought about a rapid decrease in the cage effect. Furthermore, the cage effect at 20°C is much smaller in LUV's relative to SUV's. The fact that smaller cage effects are observed in LUV's compared to SUV's and that the cage effect in LUV's is not dramatically changed as the temperature is increased indicates a pathway already exists (even at room temperature) for a relatively fast route for exit from the large vesicles and consequent recombination in the bulk water.

4.3.4.1 Magnetic Field Effects on Product Distributions

In small vesicles, an external magnetic field reduces the observed cage effect in the product studies by 15% and 16% (absolute values) at 20°C and 58°C, respectively. Application of magnetic fields decreased the observed cage effect in large vesicles by only 8% (absolute value) at both 20°C and 58°C. If the large vesicles are more ordered, an increase in either the temperature or magnetic field would have a much larger effect assuming that radicals are recombining (geminate or random) inside the vesicle bilayer. The small decrease of the cage effect with application of MF's in the large vesicles possibly indicates that exit is faster than ISC and so the necessary competition between the two pathways may not fully

exist. Therefore, we arrive at the conclusion that it is not the structure or organization that is critical in determining the cage effect.

4.3.5 Random Radical Recombination in the Bulk Water and Internal Water Pools

In order to ascertain the likelihood of recombination in either the bulk water or inner water pool, the concentrations of vesicles as well as the respective volumes for the trapped water pools is required. For small vesicles, which consist of 48 500 monomers,[40] the 40 mM solution of surfactant monomer yields 8.3×10^{-7} M of vesicles (Table 4.7). The large vesicles are produced with a 10 mM DODAC monomer concentration (*cf.* 2.3.3) and each aggregate contains many more monomers than in the small vesicles. Thus, the concentration of aggregates is reduced for large vesicles upon comparison to the small vesicles.

Table 4.7: Data for determination of encapsulated water pools and vesicle concentrations.*

	Small DODAC Vesicles	Large DODAC Vesicles
experimental diameter (nm)	30	150
bilayer thickness[139] (nm)	5	5
inner water pool radius (nm)	10	70
bilayer volume* (m^3)	9.95×10^{-24}	3.30×10^{-22}
inner water pool volume (m^3)	4.19×10^{-24}	1.44×10^{-21}
Volume per monomer (m^3/monomer)	2.05×10^{-28}	2.05×10^{-28} (assumed)
N_{ag}	48 500 [165]	1.61×10^{6} (calculated)
[Vesicles] (nM)	830	6.2
Total entrapped water pools in 2 mL solution (μL)**	4.2	10.7
Proportion of entrapped water in a 2 mL solution (%)	0.21	0.54

* Volume (V) calculated from the radius (r) by the equation: $V = \frac{4}{3}\pi r^3$

** The proportion of entrapped water relative to total water in a 2 mL solution was calculated by determining the number of vesicle aggregates and then determining the total volume of the entrapped water pools. This was compared to the total amount of water (2 mL).

4.3.5.1 Inner Water Pools

To compare the kinetic pathways shown above (Scheme 4.1), one must first comprehend the volume differences in the respective inner water pools. There are many fewer aggregates in the solutions containing the large aggregates, but each holds a greater pocket of water. Thus, for both sizes of vesicles, the proportion of trapped water in a 2 mL (approximate amount used in a static cell for LFP and

product study experiments) sample differs by about a factor of 2, but the overall fraction of water in the sequestered water is very small. Therefore, only a very small fraction of the radicals recombine in the inner pool and thus there will be a negligible alteration of the cage effect value.

In most surfactant assemblies, the probe molecule binds to the surfactant-water interface. Ketones exhibit this behaviour so that the carbonyl moiety can be stabilized by hydrogen bonding. In small DODAC vesicles, it is known that the outer monolayer contains many more lipids/surfactants compared to the inner monolayer (a ratio of 3:2).[139] This stems from the packing arrangement of the hydrophobic and hydrophilic portions of the surfactant. It also serves to illustrate that the probe will predominately (if not exclusively) bind in the region where there is less restriction on its mobility. Thus, if a radical is generated on the outer leaflet and then follows a random walk path, it will encounter a stiffer "wall" upon entering the inner monolayer. For this reason, the radical is more likely to diffuse outwards, towards the bulk water. In essence this demonstrates that for both sizes of vesicles, escape into the inner water pocket is unlikely as (*i*) there is only a very small percentage of water in the inner pool; (*ii*) the radicals are initially situated much closer to the bulk water; and (*iii*) the probe has more mobility in the outer leaflet.

4.3.5.2 Escape Into the Bulk Water

Escape into the bulk water requires complete exit from the vesicle. In the main aqueous phase, the radicals have a very low effective concentration because they are not sequestered in a supramolecule. Approximately the same amount of radicals are formed in SDS micelles and DODAC vesicles. So, the concentration of radicals is less than <3 μM in most experiments (ε= 7200 $M^{-1}cm^{-1}$, *cf.* 3.3.5.2.1)[72]

Comparing the relative concentrations of vesicles and generated radicals, and assuming that diffusion back into the vesicle is diffusion controlled, then the two rates for radical-radical encounter and radical-vesicle encounter are expected to be competitive in the case of small vesicles. The large vesicles have a much smaller concentration of aggregates, so the aqueous radical-radical bimolecular reaction should occur more frequently compared to vesicle re-entry.

4.3.5.3 Re-Entry and Reaction Within the Bilayer

For small vesicles, the reaction in the bulk water and that in the bilayer are expected to be competitive. However, it is expected that the benzyl radical will preferentially partition within the bilayer (or at the interface) rather than in the bulk water. For this reason, the effective concentration of the benzyl radical is increased when in the bilayer. So, reaction within the bilayer should be more favoured compared to reaction in the bulk water.

We have already determined (*cf.* 4.3.5.2) that recombination in the bulk water will occur for solutions of large vesicles. Thus, this mode of analysis shows that for small vesicles, recombination in the aqueous phase and within the bilayer is competitive, but in large vesicle solutions, random radical recombination occurs predominantly in the bulk water. For LUV's, path c is the major pathway, but path b may also operate (Scheme 4.1).

4.3.6 Correlation of Time-Resolved and Steady-State Experiments

4.3.6.1 Occupation Level in Vesicles

The [ketone] per [vesicle] value provides an estimate of the average occupation number to be greater than 1200 probe molecules in a single small vesicle. If recombination among the radicals formed from different precursors in a

single vesicle was occurring, not only would there be a small or no cage effect (a 1:2:1 ratio would be expected), but at least two types of decays would be seen in the LFP experiments. The large cage effect observed in the steady-state experiments and the lack of fast decay kinetics demonstrate that scrambling of radicals inside the vesicle does not happen. Under the experimental conditions utilized, a decrease in the concentration of ketone by a factor of 2 (0.5-1 mM), did not change the overall cage effect derived from product studies. This provides evidence that rules out the possibility of escape occurring by diffusion in the plane of the bilayer in a direction away from the radical partner the cage effect in the product studies would be markedly altered by a change in the ketone concentration .

4.3.6.2 Small DODAC Vesicles - Exit Processes

Magnetic fields alter the rate of recombination in the absence of a fast, geminate process. The ramification of the observation of MF effects is that the radicals can exit from the vesicle very easily. Since no fast process is observed in LFP experiments, a lower limit for the exit rate constant may be set at 1×10^7 s^{-1}. Even though the radicals can separate easily by exit from the vesicle, there is still an observed cage effect. No geminate recombination is observed in the small vesicles which indicates that diffusive separation is fast. This leads to the idea that the cross-termination product is enhanced by the partition effect where the radicals may exit the small vesicle, re-enter and then promptly recombine inside the bilayer.

4.3.6.3 The Partition Effect in Vesicles

The partition effect is based on binding constants of the radicals to the vesicle. In the case of an asymmetric ketone precursor, as the binding of one radical over another is favoured, different termination reaction rates develop and the amount of asymmetric product generated can become larger. The partitioning of the

two radical halves between the hydrophobic pseudophase and the bulk water leads to a higher cross-termination rate constant. In small vesicles, a large cage effect in the product studies was observed in the absence of a fast, geminate process. In addition, a magnetic field effect was seen for the random encounters. These characteristics are similar to the observations made in micelles at higher temperatures. The partitioning of the two radicals between the vesicle and the aqueous phase determine the product distribution. In large vesicles, the observed overall cage effect was much smaller than that in the small vesicles and even smaller than that seen in SDS micelles because the random encounters were occurring in the water phase. The partition effect can still be invoked because the partition effect is based on the binding constant which reflects the concentration of vesicles. Equation 4.1 is defined for an equilibrium of a single radical in a vesicular solution.

$$K = \frac{[\text{radical} - \text{vesicle}]}{[\text{radical}][\text{vesicle}]} \qquad (4.1)$$

Assuming that due to the hydrophobic nature of the ketone probe, the ketone is initially bound to the vesicle. The concentration of LUV's is so low that upon photolysis, the generated radicals preferentially partition into the bulk water. In a kinetic manner, this may be viewed as exit followed by recombination in the aqueous phase without ever returning back to a vesicle bilayer. This mechanistic behaviour is in full agreement with the experimental observations and utilizes the newly termed partition effect to describe the experimental results.

4.3.7 Conclusions

Evidence derived from work in small and large vesicles has demonstrated that no geminate recombination reactions are observed. In the case of small vesicles, calculations revealed that the random encounters could be occurring inside the vesicle as well as in the bulk water. For large vesicles, calculations that agree with experimental observations, showed that most of the random radical recombination reactions were occurring in the bulk water. While these observations were once puzzling, the results in micelles have introduced the concept of the partition effect. The product distributions were altered based on the binding constant. In the case of large vesicles, recombination in the bulk water was preferred due to the very small concentration of vesicles which reduced the probability that a radical would re-enter a vesicle. For small vesicles, exit from the vesicle occurs rapidly, but due to the concentration of vesicles in solution, radical re-entry and subsequent recombination is competitive with radical-radical reactions in the bulk water.

CHAPTER 5: CONCLUSIONS AND IMPLICATIONS

5.1 Conclusions

The main objective of this work is to understand the dynamics of radical pairs in micelles and vesicles. Extrapolating the new findings in vesicles to cell membranes should allow novel insights into the behaviour of radicals in these biological systems. There are many paramagnetic materials in biological systems that can be affected by the application of magnetic fields. The MF's used in this study not only provide an impetus for research in biomimetic systems, but also furnish a method for changing the competitive kinetic pathways.

5.2 Conclusions - Micelles

Older models of radical pair dynamics in organized systems have dealt with micelles as "supercages" and have interpreted data in terms of the "superstructure".[68] The results obtained in micelles show that there is a constraint imposed on radical pairs by the micellar structure, so that geminate radical recombination reactions are enhanced. This type of cage effect is termed the geminate cage effect. Smaller micelle sizes brought about by a temperature increase, enhance the amount of exit of the radical pairs. Furthermore, an enhancement of the cross-termination product was observed under conditions when all of the radicals exited from the micelle and no geminate reaction occurred. This is counter-intuitive when one considers only the notion of geometrical constraint. In this situation, it is not the restraint imposed by the supramolecular structure that enhances the cross-termination reaction. The new model proposes that the effect is due to the microheterogeneity of the micelle and the inherent partition of hydrophobic solutes between the bulk water and the nonpolar micellar environment. The formation of the cross-termination photoproduct occurs based on re-entry of

the solute into the micelle after prior exit. This effect is termed the partition effect because the extent of the cross-termination product enhancement is based on the difference in the binding constants of the solutes.

5.3 Conclusions - Vesicles

Two sizes of DODAC vesicles were investigated. In small unilamellar vesicles with a diameter of 30 nm, the cage effect derived from product studies showed a significant enhancement of the cross-termination product below and above the phase transition. However, time-resolved experiments showed that all radicals were exiting the vesicle and thus, all of the enhanced cross-termination reactions from the product studies were derived from random radical encounters and not from geminate encounters.

Large vesicles produced by injection were sized to be ~150 nm. The solutions were turbid, so transmittance measurements with LFP could not be successfully accomplished. Further, the solutions were too clear for use with diffuse-reflectance detection. The product studies demonstrated that the cross-termination product was enhanced to an extent that was even smaller than in SDS micelles and small DODAC vesicles. Calculations revealed that a significant proportion of the random encounters were occurring in the bulk aqueous phase, rather than in the vesicle. In the case of large vesicles, almost no restraint was imposed on dynamics of the radical pair. It is now evident that structure is not as crucial as was once thought in the investigations of radical pair dynamics.

5.4 General Implications

The proposed model demonstrates how it is not necessary to generate a geminate triplet radical pair in order to observe a magnetic field effect on product distribution. Rather, any two radicals that can partition between two

(pseudo)phases and have corresponding different self- and cross-termination reaction rates can be affected by the application of an external magnetic field.

Structural rigidity, differential binding sites, micro-organization and curvature and hydrophobicity have been shown to play a role in altering product distributions in many types of microheterogeneous systems. The product distributions are altered because the mobility of the radical pair is restricted in some fashion. Biological systems have many types of constrained environments, so it seems logical to be able to extrapolate the results to enzyme active sites, cell membranes, and even to intercalation within a DNA helix. This study has demonstrated that in many cases, differential binding affinity is more important than structural considerations.

5.5 Biological Implications

Radical pair dynamics was studied in vesicles as an effort to determine the extent to which the model can be applied to more complex microheterogeneous systems. In biological systems, where radicals may partition among many sites with different affinities, it stands to reason that the partition effect is probably more important than the geminate cage effect.

The possible harmful effects of power lines and other electronics on biological organisms is the subject of much interest and debate. In this study, magnetic field effects have served to identify specific mechanistic interpretations, but were also crucial when attempting to understand the potential effects of magnetic fields on health at a molecular level. Comprehension of the effect of magnetic fields can be heightened by understanding the binding of the radical pair precursor in a constrained or restricted environment. In contrast to previous models, this new model predicts that magnetic field effects can be observed by studying enhanced CTP formation from radicals generated in an aqueous phase.

This new proposal also predicts that regardless of the multiplicity of the radical pair precursor, or site of generation, magnetic field effects in biological systems can be observed as long as mobility between different solubilization sites occurs.

CHAPTER 6: REFERENCES

(1) Jablonski, A. Z. *Phys.* **1935**, *94*, 38-46.

(2) Turro, N. J. *Modern Molecular Photochemistry*; Benjamin/Cummings Publishing Co.: Menlo Park, 1978.

(3) Porter, G. *Proc. R. Soc. Lond. A.* **1949**, *200*, 284-300.

(4) Norrish, R. G. W.; Porter, G. *Nature* **1949**, *164*, 658.

(5) Goodall, D. M.; Harrison, P. W.; Wedderburn, J. H. M. *J. Chem. Educ.* **1972**, *49*, 669-674.

(6) Novak, J. R.; Windsor, M. W. *J. Chem. Phys.* **1967**, *47*, 3075-3076.

(7) Novak, J. R.; Windsor, M. W. *Proc. R. Soc. Lond. A.* **1968**, *308*, 95-110.

(8) Brown, R. E.; Legg, K. D.; Wolf, M. W.; Singer, L. A.; Parks, J. H. *Anal. Chem.* **1974**, *46*, 1690-1694.

(9) Turro, N. J.; Aikawa, M.; Butcher Jr., J. A. *IEEE J. Quantum Electronics* **1980**, *QE-16*, 1218-1222.

(10) Turro, N. J. *Tetrahedron* **1982**, *38*, 809-817.

(11) Scaiano, J. C. *J. Am. Chem. Soc.* **1980**, *102*, 7747-7753.

(12) Liao, Y.; Bohne, C. *J. Phys. Chem.* **1996**, *100*, 734-743.

(13) Gilbert, A.; Baggott, J. *Essentials of Molecular Photochemistry*; CRC Press: Boca Raton, 1991.

(14) Kleinman, M. H.; Bohne, C. In *Organic Photochemistry: Molecular and Supramolecular Photochemistry*; V. Ramamurthy and K. S. Schanze, Ed.; Marcel Dekker, Inc.: New York, 1997; Vol. 1; pp 391-466.

(15) Tanford, C. *The Hydrophobic Effect: Formation of Micelles and Biological Membranes;* 2nd ed.; John Wiley & Sons: New York, 1980.

(16) Turro, N. J.; Cox, G. S.; Paczkowski, M. A. *Topics in Current Chemistry* **1985**, *129*, 59-97.

(17) Menger, F. M.; Zana, R.; Lindman, B. *J. Chem. Educ.* **1998**, *75*, 115.

(18) Kalyanasundaram, K. *Photochemistry in Microheterogeneous Systems*; Academic Press: Orlando, 1987.

(19) Tascioglu, S. *Tetrahedron* **1996**, *52*, 11113-11152.

(20) Gennis, R. B. *Biomembranes: Molecular Structure and Function*; Springer-Verlag: New York, 1989.

(21) Blatt, E.; Sawyer, W. H. *Biochim. Biophys. Acta* **1985**, *822*, 43-62.

(22) Almgren, M.; Grieser, F.; Thomas, J. K. *J. Chem. Soc., Faraday Trans. 1* **1979**, *75*, 1674-1687.

(23) Reekmans, S.; De Schryver, F. C. In *Frontiers in Supramolecular Organic Chemistry and Photochemistry*; H.-J. Schneider and H. Dürr, Ed.; VCH Verlagsgesellschaft: Weinheim, 1991; pp 287-310.

(24) Croonen, Y.; Geladé, E.; Van der Zegel, M.; Van der Auweraer, M.; De Schryver, F. C.; Almgren, M. *J. Phys. Chem.* **1983**, *87*, 1426-1431.

(25) Dominguez, A.; Fernandez, A.; Montenegro, L. *J. Chem. Educ.* **1997**, *74*, 1227-1231.

(26) Missel, P. J.; Mazer, N. A.; Benedek, G. B.; Young, C. Y.; Carey, M. C. *J. Phys. Chem.* **1980**, *84*, 1044-1057.

(27) Quina, F. H.; Nassar, P. M.; Bonilha, J. B. S.; Bales, B. L. *J. Phys. Chem.* **1995**, *99*, 17028-17031.

(28) Briggs, J.; Nicoli, D. F.; Ciccolello, R. *Chem. Phys. Lett.* **1980**, *73*, 149-152.

(29) Bales, B. L.; Almgren, M. *J. Phys. Chem.* **1995**, *99*, 15153-151562.

(30) Turro, N. J.; Zimmt, M. B.; Lei, X. G.; Gould, I. R.; Nitsche, K. S.; Cha, Y. *J. Phys. Chem.* **1987**, *91*, 4544-4548.

(31) Coello, A.; Meijide, F.; Mougán, M. A.; Núñez, E. R.; Tato, J. V. *J. Chem. Educ.* **1995**, *72*, 73-75.

(32) Hayashi, S.; Ikeda, S. *J. Phys. Chem.* **1980**, *84*, 744-751.

(33) Mazer, N. A.; Benedek, G. B.; Carey, M. C. *J. Phys. Chem.* **1976**, *80*, 1075-1085.

(34) Missel, P. J.; Mazer, N. A.; Benedek, G. B.; Carey, M. C. *J. Phys. Chem.* **1983**, *87*, 1264-1277.

(35) Young, C. Y.; Missel, P. J.; Mazer, N. A.; Benedek, G. B.; Carey, M. C. *J. Phys. Chem.* **1978**, *82*, 1375-1378.

(36) Miller, D. J.; Klein, U. K. A.; Hauser, M. *Ber. Bunsenges. Phys. Chem.* **1980**, *84*, 1135-1140.

(37) Stryer, L. *Biochemistry*; W.H. Freeman and Company: New York, 1988.

(38) Kano, K.; Romero, A.; Djermouni, B.; Ache, H. J.; Fendler, J. H. *J. Am. Chem. Soc.* **1979**, *101*, 4030-4037.

(39) Carmona Ribeiro, A. M.; Chaimovich, H. *Biochim. Biophys. Acta* **1983**, *733*, 172-179.

(40) Fendler, J. H. *Acc. Chem. Res.* **1980**, *13*, 7-13.

(41) Tran, C. D.; Klahn, P. L.; Romero, A.; Fendler, J. H. *J. Am. Chem. Soc.* **1978**, *100*, 1622-1624.

(42) Deamer, D.; Bangham, A. D. *Biochim. Biophys. Acta* **1976**, *443*, 629-634.

(43) Aniansson, E. A. G.; Wall, S. N.; Almgren, M.; Hoffman, H.; Kielmann, I.; Ulbricht, W.; Zana, R.; Lang, J.; Tondre, C. *J. Phys. Chem.* **1976**, *80*, 905-922.

(44) Abuin, E. B.; Scaiano, J. C. *J. Am. Chem. Soc.* **1984**, *106*, 6274-6283.

(45) Atik, S. S.; Thomas, J. K. *J. Am. Chem. Soc.* **1981**, *103*, 3550-3555.

(46) Dauben, W. G.; Salem, L.; Turro, N. J. *Acc. Chem. Res.* **1975**, *8*, 41-54.

(47) Wagner, P. J. In *CRC Hanbook of Photochemistry and Photobiology*; W. M. Horspool and P.-S. Song, Ed.; CRC Press: Boca Raton, 1995; pp 449-470.

(48) Lei, X.; Wang, G.; Liu, Y.; Turro, N. J. *J. Photochem. Photobiol. A:Chem.* **1992**, *67*, 57-65.

(49) Scaiano, J. C.; Abuin, E. B.; Stewart, L. C. *J. Am. Chem. Soc.* **1982**, *104*, 5673-5679.

(50) Scaiano, J. C.; Abuin, E. B. *Chem. Phys. Lett.* **1981**, *81*, 209-213.

(51) Griller, D.; Ingold, K. U. *Acc. Chem. Res.* **1976**, *9*, 13-19.

(52) Arbour, C.; Atklinson, G. H. *Chem. Phys. Lett.* **1989**, *159*, 520-525.

(53) Lipson, M.; Noh, T.; Doubleday, C. E.; Zaleski, J. M.; Turro, N. J. *J. Phys. Chem.* **1994**, *98*, 8844-8850.

(54) Hany, R.; Fischer, H. *Chem. Phys.* **1993**, *172*, 131-146.

(55) Sakata, T.; Takahashi, S.; Terazima, M.; Azumi, T. *J. Phys. Chem.* **1991**, *95*, 8671-8676.

(56) Robbins, W. K.; Eastman, R. H. *J. Am. Chem. Soc.* **1970**, *92*, 6076-6077.

(57) Engel, P. S. *J. Am. Chem. Soc.* **1970**, *92*, 6074-6076.

(58) Lunazzi, L.; Ingold, K. U.; Scaiano, J. C. *J. Phys. Chem.* **1983**, *87*, 529-530.

(59) Turro, N. J.; Gould, I. R.; Baretz, B. H. *J. Phys. Chem.* **1983**, *87*, 531-532.

(60) Tsentalovich, Y. P.; Fischer, H. *J. Chem. Soc., Perkin Trans. 2* **1994**, *1994*, 729-733.

(61) Robbins, W. K.; Eastman, R. H. *J. Am. Chem. Soc.* **1970**, *92*, 6077-6079.

(62) Turro, N. J. *Pure & Appl. Chem.* **1981**, *53*, 259-286.

(63) Turro, N. J.; Kraeutler, B. *Acc. Chem. Res.* **1980**, *13*, 369-377.

(64) Turro, N. J.; Grätzel, M.; Braun, A. M. *Angew. Chem. Int. Ed. Engl.* **1980**, *19*, 675-696.

(65) Turro, N. J.; Chow, M.-F.; Kraeutler, B. *Chem. Phys. Lett.* **1980**, *73*, 545-549.

(66) Turro, N. J.; Chow, M.-F.; Chung, C.-J.; Weed, G. C.; Kraeutler, B. *J. Am. Chem. Soc.* **1980**, *102*, 4843-4845.

(67) Turro, N. J.; Cherry, W. R. *J. Am. Chem. Soc.* **1978**, *100*, 7431-7432.

(68) Turro, N. J.; Weed, G. C. *J. Am. Chem. Soc.* **1983**, *105*, 1861-1868.

(69) Turro, N. J.; Chow, M.; Chung, C.; Tanimoto, Y.; Weed, G. C. *J. Am. Chem. Soc.* **1981**, *103*, 4574-4576.

(70) Sakaguchi, Y.; Hayashi, H.; Nagakura, S. *J. Phys. Chem.* **1982**, *86*, 3177-3184.

(71) Hayashi, H.; Sakaguchi, Y.; Nagakura, S. *Chem. Lett.* **1980**, 1149-1152.

(72) Cozens, F. L.; Scaiano, J. C. *J. Am. Chem. Soc.* **1993**, *115*, 5204-5211.

(73) Gould, I. R.; Zimmt, M. B.; Turro, N. J.; Baretz, B. H.; Lehr, G. F. *J. Am. Chem. Soc.* **1985**, *107*, 4607-4612.

(74) Turro, N. J.; Zimmt, M. B.; Gould, I. R. *J. Am. Chem. Soc.* **1983**, *105*, 6347-6349.

(75) Almgren, M.; Grieser, F.; Thomas, J. K. *J. Am. Chem. Soc.* **1979**, *101*, 279-291.

(76) Steiner, U. E.; Wolff, H.-J. In *Photochemistry and Photophysics*; J. F. Rabek, Ed.; CRC Press: Boca Raton, 1991; Vol. 4; pp 1-130.

(77) Steiner, U. E.; Ulrich, T. *Chem. Rev.* **1989**, *89*, 51-147.

(78) Closs, G. L.; Miller, R. J.; Redwine, O. D. *Acc. Chem. Res.* **1985**, *18*, 196-202.

(79) Closs, G. L.; Doubleday Jr., C. *J. Am. Chem. Soc.* **1973**, *95*, 2735-2736.

(80) Bohne, C. *Science Progress* **1994**, *76*, 225-246.

(81) Hayashi, H. In *Photochemistry and Photophysics*; J. F. Rabek, Ed.; CRC Press: Boca Raton, 1990; Vol. 1; pp 60-136.

(82) Buchachenko, A. L. *Russ. Chem. Rev.* **1995**, *64*, 809-816.

(83) Salikhov, K. M.; Molin, Y. N.; Sagdeev, R. Z.; Buchachenko, A. L. *Spin Polarization and Magnetic Effects in Radical Reactions*; Elsevier: New York, 1984; Vol. 22.

(84) Sakaguchi, Y.; Hayashi, H.; Nagakura, S. *Bull. Chem. Soc. Jpn.* **1980**, *53*, 39-42.

(85) Hayashi, H.; Nagakura, S. *Bull. Chem. Soc. Jpn.* **1978**, *51*, 2862-2866.

(86) Turro, N. J.; Lei, X.; Gould, I. R.; Zimmt, M. B. *Chem. Phys. Lett.* **1985**, *120*, 397-400.

(87) Suzuki, T.; Obi, K. *Chem. Phys. Lett.* **1995**, *246*, 130-134.

(88) Imamura, T.; Onitsuka, O.; Obi, K. *J. Phys. Chem.* **1986**, *90*, 6741-6744.

(89) Kawai, A.; Obi, K. *J. Phys. Chem.* **1992**, *96*, 52-56.

(90) Kawai, A.; Okutsu, T.; Obi, K. *J. Phys. Chem.* **1991**, *95*, 9130-9134.

(91) Blättler, C.; Jent, F.; Paul, H. *Chem. Phys. Lett.* **1990**, *166*, 375-380.

(92) Khudyakov, I. V.; Serebrennikov, Y. A.; Turro, N. J. *Chem. Rev.* **1993**, *93*, 537-570.

(93) Buchachenko, A. L.; Galimov, E. M.; Ershov, V. V.; Nikiforov, G. A.; Pershin, A. D. *Akad. Navik SSSR Doklad. Phys. Chem.* **1976**, *228*, 451-453.

(94) Buchachenko, A. L. *Russ. Chem. Rev.* **1976**, *45*, 375-390.

(95) Buchachenko, A. L. *Chem. Rev.* **1995**, *95*, 2507-2528.

(96) Turro, N. J.; Kraeutler, B. *J. Am. Chem. Soc.* **1978**, *100*, 7432-7434.

(97) Kraeutler, B.; Turro, N. J. *Chem. Phys. Lett.* **1980**, *70*, 270-275.

(98) Turro, N. J.; Kraeutler, B.; Anderson, D. R. *J. Am. Chem. Soc.* **1979**, *101*, 7435-7437.

(99) Turro, N. J.; Anderson, D. R.; Chow, M.; Chung, C.; Kraeutler, B. *J. Am. Chem. Soc.* **1981**, *103*, 3892-3896.

(100) Turro, N. J.; Anderson, D. R.; Kraeutler, B. *Tetrahedron Lett.* **1980**, *21*, 3-6.

(101) Turro, N. J.; Chow, M.; Chung, C.; Kraeutler, B. *J. Am. Chem. Soc.* **1981**, *103*, 3886-3891.

(102) Turro, N. J.; Chung, C.; Jones II, G.; Becker, W. G. *J. Phys. Chem.* **1982**, *86*, 3677-3679.

(103) Laidler, K. J. *Chemical Kinetics;* 3rd ed.; Harper and Row Publishers: New York, 1987.

(104) Evans, C. H.; Scaiano, J. C.; Ingold, K. U. *J. Am. Chem. Soc.* **1992**, *114*, 140-146.

(105) Evans, C. H.; Scaiano, J. C. *J. Am. Chem. Soc.* **1990**, *112*, 2694-2701.

(106) Turro, N. J.; Zimmt, M. B.; Gould, I. R. *J. Phys. Chem.* **1988**, *92*, 433-437.

(107) Scaiano, J. C.; Tanner, M.; Weir, D. *J. Am. Chem. Soc.* **1985**, *107*, 4396-4403.

(108) Gould, I. R.; Baretz, B. H.; Turro, N. J. *J. Phys. Chem.* **1987**, *91*, 925-929.

(109) Barra, M.; Bohne, C.; Zanocco, A.; Scaiano, J. C. *Langmuir* **1992**, *8*, 2390-2395.

(110) Scaiano, J. C.; Shi, J. *Chem. Phys. Lett.* **1990**, *173*, 271-276.

(111) Rao, B. N.; Turro, N. J.; Ramamurthy, V. *J. Org. Chem.* **1986**, *51*, 460-464.

(112) Turro, N. J. *Tetrahedron* **1987**, *43*, 1589-1616.

(113) Johnston, L. J.; King Wong, S. *Can. J. Chem.* **1984**, *62*, 1999-2005.

(114) Turro, N. J.; Cheng, C.-C.; Wan, P.; Chun, C.-J.; Mahler, W. *J. Phys. Chem.* **1985**, *89*, 1567-1568.

(115) Turro, N. J.; Paczkowski, M. A.; Wan, P. *J. Org. Chem.* **1985**, *50*, 1399-1404.

(116) Turro, N. J. *Pure & Appl. Chem.* **1986**, *58*, 1219-1228.

(117) Turro, N. J.; Wan, P. *J. Am. Chem. Soc.* **1985**, *107*, 678-682.

(118) Turro, N. J.; Cheng, C.-C.; Lei, X.-G. *J. Am. Chem. Soc.* **1985**, *107*, 3739-3741.

(119) Turro, N. J.; Lei, X.; Cheng, C.-C.; Corbin, D. R.; Abrams, L. *J. Am. Chem. Soc.* **1985**, *107*, 5824-5826.

(120) Taraban, M. B.; Leshina, T. V.; Anderson, M. A.; Grissom, C. B. *J. Am. Chem. Soc.* **1997**, *119*, 5768-5769.

(121) Harkins, T. T.; Grissom, C. B. *Science* **1994**, *263*, 958-960.

(122) Grissom, C. B. *Chem. Rev.* **1995**, *95*, 3-24.

(123) Scaiano, J. C.; Monahan, S.; Renaud, J. *Photochem. Photobiol.* **1997**, *65*, 759-762.

(124) Kaiser, J. *Science* **1996**, *274*, 910.

(125) Stone, R. *Science* **1992**, *258*, 1724-1725.

(126) Taubes, G. *Science* **1993**, *262*, 649.

(127) Taubes, G. *Science* **1997**, *277*, 29.

(128) Hileman, B. *C&EN* **1993**, 15-29.

(129) Linet, M. S.; Hatch, E. E.; Kleinerman, R. A.; Robison, L. L.; Kaune, W. T.; Friedman, D. R.; Severson, R. K.; Haines, C. M.; Hartsock, C. T.;

Niwa, S.; Wacholder, S.; Tarone, R. E. *New England J. Med.* **1997**, *337*, 1-7.

(130) Kang, G. H.; Lee, C. H.; Seo, J.-W.; Sung, R. H.; Chung, Y. H.; Lee, S. K.; Suh, Y.-H.; Chi, J. G. *Journal of Korean Med. Sci.* **1997**, *12*, 128-134.

(131) Mohtat, N.; Cozens, F. L.; Hancock-Chen, T.; Scaiano, J. C.; McLean, J.; Kim, J. *Photochem. Photobiol.* **1998**, *67*, 111-118.

(132) Scaiano, J. C.; Cozens, F. L.; Mohtat, N. *Photochem. Photobiol.* **1995**, *62*, 818-829.

(133) Scaiano, J. C. *The Spectrum* **1995**, *8*, 1-10.

(134) Scaiano, J. C.; Mohtat, N.; Cozens, F. L.; McLean, J.; Thansandote, A. *Bioelectromagnetics* **1994**, *15*, 549-550.

(135) Scaiano, J. C.; Cozens, F. L.; McLean, J. *Photochem. Photobiol.* **1994**, *59*, 585-589.

(136) Brocklehurst, B.; McLauchlan, K. A. *Int. J. Radiat. Biol.* **1996**, *69*, 3-24.

(137) Brocklehurst, B. *Int. J. Radiat. Biol.* **1997**, *72*, 587-596.

(138) Perrin, D. D.; Armarego, W. L. F. *Purification of Laboratory Chemicals*; Pergamon Press, Ltd.: Oxford, 1988.

(139) Lim, Y. Y.; Fendler, J. H. *J. Am. Chem. Soc.* **1979**, *101*, 4023-4029.

(140) Noh, T.; Step, E.; Turro, N. J. *J. Photochem. Photobiol. A:Chem.* **1993**, *72*, 133-145.

(141) Boch, R.; Whittlesey, M. K.; Scaiano, J. C. *J. Phys. Chem.* **1994**, *98*, 7854-7857.

(142) Hutton, R. S.; Roth, H. D.; Kraeutler, B.; Cherry, W. R.; Turro, N. J. *J. Am. Chem. Soc.* **1979**, *79*, 2227-2228.

(143) Johnston, L.; de Mayo, P.; King Wong, S. *J. Am. Chem. Soc.* **1982**, *104*, 307-309.

(144) Lei, X. *Res. Chem. Intermed.* **1990**, *14*, 15-46.

(145) Step, E. N.; Tarasov, V. F.; Buchachenko, A. L.; Turro, N. J. *J. Phys. Chem.* **1993**, *97*, 363-373.

(146) Lehni, M.; Schuh, H.; Fischer, H. *Int. J. Chem. Kinetics* **1979**, *11*, 705-713.

(147) Huggenberger, C.; Fischer, H. *Helv. Chim. Acta* **1981**, *64*, 338-353.

(148) Claridge, R. F. C.; Fischer, H. *J. Phys. Chem.* **1983**, *87*, 1960-1967.

(149) Maouf, A.; Lemmetyinen, H.; Koskikallio, J. *Acta Chem. Scan.* **1990**, *44*, 336-338.

(150) Forbes, M. D. E.; Closs, G. L.; Calle, P.; Gautam, P. *J. Phys. Chem.* **1993**, *97*, 3384-3389.

(151) Roelants, E.; Geladé, E.; Smid, J.; De Schryver, F. C. *J. Colloid Interface Sci.* **1985**, *107*, 337-344.

(152) Fischer, H. *J. Am. Chem. Soc.* **1986**, *108*, 3925-3927.

(153) Daikh, B. E.; Finke, R. G. *J. Am. Chem. Soc.* **1992**, *114*, 2938-2943.

(154) Bravo, A.; Bjørsvik, H.-R.; Fontana, F.; Liguori, L.; Minisci, F. *J. Org. Chem.* **1997**, *62*, 3849-3857.

(155) Arends, I. W. C. E.; Ingold, K. U.; Wayner, D. D. M. *J. Am. Chem. Soc.* **1995**, *117*, 4710-4711.

(156) MacFaul, P. A.; Arends, I. W. C. E.; Ingold, K. U.; Wayner, D. D. M. *J. Chem. Soc., Perkin Trans. 2* **1997**, 135-145.

(157) Quina, F. H.; Alonso, E. O.; Farah, J. P. S. *J. Phys. Chem.* **1995**, *99*, 11708-11714.

(158) Abraham, M. H.; McGowan, J. C. *Chromatographia* **1987**, *23*, 243-246.

(159) Abraham, M. H. *Chem. Soc. Rev.* **1993**, 73-83.

(160) Wilkinson, F. *J. Chem. Soc., Faraday Trans.* **1986**, *82*, 2073-2081.

(161) Kessler, R. W.; Wilkinson, F. *J. Chem. Soc., Faraday Trans.* **1981**, *77*, 309-320.

(162) Kortüm, G.; Braun, W.; Herzog, G. *Angew. Chem., Int. Ed. Engl.* **1963**, *2*, 333-404.

(163) Vanderkooi, J. M.; Callis, J. B. *Biochemistry* **1974**, *13*, 4000-4006.

(164) Naqvi, K. R.; Behr, J. P.; Chapman, D. *Chem. Phys. Lett.* **1974**, *26*, 440-444.

(165) Herrmann, U.; Fendler, J. H. *Chem. Phys. Lett.* **1979**, *64*, 270-274.